

Republic of Iraq
Ministry of Higher Education
And Scientific Research
Al-Nahrain University
College of Science
Department of Chemistry



Characterization of Red Apple and Pomegranate Peels Extracts as Corrosion Inhibitors for α - Brass in Acidic Media

A Thesis

Submitted to the College of Science/Al-Nahrain University as a partial fulfillment of the requirements for the Degree of Master of Science in Chemistry

By

Mustafa Sabri Cheyad

B.Sc. Chemistry/College of Science/Al-Nahrain University
2015

Supervised by

Dr. Taghried Ali Salman

(Asst. Prof.)

Feb. 2018

Jumada I. 1439

Supervisor Certification

I, certify that this thesis entitled “**Characterization of Red Apple and Pomegranate Peels Extracts as Corrosion Inhibitors for α -Brass in Acidic Media**” was prepared by “**Mustafa Sabri Cheyad**” under my supervision at the College of Science/Al-Nahrain University as a partial fulfillment of the requirements for the Degree of Master of Science in Chemistry (Physical Chemistry).

Signature: 

Name: **Dr. Taghried A. Salman**

Scientific Degree: Assistant Professor

Date: 29 - 1 - 2018

In view of the available recommendations, I forward this Thesis for debate by Examining Committee.

Signature: 

Name: **Dr. Emad Al-Sarraj**

Title: Head of the Department of Chemistry

Committee Certification

We, the examining committee certify that we have read this thesis entitled “**Characterization of Red Apple and Pomegranate Peels Extracts as Corrosion Inhibitors for α -Brass in Acidic Media**” and examined the student “**Mustafa Sabri Cheyad** “ in its contents and that in our opinion, it is accepted for the Degree of Master of Science, in Physical Chemistry.

Signature: 

Name: **Dr. Ahmed Abdulilah Ahmed**

Scientific Degree: Assistant Professor

Date: **25-1-2018**

(Chairman)

Signature: 

Name: **Dr. Alaa Al-Khalaf**

Scientific Degree: Assistant Professor

Date: **28-1-2018**

(Member)

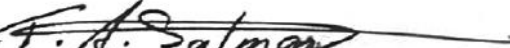
Signature: 

Name: **Dr. Khalida A. Samawi**

Scientific Degree: Lecturer

Date: **24-1-2018**

(Member)

Signature: 

Name: **Dr. Taghried A. Salman**

Scientific Degree: Assistant Professor

Date:

(Member/Supervised)



I, hereby certify upon the decision of the examining committee.

Signature: 

Name: **Dr. Hadi M. A. Abood**

Scientific Degree: Professor

Title: Dean of College of Science

Date: **4/1/2018**

بِسْمِ اللَّهِ الرَّحْمَنِ الرَّحِيمِ

﴿وَهُوَ الَّذِي أَنْزَلَ مِنَ السَّمَاءِ مَاءً فَأَخْرَجْنَا بِهِ نَبَاتَ كُلِّ
شَيْءٍ فَأَخْرَجْنَا مِنْهُ خَضِرًا نُخْرِجُ مِنْهُ حَبًّا مُتَرَاكِبًا وَمِنْ
النَّخْلِ مِنَ طَلْعِهَا قِنْوَانٌ دَانِيَةٌ وَجَنَّاتٍ مِّنْ أَعْنَابٍ
وَالزَّيْتُونِ وَالرُّمَّانِ مُشْتَبِهًا وَغَيْرَ مُتَشَابِهٍ انظُرُوا إِلَى ثَمَرِهِ
إِذَا أَثْمَرَ وَيَنْعِهِ إِنَّ فِي ذَلِكُمْ لَآيَاتٍ لِّقَوْمٍ يُؤْمِنُونَ ﴿٩٩﴾﴾

صدق الله العلي العظيم

سورة الانعام

Dedication

This thesis is dedicated to a strong and gentle soul, my mother

To my beloved father who has supported me throughout my life

To all the doctors who taught me and advised me in my master program

To all my friends

Acknowledgment

*First of all, I am deeply grateful to almighty **Allah** the most merciful, the most gracious for stood beside me throughout my entire life and gives the necessary strength and will to accomplish my work.*

*I would like to express my gratitude and my appreciation to my supervisor **Dr. Taghried Ali Salman** for her countless efforts, her guidance and her advises.*

*I address my thanks to the department of Chemistry in Al-Nahrain University and to head of the department **Dr. Emad Al-Sarraaj***

*I extend my thanks to **Dr. Nasreen Raheem Jber** and **Dr. Dheaa Zageer** and other staff of the department*

*I address many thanks to **Dr. AbdulKareem AL-Samarraie** for his help and motivating discussions.*

*Many thanks go to **Dr. Hassan N. Hashim** for his help in the experimental work.*

*My deeply-gratitude and appreciation go to my dearest friend **Ala'a Bader Mohammed** for her efforts and interesting discussion.*

*Special thanks go to the kindest person I ever know my friend **Namariq Amer Lafta** for her helping during my study.*

*I extend my thanks to my friends **Sarah Jwad** and **Ahmed Abbas***

Summary:

The present thesis consists of four chapters that throws the light on studying the corrosion behavior of α -brass in the acidic media using the potentiostatic polarization. Each chapter discusses many topics can be demonstrated as following:

1. Chapter one discusses the introduction topics about corrosion, corrosion forms, electrochemical aspects and copper alloys.
2. Chapter two discusses the experimental procedures and techniques about characterization of the pomegranate and red apple peels and the polarization study.
3. Chapter three discusses the outcome results from experimental work, the activation calculations and adsorption calculations.
4. Chapter four demonstrates the highlights, conclusions and recommendations that come from the discussed results.

The outcome results can be summarized as follow:

1. The characterization techniques (GC-MS) and (FT-IR) proved the presence of many organic compounds that responsible for the inhibition performance of the pomegranate and red apple peels.
2. The potentiostatic results show that the corrosion current density, corrosion rate and penetration rate increase with increasing temperature within the range (293-313) K.
3. The inhibition efficiency and surface coverage increase with increasing the concentration of both of the inhibitors (pomegranate and red apple peels). And decrease with increasing temperature.
4. The polarization results revealed that red apple peels was best inhibitor in both of acidic media.
5. Pomegranate and red apple peels were act as mixed-type inhibitor in H_2SO_4 solution and as cathodic inhibitor in HCl solution.

6. The activation parameters revealed that the values of E_a were positive and its values were found to be higher in presence of the inhibitors compared to blank solutions which indicate the difficulty of corrosion process in presence of inhibitor. The values of ΔH_a were positive meaning the endothermic nature of corrosion process. The ΔS_a values were mostly negative and increase toward positive direction indicating that the activated complex represents association rather than dissociation.
7. The thermodynamic parameters of adsorption showed that the values of ΔG_{ads}° were large and negative which indicating that the adsorption process is spontaneous and its values were between (37.27 - 42.25) kJ.mol^{-1} which indicate that the adsorption of these inhibitors operate mostly via chemisorption mechanism. The large values of K_{ads} indicate the formation of stable protective film by those inhibitors. The values of ΔH_{ads}° were negative indicating the exothermic nature of the adsorption process. The ΔS_{ads}° values were positive meaning the increase in randomness when the adsorption process occurred.
8. The XRD analysis proved the formation of ZnS and CuCl in H_2SO_4 and HCl respectively and proved that the inhibitive performance of the pomegranate and red apple peels which they preventing formation of those compounds.
9. The SEM micrographs show that damage of the alloy surface in the corrosive solutions (H_2SO_4 and HCl) and proved the adsorption of the used inhibitors.

Contents

Item number	Subject	Page number
	List of Content	I
	List of Abbreviations and Symbols	IV
	List of Figures	VI
	List of Tables	IX
Chapter One / Introduction and Literature Survey		1
1.1	Chemistry of Copper and Zinc	2
1.2	General Concepts of Corrosion	2
1.3	Copper and Copper Alloys	3
1.3.1	Brasses Alloys	4
1.3.2	Literature Survey on Corrosion of Brass alloys in Aqueous Solutions	6
1.4	Corrosion Forms	10
1.4.1	Uniform Corrosion	10
1.4.2	Erosion Corrosion	11
1.4.3	Pitting Corrosion	11
1.4.4	Inter-granular Corrosion	12
1.4.5	Galvanic Corrosion	12
1.4.6	Stress Corrosion Cracking	13
1.4.7	Crevice Corrosion	13
1.5	Electrochemical Aspects of Corrosion	13
1.5.1	Corrosion Rate and Penetration Rate	16
1.5.2	Transfer Coefficients	17
1.5.3	Polarization Resistances and Exchange Current Densities	18
1.6	Corrosion Thermodynamic	19
1.6.1	Arrhenius Equation	19
1.6.2	Adsorption Isotherm Model	19
1.7	Corrosion Inhibitors	19
1.7.1	Corrosion Inhibitors Classification	21
1.7.1.1	Environmental Conditioners (Scavengers)	21
1.7.1.2	Interface Inhibitors	22
1.7.1.2.1	Vapor-Phase Inhibitors	22
1.7.1.2.2	Liquid-Phase Inhibitors	22
1.7.1.2.2.1	Anodic Inhibitors (Inorganic Inhibitors)	22
1.7.1.2.2.2	Cathodic Inhibitors	23
1.7.1.2.2.3	Mixed-type Inhibitors (Organic Inhibitors)	23
1.8	Green Chemistry Approach in Corrosion	24

1.8.1	Literature Survey on using Natural Products as Corrosion Inhibitors	25
1.9	The Aim of the Research	27
Chapter Two / Experimental		28
2.1	Chemicals and Materials	29
2.1.1	α -Brass Alloy	29
2.1.2	Chemicals	29
2.2	Preparation of Electrolytes	29
2.3	Extraction	30
2.3.1	Pomegranate Peel Extraction	30
2.3.2	Red Apple Peel Extraction	31
2.4	Specimen Preparation	31
2.5	Instrumental Techniques	31
2.6	The Potentiostatic Polarization Set-Up and Procedure	32
2.6.1	Potentiostat/Galvanostat Device-M lab 200	33
2.6.2	Three-Electrodes System	33
2.6.2.1	Working Electrode	34
2.6.2.2	Reference Electrode	34
2.6.2.3	Auxiliary Electrode	35
2.6.3	Corrosion Cell	35
2.6.4	Thermostat	35
2.6.5	Procedure of Corrosion Test	36
2.6.5.1	Open Circuit Potential	36
2.6.5.2	Polarization Measurements (Tafel Extrapolation)	37
2.7	Characterization Techniques	37
2.7.1	Fourier Transform Infrared Spectroscopy (FTIR)	38
2.7.2	Gas Chromatography Mass Spectroscopy (GC-MS)	38
2.8	Surface Examination Techniques	40
2.8.1	X-Ray Diffraction (XRD) Powder	40
2.8.2	Scanning Electron Microscope (SEM)	41
Chapter Three / Results and Discussion		42
3.1	Characterization Techniques	43
3.1.1	Fourier Transform Infrared Spectroscopy (FTIR)	43
3.1.2	Gas Chromatography Mass Spectroscopy (GC-MS)	46
3.2	Potentiostatic Polarization Measurements	54
3.2.1	Corrosion Parameters	65
3.2.2	Tafel Slopes and Transfer Coefficients	71
3.2.3	Polarization Resistances and Exchange Current Densities	76
3.3	Surface Coverage and Inhibition Efficiency	76

3.4	Activation Parameters of α -Brass Corrosion	79
3.5	Thermodynamic Parameters of Adsorption Isotherm Modeling	83
3.6	Surface Characterization Techniques	89
3.6.1	X-Ray Diffraction (XRD) Powder	89
3.6.2	Scanning Electron Microscope (SEM)	93
Chapter Four / Conclusions and Recommendations		95
4.1	Conclusions	96
4.2	Recommendations	98
References		99

Abbreviations and Symbols

Abbreviations	Meaning
A	The pre-exponential factor
a	Atomic weight
ads	Adsorption
AE	Auxiliary electrode
b_a	Anodic Tafel slope
b_c	Cathodic Tafel slope
C	Coulomb
c	Concentration
c_{inh}	The inhibitor concentration
corr	Corrosion
CR	Corrosion rate
E	Potential
e	Equivalent weight
e^-	Electron
E_a	The activation energy
E_{corr}	Corrosion potential
EIS	Electrochemical impedance spectroscopy
E_{Total}	Total energy
ev	Electron volt
F	The Faraday constant
FTIR	Fourier transform infrared spectroscopy
g	Gas
GC-MS	Gas chromatography mass spectroscopy
h	The planks constant
hrs	Hours
i	Current density
I	Current
i_{corr}	Corrosion current density
IE%	The inhibition efficiency
Inh	Inhibitor
i_o	The exchange current
K_{ads}	The equilibrium constant
M	Molarity
m	Mass
M/Z	Mass to charge ratio
n	The number of electrons
N	The Avogadro's number
OCP	Open circuit potential

ox	Oxidation
ppm	Part per million
ppt	Precipitation
PR	Pentration rate
R	Gas constant
RE	Reference electrode
red	Reduction
R_p	Polarization resistance
RT	Retention time
s	Solid
SA	Surface area
SCE	Saturated calomel electrode
SEM	Scanning electron microscope
sol	Solution
T	Absolute temperature
t	Time
VPIs	Vapor-Phase inhibitors
WE	Working electrode
XRD	X-ray diffraction
Z_f	Dezincification factor
α	Alpha
α_a	The transfer coefficients of the anodic
α_c	The transfer coefficients of the cathodic
β	Beta
ΔG	The Gibbs free-energy change
ΔH	Enthalpy change
ΔS	Entropy change
η	Over potential
θ	The surface coverage
π	Pi
ρ	Density

List of figures

Figure number	Name of figures	Page number
1.1	An illustrated diagram of dezincification	6
1.2	Simple uniform corrosion	10
1.3	Erosion corrosion	11
1.4	Illustration diagram for copper alloys undergo pitting corrosion.	11
1.5	Inter- granular corrosion	12
1.6	Illustration diagram for galvanic corrosion	12
1.7	Stress cracking corrosion	13
1.8	Illustration diagram for crevice corrosion	13
1.9	Illustration diagram for adsorption of inhibitor molecules on copper surface.	20
1.10	General Classification of Inhibitors	21
2.1	Pomegranate peel extraction steps	30
2.2	Red Apple peel extraction steps	31
2.3	Front facing panel Potentiostat/Galvanostat	33
2.4	Working electrode	34
2.5	Reference electrode	34
2.6	Corrosion cell set-up	35
2.7	The complete set-up of polarization measurement	36
2.8	Experimentally polarization plot	37
2.9	Fourier Transform Infrared Spectrophotometer	38
2.10	Gas Chromatography Mass Spectrometer	39
2.11	Methanolic extracts (a): Pomegranate peel (b): Red apple peel	40
2.12	X-Ray Diffractometer	41
2.13	Scanning Electron Microscope	41
3.1	FTIR spectrum of pomegranate peels powder	43
3.2	FTIR spectrum of red apple peel powder	45
3.3	Chromatogram of methanolic extract of pomegranate peel	46
3.4	Chemical structure of 5-Hydroxymethylfurfural	47
3.5	Chromatogram of methanolic extract of red apple peel	49
3.6	Chemical structure of cyclobutyl decyl oxalate	50
3.7	Polarization curves for α -brass corrosion in blank acidic medium (H_2SO_4 solution) at different concentrations at temperature range (293-313) K.	54

3.8	Polarization curves for α -brass corrosion in the blank (H_2SO_4 solution) and in presence of different pomegranate peel concentrations at temperature range (293-313) K.	56
3.9	Polarization curves for α -brass corrosion in the blank (H_2SO_4 solution) and in presence of different apple peel concentrations at temperature range (293-313) K.	58
3.10	Polarization curves for α -brass corrosion in blank acidic medium (HCl solution) at different concentrations at temperature range (293-313) K.	60
3.11	Polarization curves for α -brass corrosion in the blank (HCl solution) and in presence of different pomegranate peel concentrations at temperature range (293-313) K.	62
3.12	Polarization curves for α -brass corrosion in the blank (HCl solution) and in presence of different apple peel concentrations at temperature range (293-313) K.	64
3.13	Arrhenius plots of $\log i_{\text{corr}}$ versus $1/T$ for the corrosion of α -brass in 2 M H_2SO_4 and in the presence of inhibitors (Pomegranate and Red apple Peels) at various concentrations.	80
3.14	Arrhenius plots of $\ln (i_{\text{corr}}/T)$ versus $1/T$ for the corrosion of α -brass in 2 M H_2SO_4 and in the presence of inhibitors (Pomegranate and Red apple Peels) at various concentrations.	80
3.15	Arrhenius plots of $\log i_{\text{corr}}$ versus $1/T$ for the corrosion of α -brass in 2 M HCl and in the presence of inhibitors (Pomegranate and Red apple Peels) at various concentrations.	81
3.16	Arrhenius plots of $\ln (i_{\text{corr}}/T)$ versus $1/T$ for the corrosion of α -brass in 2 M HCl and in the presence of inhibitors (Pomegranate and Red apple Peels) at various concentrations.	81
3.17	Langmuir isotherm plots for the adsorption of (Pomegranate and Red apple Peels) on α -brass in 2 M H_2SO_4 .	85
3.18	Langmuir isotherm plots for the adsorption of (Pomegranate and Red apple Peels) on α -brass in 2 M HCl.	85
3.19	The variation of Gibbs free energies (ΔG_{ads}) with temperature for the adsorption of (Pomegranate and Red apple Peels) on α -brass in 2 M H_2SO_4 .	86

3.20	The variation of Gibbs free energies (ΔG_{ads}) with temperature for the adsorption of (Pomegranate and Red apple Peels) on α -brass in 2 M HCl.	86
3.21	XRD interpreted patterns for α -brass in 2 M of blank solution (H_2SO_4).	89
3.22	XRD interpreted patterns for α -brass in 2 M of blank solution (H_2SO_4) and in presence of 500 ppm of pomegranate peels.	90
3.23	XRD interpreted patterns for α -brass in 2 M of blank solution (HCl).	90
3.24	XRD interpreted patterns for α -brass in 2 M of blank solution (HCl) and in presence of 500 ppm of red apple peels.	91
3.25	Scanning electron micrographs of (a) Polished α -brass alloy (b) α -brass alloy immersed 24 hrs in 2 M H_2SO_4 solution (c) α -brass alloy immersed 24 hrs in 2 M H_2SO_4 solution and in presence of 500 ppm red apple peels extract and (d) α -brass alloy immersed 24 hrs in 2 M H_2SO_4 solution and in presence of 500 ppm pomegranate peels extract.	94
3.26	Scanning electron micrographs of (a) Polished α -brass alloy (b) α -brass alloy immersed 24 hrs in 2 M HCl solution (c) α -brass alloy immersed 24 hrs in 2 M HCl solution and in presence of 500 ppm red apple peels extract and (d) α -brass alloy immersed 24 hrs in 2 M HCl solution and in presence of 500 ppm pomegranate peels extract.	95

List of tables

Table number	Name of tables	Page number
2.1	The list of chemicals used in the research.	29
2.2	The Instruments were use in this study.	32
3.1	The main FTIR bands in pomegranate peel powder.	44
3.2	The main FTIR bands red apple peel powder.	45
3.3	Major identification compounds in methanolic extract of pomegranate peels.	47
3.4	Major identification compounds in methanolic extract of red apple peels.	50
3.5	Corrosion parameters of α -brass in blank acidic medium (H_2SO_4 solution) at different concentrations at temperature range (293-313) K.	55
3.6	Corrosion parameters of α -brass in the blank (H_2SO_4 solution) and in presence of different pomegranate peel concentrations at temperature range (293-313) K.	57
3.7	Corrosion parameters of α -brass in the blank (H_2SO_4 solution) and in presence of different red apple peel concentrations at temperature range (293-313) K.	59
3.8	Corrosion parameters of α -brass in blank acidic medium (HCl solution) at different concentrations at temperature range (293-313) K.	61
3.9	Corrosion parameters of α -brass in the blank (HCl solution) and in presence of different pomegranate peel concentrations at temperature range (293-313) K.	63
3.10	Corrosion parameters of α -brass in the blank (HCl solution) and in presence of different apple peel concentrations at temperature range (293-313) K.	65
3.11	Values of transfer coefficient (α_c , α_a), the polarization resistance (R_p) and equilibrium exchange current density (i_o) for corrosion of α -brass in 2 M H_2SO_4 solution in the absence and presence of pomegranate peels at temperature range (293-313) K.	72
3.12	Values of transfer coefficient (α_c , α_a), the polarization resistance (R_p) and equilibrium exchange current density (i_o) for corrosion of α -brass in 2 M H_2SO_4 solution in the absence and presence of red apple peels at temperature range (293-313) K.	73
3.13	Values of transfer coefficient (α_c , α_a), the polarization resistance (R_p) and equilibrium exchange current density (i_o) for corrosion of α -brass in 2 M HCl	74

	solution in the absence and presence of pomegranate peels at temperature range (293-313) K.	
3.14	Values of transfer coefficient (α_c , α_a), the polarization resistance (Rp) and equilibrium exchange current density (i_0) for corrosion of α -brass in 2 M HCl solution in the absence and presence of red apple peels at temperature range (293-313) K.	75
3.15	Inhibition efficiencies and surface coverages of pomegranate and red apple peels at various concentration with temperature range (293-313)K in 2 M H ₂ SO ₄ .	77
3.16	Inhibition efficiencies and surface coverages of pomegranate and red apple peels at various concentration with temperature range (293-313)K in 2 M HCl.	78
3.17	Activation energy (E_a), activation enthalpy (ΔH_a), and the entropy of activation (ΔS_a) for the corrosion of α -brass in 2 M H ₂ SO ₄ and in the presence of inhibitors (Pomegranate and Red apple Peels) at various concentrations.	82
3.18	Activation energy (E_a), activation enthalpy (ΔH_a), and the entropy of activation (ΔS_a) for the corrosion of α -brass in 2 M HCl and in the presence of inhibitors (Pomegranate and Red apple Peels) at various concentrations.	82
3.19	Thermodynamic parameters for adsorption of (Pomegranate and Red apple Peels) on α -brass in 2 M H ₂ SO ₄ .	87
3.20	Thermodynamic parameters for adsorption of (Pomegranate and Red apple Peels) on α -brass in 2 M HCl.	87

Chapter One

Introduction and Literature

Survey

1.1 Chemistry of Copper and Zinc

Copper is one of the oldest metal used by human centuries ago it has chemical configuration $[\text{Ar}]3d^{10}4s^1$ it has one electron outside a filled electronic subshell. Copper has a remarkable physical properties such as being high conductor for both of electricity and heat. The metal is also ductile and malleable. Copper is widely considered unreactive toward many diluted acid such sulfuric or hydrochloric acids that's considered main reason of its usefulness in many industrial fields with or without alloying with other metals ⁽¹⁾.

Zinc is a metallic element with chemical configuration $[\text{Ar}]3d^{10}4s^2$ it has only one oxidation stats (II) unlike copper, zinc is highly reactive due to its large electrode potential that's why it used as a sacrificial protection. In order to enhance its corrosion resistance zinc can be coupled with many high resistant metal such as copper in process known as galvanizing ⁽²⁾.

1.2 General Concepts of Corrosion

Corrosion terminology comes from a Latin word "corrodere" which means (to gnaw), corrosion can be defined in different ways but the most interpretation definition of the term is a destructive attack on the metallic materials (metals) within the surrounded environments. It's an electrochemical reaction and ordinarily begins at a metal surface which can be determined by either the change in weight of a given metal or by change in the chemical or physical properties with time ⁽³⁾. Corrosion causes consequences series that become globally as a significant problem; besides our everyday experiencing with this kind of degradation it also leads to shutdown of plants, destruction of metallic infrastructures and waste valuable resources which required a costly maintenance. In order to minimize its effect, major corporations, establishments and governments have been recruited groups and committees to investigate corrosion-issues related. Corrosion control is done by first understanding its

mechanisms and by using corrosion-resistant materials as possible, protective systems or devices ⁽⁴⁾. Corrosion is undesired phenomenon naturally occurred due to the fact that metals and their temporary unstable form of a pure metallic state have great tendency to convert to a high thermodynamically stable form which represent as ores or natural minerals that's the main reason metals are existed in many forms such as oxides or hydroxides, etc., according to their existing environment ⁽⁵⁾. Corrosion prevention is the most important topic in industrial engineering as a result its necessary to have a full awareness insight into electrochemistry, physical chemistry, chemical metallurgy and composition such of these related areas of knowledge is what the corrosion fundamentals is based on ⁽⁶⁾.

1.3 Copper and Copper Alloys

Copper is the one of the few metals that occurs in nature in directly usable metallic form as opposed to need extraction from an ore, also its oldest metal for human use. It was widely used in many applications due to its good electrical, mechanical and physical properties, so it used in electronics manufacturing, wires, sheets and alloys. Copper is known being resistant toward atmospheric conditions and many chemicals solutions; however, it's well known that could be susceptible to corrosion in aggressive media such as sulfuric and hydrochloric acids. The corrosion prevention of copper has been taken an intention of many researchers to discover new approaches to reduce its corrosion ⁽⁷⁾. The inhibition possibility of copper corrosion have been topics of interest for a wide scientific society for quite time which clear obvious from the studies that conducted and published about that subject ⁽⁸⁾. Copper can be used in industry applications as either in a pure metal state or alloying with other elements (e.g. Zn ,Ni ,Al, etc.) doping copper with such these elements can enhance its mechanical properties and higher corrosion resistance ⁽⁹⁾. A pure unalloyed copper have a red dark color in nature which converted gradually towards

yellow, bronze and gray when alloyed with other elements. Alloyed copper with main elements for different industrial purposes which can be mentioned as below:

- ❖ Coppers: alloys which contain 99.3% of copper metal as minimal percentage.
- ❖ Brasses: the main type of copper alloys (Cu+Zn) that use in different industrial fields which contain zinc as principle element with various percentages reaching up to 45%.
- ❖ Bronzes: alloys that contain tin as the only or principle element these alloys used for many outdoor applications.
- ❖ Copper-Nickel: these alloys contain nickel as the principle element also known as nickel-silver when doped with zinc as second principle element.
- ❖ Copper-Leaded alloys: are alloys that contain lead with 20% or low as the principle element.
- ❖ Special alloys: other copper alloys that containing other elements didn't mention above ⁽⁴⁾.

1.3.1 Brasses Alloys

Brasses are alloys that made primary of copper containing different percentage of zinc; they exhibit remarkable strength, ductility and easily cold-worked properties which enhanced with increasing zinc content up to 45% brasses color ranges between red to golden yellow depends on zinc content ⁽¹⁰⁾. Brasses can be classified according to zinc content as follows:

- ❖ α -Brass: alloys with homogenous crystalline structure (FCC) with zinc content of 30% or below they have a golden yellow color.
- ❖ β -Brass: alloys that have greater zinc content up to 45% they considered strongest type of brasses and far less ductile.

- ❖ α - β (Dublex Brasses): alloys that have a heterogeneous crystalline structure with zinc content ranging between 30-45 % depending on the ratio between alpha and beta contents ⁽¹¹⁾.

α -Brass is most versatile copper alloys that widely used in many industrial and engineering application such as heat exchange tubes for instance cooling water systems, power generations, heat exchangers, valves and condensers ⁽¹²⁾. These alloys contain zinc content up to 30% or less with or without other elements which acquire them a yellow golden color. α -brass considered as most copper-zinc alloys type to use in many industrial fields, this attributed to its great corrosion resistance. α -brass also used in non-industrial applications like decorative, casting and other outdoor applications due to its being more dutiable ⁽¹³⁾.

α -Brass alloys are widely used in industrial fields due to its good machinability, high thermal and electrical conductivity and their low cost. However, these alloys are susceptible to a special De-alloying form called Dezincification as shown in figure (1.1) which defined as a selective form of corrosion of brasses alloys that leads to a preferential leaching of zinc from alloy surface leaving a porous layer (plug type) or uniform (layer type) of copper which can be observed by naked eyes from turning its color from yellow to red. This undesired phenomenon leads to serious destruction of the surface and mechanical properties of the remaining alloy as a result; many studies have been established on the mechanism of dezincification and knowing the possible ways to prevent this type of corrosion failure ⁽¹⁴⁾.

Despite of many researches about dezincification, yet it's still unclear how brasses alloys undergo that phenomenon but there are three accepted mechanisms that proposed as a result of the studies by Heidersback and Verink which are ⁽¹⁵⁾:

- ❖ A preferential dissolution of zinc from the alloy.

- ❖ Dissolution of copper and zinc simultaneously, followed by re-plate of spongy copper due to the reduction of cupric ions at cathodic region and then redeposition on the surface
- ❖ The above mechanisms occurred simultaneously at the time.

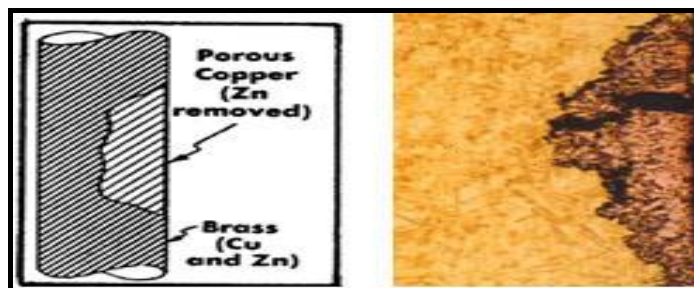


Figure (1.1): An illustrated diagram of dezincification.

In industrial fields brasses are more susceptible to dezincification because of many plants, factories and water systems are used many acids like oxidizing acids (H_2SO_4 , HNO_3) or non-oxidizing acids (HCl) as primary chemicals for cleaning, pickling and descaling. These acids play an important role in industry because these chemicals remove the accumulated precipitates and oxides layers that formed on brass surface as a result of their heating transmission which leads to diminish its performance which required to be regularly cleaned with these acids ⁽¹³⁾.

1.3.2 Literature Survey on Corrosion of Brass alloys in Aqueous Solutions

H. S Hegazy (2001) ⁽¹⁶⁾ investigated the inhibition performance of Benzotriazole (BTAH) for α -brass in sulfide-polluted salted water using weight loss method. BTAH results showed to be effective against the localized corrosion of the contaminated sulfide ions due to the increase of the surface coverage of the inhibitor which led to decrease the sulfide concentration which decrease of the corrosion rate.

S. A. M. Refaey et.al (2007) ⁽⁹⁾ investigated the inhibition action of inorganic anions (permanganate and phosphate) on brass (Cu-Zn alloys) in NaCl

solution. The corrosion behavior have been investigated using electrochemical techniques (open circuit potential, potentiodynamic, and impedance spectroscopy EIS). The corrosion rate was reduced remarkably with increase the concentration of the anions. The adsorption characteristics of the anions was also studied. The polarization measurements revealed the order of inhibition was phosphate > permanganate.

S. A. M. Refaey et .al (2008) ⁽¹⁷⁾ investigated the effect of adding isatin to Cu-Zn alloys in acidic media (H_2SO_4 , HCl) by using open circuit potential, potentiodynamic polarization, and electrochemical impedance spectroscopy (EIS). The corrosion rate was found to be decreased by increase the addition of isatin the polarization measurement revealed that isatin acts as anodic inhibitor in HCl and as cathodic inhibitor in H_2SO_4 .

M. Abdallah et .al (2009) ⁽¹⁸⁾ investigated the protection efficiency of some phenylhydrazone derivatives, namely, [ethyl(2Z)-cyano[(4E)-5-oxo-3-phenyl-4-(phenylhydrazono)-1,3-thiazolidin-2-ylidene] acetate (A), ethyl(2Z)-cyano[(4E)-5-oxo-3-phenyl-4-(p-methylphenylhydrazono)-1,3-thiazolidin-2-ylidene] acetate (B), ethyl(2Z)-cyano[(4E)-5-oxo-3-phenyl-4-(o-methoxyphenylhydrazono)-1,3-thiazolidin-2-ylidene] acetate (C) and ethyl(2Z)-cyano[(4E)-5-oxo-3-thiazolidin-2-ylidene] acetate (D) for corrosion of α -brass in 2 M HCl solution. the corrosion behavior was investigated using weight loss and polarization technique. The inhibition efficiency was increased with increasing concentration of these inhibitors. The adsorption of these inhibitors followed Temkin isotherm model.

A. Dadgarinezhad and F. Baghei (2010) ⁽¹³⁾ studied the effect of a new synthetic Schiff base namely bis-(2-hydroxy-3-methoxy)-1,6-diaminohexane salicyladimine for corrosion of α -brass (70Cu/Zn30) in 1 M HCl solution using weight loss method, Potentiodynamic polarization, EIS and solution analysis techniques. The polarization results revealed that the new Schiff base derivative

acts as mix-type inhibitor and also showed that it's considered good inhibitor with maximum obtained efficiency 88.82 %. The measurement of weight loss showed that the addition of inhibitor decreased the corrosion rate. The calculated dezincification factor (Z_f) in presence of the inhibitor was found to be smaller than the bulk solution which can be attributed to formation of protective film via adsorption.

X. Joseph Raj and N. Rajendran (2011) ⁽¹⁹⁾ Studied the inhibition action of thiadiazole derivatives for brass in natural seawater. It was found that the inhibition efficiency of the thiadiazole derivatives which they namely, 2-amino-5-ethyl-1,3,4-thiadiazole (AETD), 2-amino-5-ethylthio-1,3,4-thiadiazole (AETTD) and 2-amino-5-tert-butyl-1,3,4-thiadiazole (ATBTD) increased with increased concentration. The maximum inhibition efficiency was obtained by AETTD with 95% percentage. The adsorption of the inhibitor was confirmed by SEM/EDX and FTIR spectra. The adsorption of these inhibitors was found to be followed Langmuir adsorption isotherm.

B. A. Abd-El-Nabey et.al (2013) ⁽²⁰⁾ studied the inhibitive action of 6-methyl-2-thioxypyrimidinone (MTP), 6-phenyl-2-thioxypyrimidin-4-one (PhTP) and 5-cyano-6-phenyl-2-thioxypyrimidin-4-one (CPhTP) for brass alloy in presence of 0.1 M H_2SO_4 solution and at temperature 30 °C the inhibition performance was investigated using electrochemical methods such as potentiodynamic polarization and electrochemical impedance spectroscopy (EIS) techniques. The calculated protection efficiencies for these compounds were 52.6 %, 76.2% and 96.1% respectively which indicates that (CPhTP) was best and suitable inhibitor among the other. The order of increase efficiency was related to the modification of the molecular structure of these compounds. The polarization measurement revealed that the anodic behavior and limiting current density behavior was observed in increasing the concentration of PhTP which attributed to formation sparingly soluble complex $[Cu(PhTP)]^+$ on the surface.

Ranjana et.al (2013)⁽²¹⁾ studied the inhibition action of L(-) aspartic acid (I) and its derivatives namely N-benzenesulphonyl L(-) aspartic acid (II), α -benzenesulphonamido- β -2-(1, 4, 5, 6-tetrahydropyrimidinyl) propionic acid (III) and 1-benzenesulphonamido-1, 2-bis-2(1, 4, 5, 6 tetrahydropyrimidinyl) ethane (IV) for corrosion of brass in 0.6 M NaCl solution using electrochemical techniques the maximum inhibition efficiency was for compound (IV) with 94.9% the order of the inhibition efficiency was I>II>III>IV.

T. Gowrani et.al (2014)⁽²²⁾ investigated the corrosion behavior of brass alloy in 3% NaCl medium using an inhibitor namely 5-methyl benzotriazole (MBTA). The protection efficiency was calculated from chemical and electrochemical techniques which showed that MBTA reduced the corrosion rate of brass in the aggressive solution. The polarization measurement also revealed that MBTA acted as mixed-type inhibitor with obtained maximum protection efficiency was 68.17 %. The characterization of corrosion product on brass in presence of MBTA was analysed by FTIR spectroscopy.

T. Ramdé et. al (2016)⁽²³⁾ studied the inhibition action of Sulfamethoxazole for brass in synthetic acidic rainwater using electrochemical impedance spectroscopy (EIS), potentiodynamic polarization, optical microscopy, Fourier Transformed Infrared spectroscopy (FTIR) and scanning electron microscopy (SEM). The polarization measurements revealed that the SMX acts as mix-type inhibitor with maximum protection efficiency 84.56 %. The surface analysis techniques FTIR, SEM/EDX and optical microscopy of the brass alloy confirmed the adsorption of SMX and good surface coverage of the inhibitor molecules.

M. Damej et.al (2016)⁽²⁴⁾ investigated the inhibition performance of 1,2,4-triazole-5-thione derivative (MTSNH) for brass alloy in aggressive solution of aerated 3% NaCl using electrochemical impedance spectroscopy (EIS) and potentiodynamic polarization. The effect of time immersion relative to inhibition

efficiency has been studied which found to be increased with increase the time immersion. The polarization curves showed that (MTSNH) acted as mixed-type inhibitor by retarding both cathodic and anodic reaction. SEM micrographs confirmed that in presence of MTSNH a protective film was formed on the alloy surface.

By comparison the studies above with the present research. The current work focuses on using naturally occurring-substances (pomegranate and red apple peels) as green corrosion inhibitors which being cheap, easily prepared, available and eco-friendly environmental instead of toxic, costly and difficulty of synthesise organic inhibitors.

1.4 Corrosion Forms

Corrosion can be classified into several categories; these types can occur to all metallic materials and could operate and propagate by different mechanisms. With all types of corrosion there are many mutual factors that could influence the rate of corrosion. The most important factor that governing corrosion are the aggressivity of medium , degree of acidity (pH), temperature, concentration, the aeration and degree of oxidizing power. Corrosion types can be classified as follows:

1.4.1 Uniform Corrosion

A class of corrosion that occurred when a metal surface corroded at the same rate. When a metal placed in a corrosive medium the oxidizing sites (anode areas) shift to different positions until the entire metal surface has been anodic at the same time as shown in figure (1.2) ⁽²⁵⁾.

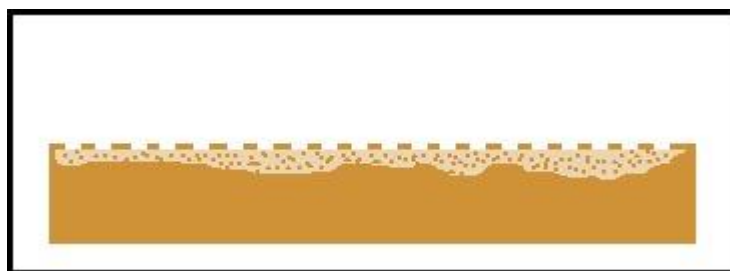


Figure (1.2): Simple uniform corrosion

1.4.2 Erosion Corrosion

Erosion corrosion ("Flow-Assisted") as illustrated in figure (1.3) refers to corrosion brought via highly-relative velocity between a corrosive environment and the metal surface. Corrosive medium can sweep away the metal ions before they can deposit on the surface which depends on its reactivity ⁽²⁶⁾.

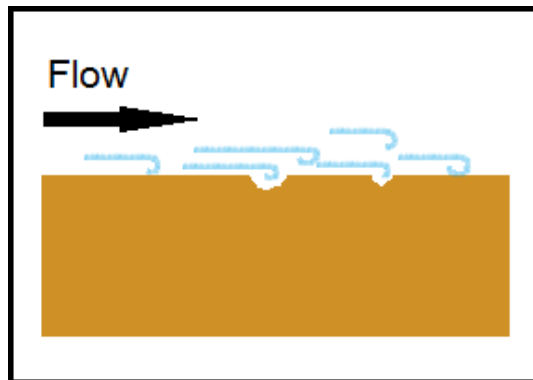


Figure (1.3): Erosion corrosion

1.4.3 Pitting Corrosion

Pitting corrosion represents a highly-localized attack on the surface resulting holes (pits) that could expand to dig in within the inside of a metal such of this type can be observed on an alloy surface that presented in certain environment such as hydrochloric acid as shown in the figure (1.4) for copper in aerated environment ⁽²⁷⁾.

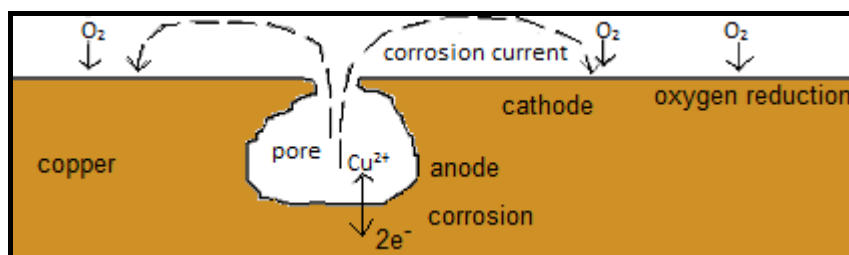


Figure (1.4): Illustration diagram for copper alloys undergo pitting corrosion.

1.4.4 Inter-granular Corrosion

The infra-microstructure of a metal makes up of grains; these grains are separated by boundaries as shown in figure (1.5). Inter-granular corrosion can be defined as a localized attack occurred among these boundaries or adjacent to it. There are many reasons for this type of corrosion such as enrichment of a certain element in manufacture alloying operation, presence of the impurities and to the decrease of one alloying element in the boundaries ⁽²⁸⁾.

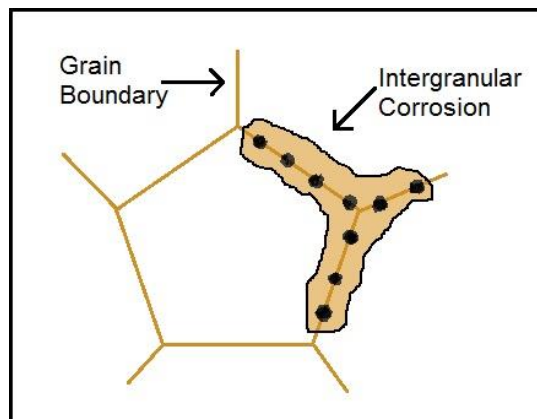


Figure (1.5): Inter- granular corrosion

1.4.5 Galvanic Corrosion

A contact or dissimilar corrosion, such type of corrosion occurred when dissimilar metals are existed in a certain corrosion electrolyte one of them is noble relative to another as shown in figure (1.6). Galvanic corrosion depends on the standard potentials of the existing metals that arranged in the galvanic series ⁽²⁹⁾.

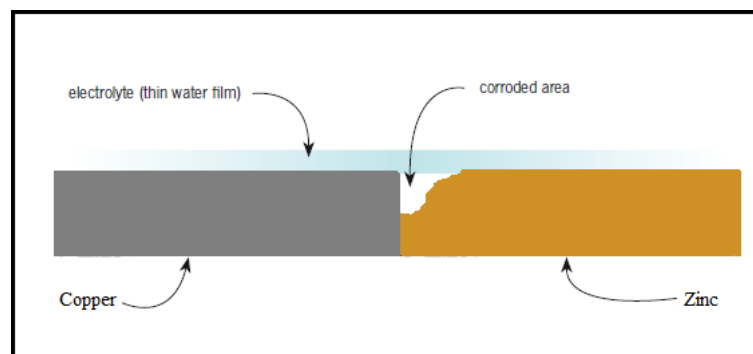


Figure (1.6): Illustration diagram for galvanic corrosion

1.4.6 Stress Corrosion Cracking

Stress corrosion cracking promotes a crack fatigue within the metallic structure as illustrated in figure (1.7). This type of corrosion occurred when a metal experience a tensile and mechanical stress at the surface which leads to form a crack that expands within the metallic structure ⁽³⁰⁾.

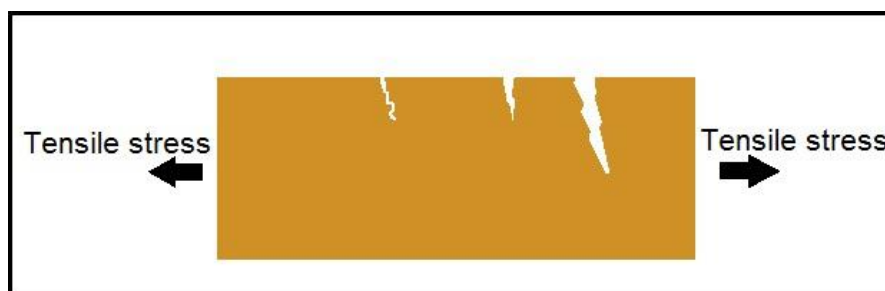


Figure (1.7): Stress cracking corrosion

1.4.7 Crevice Corrosion

Crevice corrosion is a localized attack that occurred at the narrow spaces between two metals as shown in figure (1.8). The stagnant environment within the crevice can differentiate from the bulk environment which promotes the metal dissolution ⁽³¹⁾.

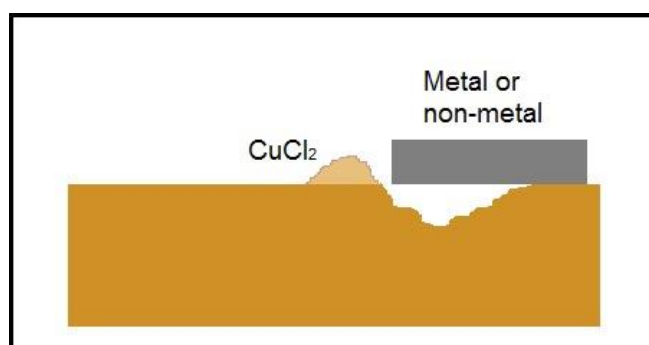


Figure (1.8): Illustration diagram for crevice corrosion

1.5 Electrochemical Aspects of Corrosion

The electrochemical basis of corrosion is based on well-known mixed-potential theory that proposed by Wagner and Traud. This theory considered as the most important ones in corrosion's explanation. It describes and demonstrates that both oxidation and reduction processes occurred at an

infinitesimal region (metal/electrolyte) interface where both a metal and an electrolyte being in contact ^(32, 33). Mixed potential theory consists of two main simple aspects which are:

- ❖ Any electrochemical reaction can be divided into or more individual reduction and oxidation reactions.
- ❖ During electrochemical reaction there is no net accumulation of electric charges ⁽³³⁾.

In any electrochemical reaction the rate of dissolution a metal equals the rate of reduction reaction. Both reactions precede at the same rate i.e. the net current equals zero as shown below in equation (1.1).

$$i_{net} = i_{red} - i_{ox} = 0 \dots\dots\dots (1.1)$$

Where i_{net} , i_{red} and i_{ox} are the net, reduction and oxidation currents respectively.

When a certain metal is in contact with a solution. The metal assumes a potential that depends on the metal itself and nature of the solution this potential is called "open-circuit potential" i.e. no external potential to the cell is referred as the corrosion potential E_{corr} ⁽³⁴⁾. In electrochemical prospective the corrosion rate can be determined from the oxidation current and then this current is called corrosion current so the equation (1.1) above can be rewritten as ⁽³⁵⁾:

$$i_{net} = i_{red} - i_{ox} = 0 \text{ at } E_{corr} \dots\dots\dots (1.2)$$

When the both reactions at the equilibrium, the equilibrium potential (E_{eq}) represented when the metal is in equilibrium with the solution. When the electrochemical reaction is forced away from its equilibrium state due to the flow of current this case called electrochemical polarization. The polarization measures the extent degree change in equilibrium potential. The degree of polarization also known as "overpotential" η which given by the equation (1.3):

$$\eta = E - E_{eq} \dots\dots\dots (1.3)$$

Where E is the resultant potential due to polarization and E_{eq} is the equilibrium potential.

The type of polarization is said to be anodic or cathodic depends on direction of shifting occurred in the equilibrium potential ⁽³⁵⁾. There are three important types of polarization:

❖ Activation Polarization (η_{act}):

Type of overpotential that always predominates at small polarization currents or voltages. This type of polarization is controlled by the sequence of electrochemical reaction that occurs at metal/electrolyte interface. The activation polarization is the controlling factor for corrosion of metals in media that have a high concentration of active species such as concentrated acids ⁽³⁶⁾.

❖ Concentration Polarization (η_{conc}):

This type of polarization results from diffusion or mass transfer at the surface of a metal during the electrochemical reaction and predominates at high polarization currents and voltages the concentration polarization is achieved at the point where increase in the negative potential will no longer effect the rate of the reaction. It's considered a controlling factor when the concentration of the species in the corrosive media is low such as in dilute acids or aerated salts solutions ⁽³⁷⁾.

❖ iR drop:

Is an ohmic potential drop, this type of polarization resulted from the pure resistance of an electrolyte in the path of current and its greatly linked to the ionic resistance of the electrolyte. In general all the metals are relativity have high ionic so the ohmic polarization is not significant ⁽³⁸⁾. The total over potential given as below in equation (1.4):

$$\eta_{total} = \eta_{act} + \eta_{conc} + iR \dots\dots\dots (1.4)$$

For the electrochemical reaction limited by activation polarization the basic law of describing the charge-transfer is given by the Butler-Volmer equation which demonstrate the relation between the rate of reaction i.e. the current density i and the driving potential E which is giving below in equation (1.5):

$$i = i_0 \exp \left[\frac{\alpha n F (E - E_{rev})}{RT} \right] - i_0 \exp \left[\frac{-(1-\alpha) n F (E - E_{rev})}{RT} \right] \dots \dots \dots (1.5)$$

Submitting eq. (1.3) gets (1.6):

$$i = i_0 \exp \left[\frac{\alpha n F \eta}{RT} \right] - i_0 \exp \left[\frac{-(1-\alpha) n F \eta}{RT} \right] \dots \dots \dots (1.6)$$

Where i_0 is an exchange current density which represents either rate of oxidation or rate of reduction at equilibrium, F : is the Faraday constant, E_{rev} : is the reversible potential, n : is the charge of ion in equivalents/mol, R : is the gas constant and α : is the charge transfer coefficient which has value usually around 0.5.

When the anodic polarization predominates at high overpotential ($\eta_{act} > \sim 50$ mV) the rate of the reverse reaction become negligible and the equation (1.6) can be rewritten as follows:

$$i_{net} = i_0 \exp \left[\frac{\alpha n F \eta_a}{RT} \right] \dots \dots \dots (1.7)$$

Rearrangement of the equation (1.7) gets:

$$\eta_a = b_a \log \left[\frac{i}{i_0} \right] \dots \dots \dots (1.8)$$

b_a : is the anodic Tafel slope ($2.3 RT/\alpha n F$), for b_a equals to (0.12 V) and α : is equal 0.5 and n : is equal 1

Similar equation can get for cathodic polarization ^(38, 39)

$$\eta_c = -b_c \log \left[\frac{|i|}{i_0} \right] \dots \dots \dots (1.9)$$

1.5.1 Corrosion Rate and Penetration Rate

In Electrochemistry prospective the corrosion is an electrochemical reaction that involves a mass transfer in addition to charge transfer so the rate of the reaction is expressed in terms of current (I , Ampere) and the mass of the

reactants. The relation between current and mass is given by Faraday's law as shown in the equation ⁽⁴⁰⁾:

$$m = \frac{I t a}{n F} \dots\dots\dots(1.10)$$

Where F is the Faraday's constant (96500 C/equivalent), t is the time in seconds, a is the atomic weight of the metal, and n is the number of valence electrons.

Corrosion rate (CR) is expressed in terms of mass loss per surface area (SA) per time (g/m²d):

$$CR = \frac{m}{SA \cdot t} = \frac{i a}{n F} \dots\dots\dots(1.11)$$

where i equal I/SA which is known current density.

Penetration rate (PR) in millimeters per year (mm/y) has been calculated from equation ⁽⁴¹⁾:

$$PR = \frac{3.27}{10^3} \times \left(\frac{e}{\rho}\right) i \dots\dots\dots(1.12)$$

Where e is the chemical equivalent of the metal, ρ its density and i is the current density.

1.5.2 Transfer Coefficients

The anodic and cathodic transfer coefficients (α_a , α_c) were evaluated from anodic and cathodic Tafel slopes respectively using the equation (1.13) and (1.14) ⁽⁴²⁾:

$$\alpha_a = \frac{2.3 RT}{b_a n F} \dots\dots\dots(1.13)$$

$$\alpha_c = \frac{2.3 RT}{b_c n F} \dots\dots\dots(1.14)$$

The transfer coefficient is considered a kinetic parameter in the mechanism of an electrode process alongside with Tafel slope. A typical Tafel slope approximately equal -0.120 V (or of $\alpha_c = 0.5$) for a simple diagnostic of a discharge-chemical desorption mechanism for hydrogen evolution.

1.5.3 Polarization Resistances and Exchange Current Densities

The polarization resistance (R_p) represents the extent of the electrode resistance when it's polarized from its equilibrium potential (E_{corr}) the current flow resulted from the polarization of the electrode. The polarization resistance (R_p) values were evaluated using the rearranged Stern-Geary equation ⁽⁴³⁾:

$$i_{corr} = \frac{b_a b_c}{2.3(b_a + b_c) R_p} \dots\dots\dots(1.15)$$

When the electrode at equilibrium the rate of oxidation and reduction are equal and can express in terms of exchange current density when the net current equals zero. For small overpotential the Tafel equation can be reduced as follows ⁽⁴⁴⁾:

$$i = \frac{i_o F \eta}{RT} \dots\dots\dots(1.16)$$

Where i_o is the equilibrium exchange current density. The polarization resistance for charge transfer reaction represents the term of η/i then the rearrangement of equation (1.16) can be as follows:

$$i_o = \frac{RT}{R_p F} \dots\dots\dots(1.17)$$

1.6 Corrosion Thermodynamic

1.6.1 Arrhenius Equation

The formation about corrosion rate and kinetic parameters may be helpful in the corrosion control. Activation parameters for some systems can be estimated from the Arrhenius equation:

$$i_{corr} = A \exp\left(\frac{-E_a}{RT}\right) \dots \dots \dots (1.18)$$

Where E_a is the activation energy, A is the pre-exponential factor, R is gas constant, T is absolute temperature and i_{corr} is the corrosion current density ⁽⁴⁵⁾.

1.6.2 Adsorption Isotherm Model

The relationship between metal surface and inhibitor molecules can be interpreted by an adsorption isotherm model. It is known that in many corrosion systems, Langmuir model met the criterion of the adsorption process of inhibitors since the metal surface is monolayer (homogenous phase) and linear proportionality can be obtained between the c and c/θ values with best fitting correlation coefficient R^2 ⁽⁴⁶⁾.

The Langmuir adsorption isotherm is given by the following equation:

$$\left(\frac{c_{inh}}{\theta}\right) = \frac{1}{K_{ads}} + c_{inh} \dots \dots \dots (1.19)$$

Where c_{inh} is inhibitor concentration, θ is surface coverage and K_{ads} is the equilibrium adsorption constant.

1.7 Corrosion Inhibitors

Corrosion inhibitors can be defined in various ways but most suitable one is, chemical compounds when added in minimal amounts to the corrosive environment they leads to lowering the corrosion rate of a metal or an alloy without a significant change in the concentration or any other properties of this environment. Inhibitors can help the metal or alloy to enhance their resistance against corrosion by various corrosion inhibition mechanisms ⁽⁴⁷⁾.

Over recent years, many researchers have dedicated considerable efforts to find suitable approaches for minimizing corrosion rate as much as possible. It's widely accepted that the most practical way to reduce the corrosion rate is by using inhibitors. The mechanism of the inhibition action is not quite understood however, there are many suggested mechanisms explained the possibility of inhibitors to reduce the corrosion rate. Which they are:

- ❖ An adsorption process in which ions or molecules of the inhibitor adsorbed onto metal surface.
- ❖ increase/decrease in the cathodic or anodic rate reactions.
- ❖ Decrease in the rate of diffusion of reactants onto the metal surface.

In acid media, nitrogen-containing compounds, sulfur-base compounds, alkaloids, aldehydes and etc. are used as inhibitors.

The significant role of the inhibitors is to form a barrier of one or multi layers against the aggressive attack of acid solution. The formation of the protective film is greatly associated with chemical and/or physical adsorption mechanisms which involving a variation in the charge of the adsorbed molecules and transfer of charge from one site to the other as shown in figure (1.9). Those adsorbed substances (ions/molecules) are adsorbed at metal/solution interface and retard cathodic or anodic reaction subsequently reduce the corrosion rate ⁽⁴⁸⁾.

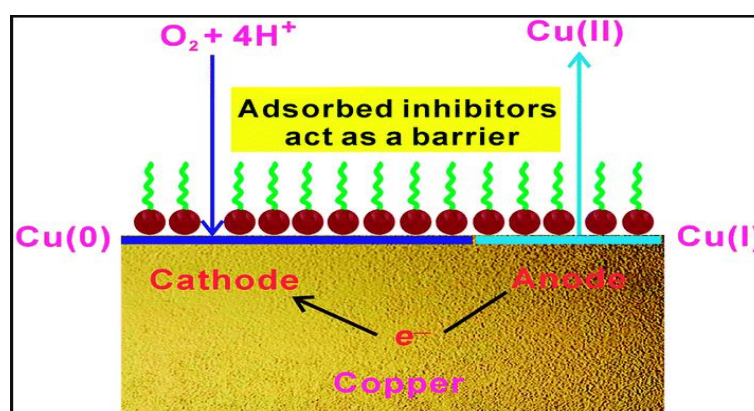


Figure (1.9): Illustration diagram for adsorption of inhibitor molecules on copper surface.

1.7.1 Corrosion Inhibitors Classification

Corrosion inhibitors being selected according to various criteria such as metal and environment. There is no particular classification for inhibitors however, the most general and comprehensive one is presented in figure (1.10) (49).

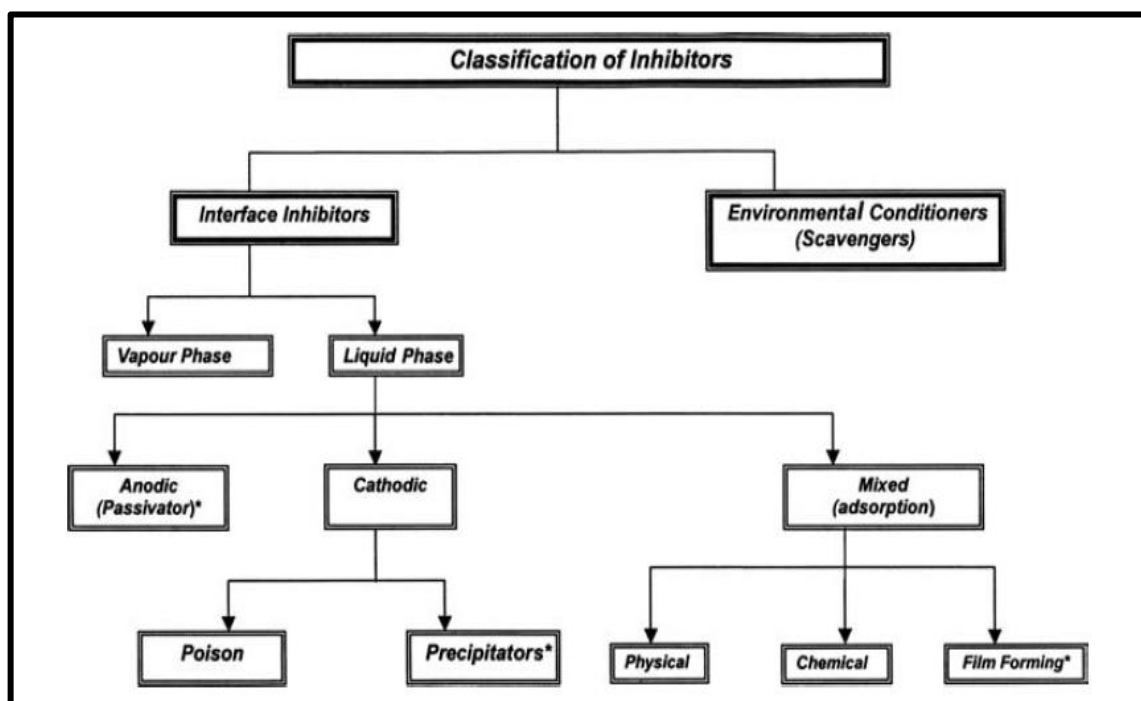
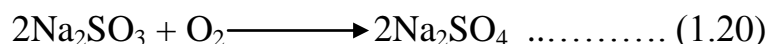


Figure (1.10): General Classification of Inhibitors

1.7.1.1 Environmental Conditioners (Scavengers)

One of most effective approach against corrosion is the removal of active corrosive species from an environment. The scavengers or conditioners have ability to scavenging the active substances and reducing the corrosion rate. In aerated acidic media the reduction of oxygen can be the main cathodic reaction besides the evolution of hydrogen gas. Such of these situations the oxygen scavengers play an important role in decrease the oxygen content and resulted to decrease in the corrosion rate. Sodium sulfite (Na_2SO_3) is most common oxygen scavenger it's reacted with oxygen to produce sodium sulfate as shown in the equation (1.10) (49):



1.7.1.2 Interface Inhibitors

The interface inhibitors inhibit the corrosion of a metal by forming a film at metal/electrolyte interface. The interface inhibitors can be categorized into vapor- and liquid- phase inhibitors ⁽⁴⁹⁾.

1.7.1.2.1 Vapor-Phase Inhibitors

Vapor-phase inhibitors abbreviated (VPIs) are the inhibitors that can be used in closed environment to provide a temporary protection against corrosion. They operate via either in a molecular form or in a dissociate form. Both of these forms can be adsorbed on a metal surface and decrease the corrosion rate ⁽⁴⁹⁾.

1.7.1.2.2 Liquid-Phase Inhibitors

Liquid-phase inhibitors can be classified according to their inhibitive action mechanism anodic, cathodic or mix-type inhibitors.

1.7.1.2.2.1 Anodic Inhibitors (Inorganic Inhibitors)

Anodic inhibitors operate by a significant shifting in corrosion potential towards anodic direction (noble direction). They block the anodic active sites by forming a protective layer; hence inhibit the dissolution of a metal. Inorganic anions such as molybdate, chromate and phosphate are usually used. The metal is exhibit a special type of coating called "passive layer" which is formed due to the adsorption of these anions on the metal surface. The passivation phenomenon that occurred for some metals in certain environments is not quite understand however, the formation of passive layer depends on the amount of oxygen, the nature of the environment and the concentration of aggressive ions ⁽⁴⁹⁾.

1.7.1.2.2.2 Cathodic Inhibitors

Cathodic inhibitors can reduce the corrosion rate by either reduce the reduction rate (cathodic poisons) or by a selective precipitating on cathodic active sites. In most cases the cathodic inhibitors decrease cathodic reaction rate by limiting the diffusion of reducible (oxygen/hydrogen) active species on metal surface hence reduce the corrosion rate ⁽⁴⁹⁾.

1.7.1.2.2.3 Mixed-type Inhibitors (Organic Inhibitors)

Mixed-type inhibitors also called (Adsorption inhibitors) are inhibitors that can be adsorbed on both cathodic and anodic active sites as a result they can retard both cathodic and anodic reactions and subsequently reduce the corrosion rate. About 80% of mixed-type inhibitors are organic inhibitors. The most significant key property of organic inhibitors effectiveness comes from its adsorption characteristics which is depend on the chemical structure of the inhibitors, type of environment and surface charge of the metal. The adsorption process of organic inhibitors occurred via two possible mechanisms: physisorption and chemisorption. The physical adsorption represents an electrostatic interaction between the metal surface and inhibitor's charged species despite occurring rapidly, physisorption breaks down with increasing temperature. Chemisorption involves charge transfer sharing between the adsorbed inhibitor molecules and the metal surface. Since chemisorption involves formation of a coordinated bond between adsorbed inhibitor molecules and the metal surface is required longer time to formulate than physisorption. In contrast of physisorption, the chemisorption is increased with increasing temperature. Chemisorption is greatly depends on the inhibitor molecular structure. Since chemisorption involves electron donation, the inhibitors must be contain heteroatoms. Heterocyclic compounds containing double or triple bonds, hydrocarbon chain, sulfur containing compounds and nitrogen containing compounds are considered to be effective inhibitors. The ability of a compound

to adsorb chemically depends on amount of heteroatoms and their chemical characteristics such as electronegativity and basicity. The greater electronegativity of an atom the lower its tendency to coordinate as the follow order ⁽⁴⁹⁾:



← Increase the electronegativity

→ Increase the basicity (Inhibition performance)

1.8 Green Chemistry Approach in Corrosion

The term of "Green Chemistry" provides a suitable design of any related research in non-polluting way with minimal waste and toxic levels ⁽⁵⁰⁾. Over decades in corrosion-related researches field the main practical approach against corrosion is the use of synthetic organic inhibitors. Numerous organic compounds have been used as anti-corrosion inhibitors for various metals and alloys. The synthetic organic inhibitors having heteroatoms (O, N, S, and P) showed remarkable inhibition efficiency, but most of organic inhibitors are highly toxic and greatly affected both human and environment. The growing concern of the harmful of organic inhibitors led to discover alternative approaches instead. Harmful impact of the organic inhibitors forced the chemical suppliers and operators who had to follow with the increasing demands and more stringent rules that could contribute to minimize impact of the organic inhibitors to nature, humans and aquatic life. Hence the use of natural originating inhibitors have been increase recently. Which provides better chances of being eco-friendly and harmless ⁽⁵¹⁾. Green corrosion inhibitors are eco-friendly, non-toxic, biodegradable, cheap and do not contain heavy metals.

In recent years many researchers have been successfully used naturally products in order to inhibit the corrosion of metals. They developed a green inhibitors such as plant extracts, fruits peel extracts, dried stems, leaves, seeds

and other natural products. The natural-occurring substances contain of many natural organic compounds such as pigments, flavonoids, ascorbic acid etc. the extracts of these substances constitute of nitrogen, oxygen and sulfur-containing compounds which make them good and effective anti-corrosion inhibitors ⁽⁴⁸⁾.

Several synthetic heterocyclic organic compounds have been used as inhibitors for corrosion of brass alloys in various aqueous media. But there is a significant lack in information regarding the use of green inhibitors for corrosion of α -brass (70% Cu+30% Zn) alloy in various environments.

The aim of the research is the use of pomegranate and red apple peels as green corrosion inhibitors due to its availability, low cost, easily to prepare and eco-friendly environment.

1.8.1 Literature Survey on using Natural Products as Corrosion Inhibitors

S.S. Mahmoud (2006) ⁽⁵²⁾ studied the corrosion of Muntz brass (63% Cu, 37% Zn) in HCl solution using naturally occurring extracts which they are A- brown skin onion, B- onion bulb, C- the cloves of garlic blub, D- orange peel and E- henna leaves. Their inhibition performance was determined by using weight loss, galvanostatic polarization, linear polarization and atomic absorption spectroscopy. It was found that these inhibitor had a high efficiency against corrosion of muntz brass in 1 M HCl the measurements revealed that extract C is the best inhibitor for the alloy with maximum efficiency 99% the order of efficiency was C>D>E>B>A the extracts acted as mixed-type inhibitor. The adsorption of these inhibitors on the alloy surface followed Frumkin adsorption isotherm. The atomic absorption analysis revealed that the addition of inhibitors reduce the dissolution of zinc.

J. C. da Rocha1et.al (2012) ⁽⁵³⁾ investigated the Grape Pomace Extracts for carbon steel in 1 mol L⁻¹ HCl solution. The inhibition action of the extract was investigated using weight loss, potentiodynamic polarization, surface analysis and impedance spectroscopy. The grape extract was found to be effective

against steel corrosion. The inhibition efficiency was increased with increasing extract concentration and decreased with increasing temperature. The adsorption of the grape extract was followed Langmuir adsorption isotherm.

K. Agarwal (2014)⁽⁵⁴⁾ studied the inhibitive action of Lemon peel (LP) and Fenugreek leaves (FL) extracts on mild steel corrosion in 1 M HCl. The investigation was carried out by using electrochemical and non- electrochemical methods which confirmed that both of extracts are good inhibitors against corrosion. The electrochemical measurements indicated that both of inhibitors acted as mixed-type inhibitors. The adsorption of these inhibitors on the steel alloy followed Langmuir adsorption isotherm via physisorption.

A. Ismail and M. A. Mohd Tajuddin (2014)⁽⁵⁵⁾ studied the inhibition action of banana peel extract on stainless steel 304 corrosion in seawater 3.5% NaCl. The electrochemical measurements revealed that the banana extract had an effective action against the breakdown of passive film on the steel alloy. The addition of the extract inhibited the localized attack of the corrosive medium.

A.M. Al-Fakih et.al (2015)⁽⁵⁶⁾ studied the effect of turmeric and ginger extracts on mild steel corrosion in 1 M HCl. Their inhibition performance was investigated using weight loss method and potentiodynamic polarization. Weight loss measurements were carried out at various temperatures for 1 h immersion time. The polarization measurements revealed that both of inhibitors acted as mixed-type inhibitors. The inhibition efficiency increased with the increasing the inhibitors concentrations reaching up to 92 and 91% at 10 g/L of turmeric and ginger respectively. The adsorption of both inhibitors showed to be obeyed Langmuir adsorption isotherm.

It is shown from this survey that there is a lack of fundamental information regarding the identification and corrosion inhibition studies particularly for red apple peels that is considers as an environmental friendly

inhibitor and expected to show inhibiting effect on the corrosion behavior for α -brass alloy in HCl and H₂SO₄ solution.

1.9 The Aim of the Research

1. Study the corrosion behavior of α -brass alloy in various concentrations (0.5, 1, 1.5 and 2) M of H₂SO₄ and HCl solutions and at different temperatures from 293 K to 313 K using potentiostatic polarization measurements.
2. Characterization of pomegranate and red apple peels using GC-MS and Fourier transform spectroscopy techniques.
3. Study the inhibitive action of the peels extracts at different concentrations (200, 300, 400 and 500) ppm for corrosion of α -brass presence in 2 M H₂SO₄ and HCl solutions over the temperature range (293-313) K.
4. Investigation of corrosion products that formed as a result of α -brass corrosion in acidic media in the absence and presence of various concentrations of peels extracts using XRD.
5. Study the surface morphology of α -brass in 2 M H₂SO₄ and HCl solutions in the absence and presence of various concentrations of peels extracts using SEM technique.

Chapter Two

Experimental

2.1 Chemicals and Materials

2.1.1 α -Brass Alloy

Commercially circular α -brass has a chemical composition 70% Cu and 30% Zn.

2.1.2 Chemicals

The chemicals were used in the research are listed in table (2.1).

Table (2.1): The list of chemicals used in the research.

material	supplier	% purity
Hydrochloric Acid	CDH	99.9
Sulphuric Acid	CDH	98
Ethanol	Sigma-aldrich	99.8
Methanol	Sigma-aldrich	99
Acetone	ROMIL-SA	99.7
Diamond product spray	Struers	High quality diamond product

2.2 Preparation of Electrolytes

Based on information of Winchester, the standards molar concentration of both of H_2SO_4 and HCl is 18 M and 11 M respectively. The stock solutions were prepared using dilution law.

- ❖ Different concentrations of the aggressive H_2SO_4 solution (0.5, 1, 1.5 and 2) M in 1 L were prepared by diluting (27.7, 55.4, 83.1 and 111) ml respectively of stock analytical grade with distilled water in 1000 ml volumetric flask.
- ❖ Various concentrations of the aggressive HCl solution (0.5, 1, 1.5 and 2) M in 1 L were prepared by diluting stock solution (41.6, 83.3, 125 and 166.6) ml respectively of stock analytical grade with distilled water in 1000 ml volumetric flask.

2.3 Extraction

Over recent years different extraction methods for plants derivatives as corrosion inhibitors have been established. There is no a specific extraction method for natural derivatives due to its phytochemicals complexity and diversity. In this research pomegranate and red apple peels have been extracted using deionized water and hydrochloric acid respectively.

2.3.1 Pomegranate Peel Extraction

Figure (2.1) shows the preparation steps of the aqueous extract of pomegranate peel which was prepared as follows ⁽⁵⁷⁾:

1. The peels were collected from local market in Baghdad then washed and left 5 days to get dry under sun light. After that dried peels are cut into small pieces and grinded using electric grinder until became fine powder.
2. The powder was sieved using a (75 μm \times 20 cm) sieve. Weight about 20 g of powder and dissolved in an appropriate amount of deionized water the mixture was heated until boiling then cooled overnight at room temperature.
3. The mixture was filtered several times to extract the same output then heated to concentrate the extract.
4. The extract was collected and placed in 250 ml volumetric flask and then different concentrations (200, 300, 400 and 500) ppm were prepared from the stock solution.



Figure (2.1): Pomegranate peel extraction steps

2.3.2 Red Apple Peel Extraction

The extract of red apple peel (Fig. (2.2)) was prepared as follows ^(58, 59):

1. The peels were collected from a local market in Baghdad, cut into small pieces, washed and left overnight in the oven at 70 °C to get dry.
2. The dried peels were grinded by electric grinder and then sieved using a (75 μm \times 20 cm) sieve.
3. Weight 20 g of powder peels and dissolved in 1 L of 0.5 M HCl and boiling for 10 min and then cooled at room temperature.
4. The cooled mixture was filtered using Whatman No.1 filter paper as shown in figure (2.2). Then different concentrations (200, 300, 400 and 500) ppm were prepared from the stock solution.



Figure (2.2): Red Apple peel extraction steps

2.4 Specimen Preparation

Circular α -brass samples with 1.5 cm diameter and 1.3 mm thickness were polished using emery paper in different grades (320, 500, 1000, 2400, 4000) with diamond product spray that contain ethanol with different size of diamond particles (1, 3, 6, 9) μm and then rinsed with ethanol, acetone and finally washed with distilled water and left to dry at room temperature.

2.5 Instrumental Techniques

The instruments were used in this study are listed in table (2.2).

Table (2.2): The Instruments were use in this study.

Instrument	Source	Model	Function
Potentiostat/ Galvanostat	Germany	M lab 200 with software	Corrosion test monitoring
Thermostat	Danmark	HETOFRIG DT	Adjust the temperature of corrosion cell
Vacum Oven	United Kingdom	Gallenkamk	For drying the samples
Electronic Balance	Germany	Sartorius	Weight Samples
Magnetic Stirrer	France	Tacussel AGIMAX	Mix the component of solution
Electric Grinder	China	HL-140	To crush the sample into fine powder
Hot Plate with Magnetic Stirrer	Germany	Heidolph	To heat the samples at certain temperature
Gas Chromatography Mass Spectrometer (GC-MS)	SHIMADZU (Japan)	GCMS- QP2010 Plus	Identify the Major organic Compounds present in a Sample
Fourier Transform Infrarid Spectrophotometer (FTIR)	SHIMADZU (Japan)	IRPrestige-21	Identify the fuctional group of organic compounds
Scanning Electron Microscopy (SEM)	FEI (Japan)	FEI Inspect- S50	Examine the morphoiogy of surface
X-ray Diffractometer (XRD) Powder	Bruker (Germany)	2D PHASER	Identify the corrosion products and crystline phases

2.6 The Potentiostatic Polarization Set-Up and Procedure

The polarization measurement system consists of a computerized Potentiostat/Galvanostat device, three electrodes, corrosion cell and thermostat. The measurements were carried out in the corrosion studies lab.

2.6.1 Potentiostat/Galvanostat Device-M lab 200

The polarization measurements were operated by a computerized Potentiostat M Lab (WENKING M Lab multichannel and SCI-MLab corrosion measuring system from Bank Electronics-Intelligent controls GmbH, Germany 2007) as shown in figure (2.3). Potentiostat is a device that applies and controls the potential of the working electrode versus reference electrode and measures the resulting current between the working electrode and the auxiliary electrode. Potentiostat provides useful information about corrosion parameters such as corrosion potential E_{corr} , corrosion current density i_{corr} and Tafel slopes. Also gives different polarization plots of (E vs. i) as required.



Figure (2.3): Front facing panel Potentiostat/Galvanostat.

2.6.2 Three –Electrodes System

For complete and comprehensive electrochemical measurements, three electrodes are involved. The potential difference between the working electrode (WE) and reference electrode (RE) is measured as long as IR drop is minimized by holding the working electrode as close as possible to reference electrode as a result the current flows between the working electrode and auxiliary electrode (AE).

2.6.2.1 Working Electrode

Circular working electrode with 20 cm in length metallic wire and 2.5 cm in diameter and has a fix disk in the center for flat specimen. α -brass specimen were placed in the middle of the fix disk and held by a holder with exposed surface area 1 cm² only. As shown in figure (2.4).



Figure (2.4): Working electrode

2.6.2.2 Reference Electrode

A saturated calomel reference electrode (SCE) was used in the research which has a standard potential 0.2444 V ⁽⁵⁾ at 25 °C the variation in potential of working electrode is measured as a function of reference electrode's potential. The electrode constructed with a glass tube filling with an examined electrolyte in order to reduce contamination that may occurred this tube called "Luggin capillary" the tip of the tube is placed closer to working electrode as much as possible. Figure (2.5) shows the schematic reference electrode.

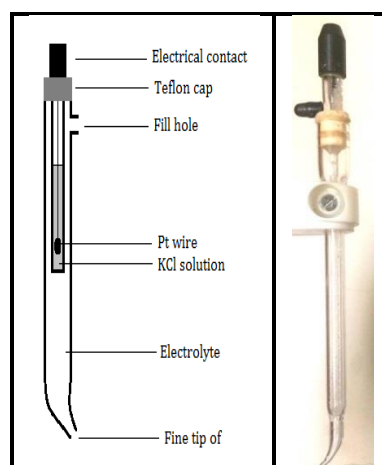
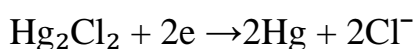
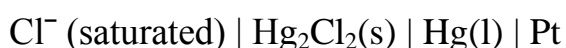


Figure (2.5): Reference electrode

2.6.2.3 Auxiliary Electrode

Platinum electrode was used as auxiliary electrode due to its large surface and its high catalytic activity. Platinum electrode has 10 cm in length and placed against working electrode in the constructed corrosion cell.

2.6.3 Corrosion Cell

The corrosion cell constructed from 1 L of a container cell made from Pyrex. The cell contains two vessels, internal vessel which contains the testing solution and the electrodes. While the external vessel connected to thermostat in order to adjust the temperature of the cell at a certain degree. The cell also contains a plastic stage that is in contact with air and contains many slots to behold the three electrodes and thermometer. Figure (2.6) shows complete construction of corrosion cell.



Figure (2.6): Corrosion cell set-up

2.6.4 Thermostat

Thermostat is a device that used to maintain the temperature of the corrosion cell. Thermostat contains water path that flows through external vessel. The thermostat was used to provide a constant temperature in

experimental range (20-40) °C. Figure (2.7) shows the complete set-up of polarization measurements.

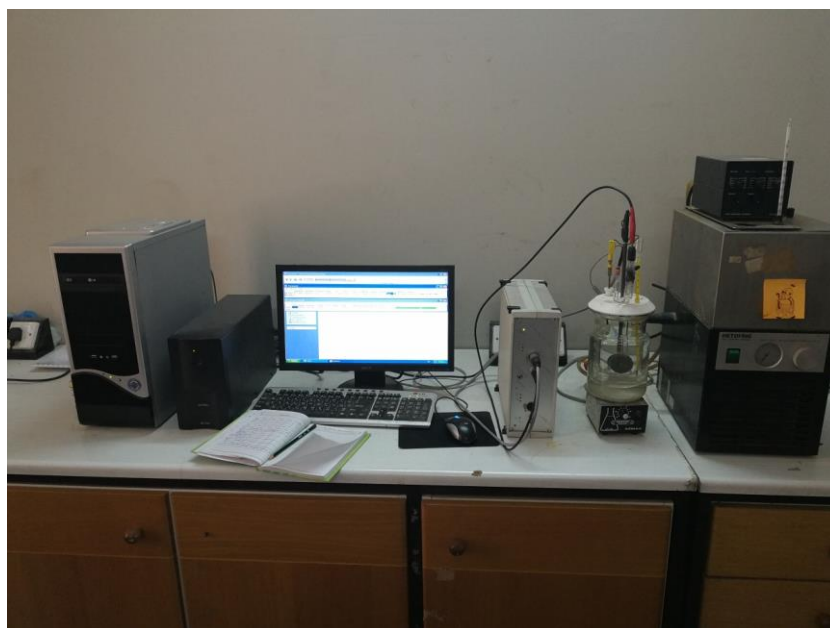


Figure (2.7): The complete set-up of polarization measurement

2.6.5 Procedure of Corrosion Test

The corrosion behavior of α -brass in acidic media and in presence and absence the inhibitors and at different temperatures has been studied by determining the open circuit potential (OCP) and corrosion parameters from Tafel slopes.

2.6.5.1 Open Circuit Potential

The open circuit potential (OCP) or steady state potential is the potential of the working electrode that's measured versus the reference electrode when there is no current flows between the working electrode and auxiliary electrode (open circuit). Open circuit potential values can be obtained by immersing α -brass specimen for 15 mins till the equilibrium condition between working electrode and electrolyte solution is achieved.

2.6.5.2 Polarization Measurements (Tafel Extrapolation)

The polarization measurements occurred directly after the open circuit potential is obtained. The entire polarization process was operated via computerized software M LabSci. The linear lines for cathodic and anodic Tafel curves were plotted in order to determine corrosion potential, corrosion current density and other corrosion parameters as shown in figure (2.8). The polarization process begins by polarize the electrode potential automatically over range -200 mV to +200 mV versus open circuit potential. Other polarization parameters include interval 10 mV and scan rate 2 mV/sec. At this polarization potential range the Potentiostat begins to construct the polarization curve in order to determine the corrosion potential (E_{corr}), corrosion current density (i_{corr}), cathodic and anodic Tafel slopes (b_a , b_c).



Figure (2.8): Experimentally polarization plot

2.7 Characterization Techniques

The peels of pomegranate and red apple were characterized using Fourier Transform Infrared Spectroscopy (FTIR) and Gas Chromatography Mass Spectroscopy (GC-MS). These characterization techniques have provided insightful information about the chemical nature and the presence of important natural organic compounds in the peels. These techniques can contribute providing evidence about the inhibitive action of the pomegranate peel and red apple peel.

2.7.1 Fourier Transform Infrared Spectroscopy (FTIR)

Fourier transform infrared spectroscopy (FTIR) is an identification technique used to identify the functional groups of organic compounds, figure (2.9) illustrated FTIR set-up. The infrared spectroscopy measures the interacting infrared radiation with a molecule and then measure the vibration of atoms of these groups. By scanning the sample over wavenumbers range $(4000-400) \text{ cm}^{-1}$ depending on the amount and intensity of transmitted light it's possible to determine the functional group of a compound.



Figure (2.9): Fourier Transform Infrared Spectrophotometer

2.7.2 Gas Chromatography Mass Spectroscopy (GC-MS)

Gas Chromatography Mass Spectroscopy (GC-MS) is an analytical technique used for identifying the chemical compounds present in a sample that has been dissolved in volatile-organic solvent. The type of mass spectrometer that used in the research is (GCMS-QP2010 Plus) as shown in figure (2.10). The measurement begins with inject $1 \mu\text{l}$ of methanolic extract by micro syringe into the column (100% dimethyl poly siloxane) which is connected to a detector that creates a signal when a compound is detected the greater the concentration of a compound the greater its signal intensity. The time from the injection to detection is called retention time (RT). When the instrument is run the computer begins to generate a graph called chromatogram which has two axis x-axis

represents the retention time of a compound after eluted from column. Y-axis represents the intensity of the compound which is greatly influenced by its concentration in the sample. The fragmentation of the sample occurred by bombardment of a sample by a steam of electrons. The fragments of the sample were deviated according to their mass to charge ratio M/Z . The temperature of the oven was 50 °C for 2 min and 280 °C for 5 min the total runtime of the experiment was 30 min. The energy of electron gun of the detector was 70 eV and helium was used as inert gas (carrier gas). Compounds were identified by comparing its mass spectra to those stored in database library where matching the sample spectra with standards based on their the retention times and abundance.



Figure (2.10): Gas Chromatography Mass Spectrometer

Procedure:

The methanolic extracts of pomegranate and red apple peels were prepared by dissolving 3 g of each of pomegranate and red apple peels powder in 30 ml of pure methanol individually and left for 3 days so that all pigments, alkaloids and all its constituents can dissolve. Then filter the extract by using

Whatman No.1 in order to get rid of remaining residue ⁽⁶⁰⁾. Figure (2.11) shows the methanolic extract of pomegranate and red apple peels.

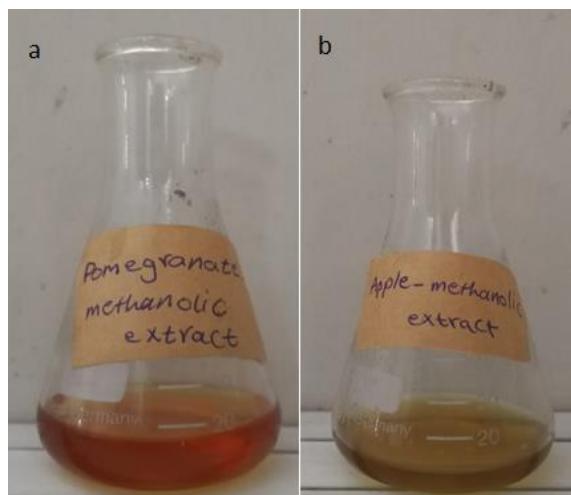


Figure (2.11): Methanolic extracts (a): Pomegranate peel (b): Red apple peel

2.8 Surface Examination Techniques

The surface examination techniques that are used in the research involve X-ray diffraction (XRD) powder and Scanning electron microscope (SEM). XRD was used in order to investigate on corrosion products that are formed after Potentiostatic measurement is done. SEM was used to examine the surface morphology of the alloy and confirm the adsorption of the inhibitor molecules.

2.8.1 X-Ray Diffraction (XRD) Powder

XRD is a rapid identification technique used to identify the phase of a crystalline material. XRD gives insightful information about the crystalline properties of a substance and identification of unknown minerals. XRD measurement operates via a diffractometer as shown in figure (2.12). The basic of XRD involves interaction of incident light (accelerating electrons) and the crystalline sample. The accelerating electrons have a sufficient energy to reach out the inner shells once the radiation hit the target it will be diffracted at specific angle called (2θ) according to the crystalline content of the substance the greater its crystalline content the greater its intensity.



Figure (2.12): X-Ray Diffractometer

The detector will convert the diffracted rays into the counts and begins to generate a graph known as "Diffractogram".

2.8.2 Scanning Electron Microscope (SEM)

SEM is a microscope used to inspect the surface morphology and its properties. SEM produces an image by using an electron beam which manages to scan the specimen's surface which is kept inside a vacuum chamber. The image is produced when electron beam emit from the source and come through vertically and hit the sample once hit the sample secondary electrons begin to eject then collect by the detector to produce the image. SEM that is used in the research is illustrated in figure (2.13).

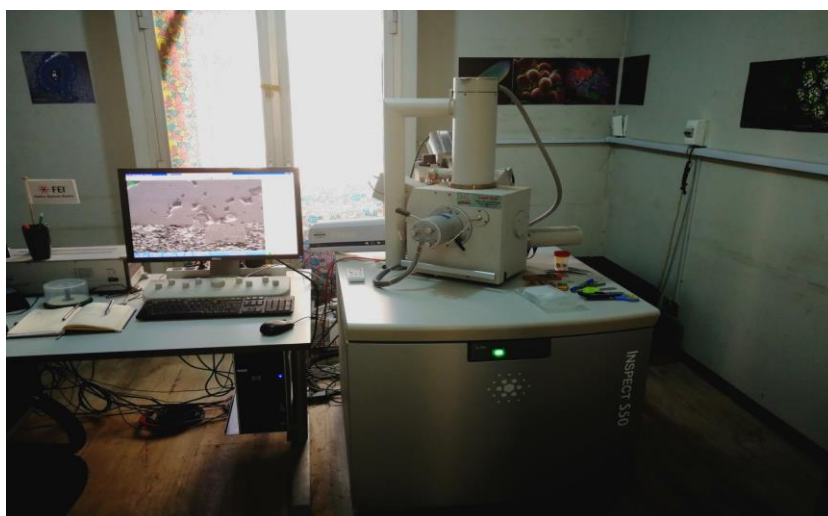


Figure (2.13): Scanning Electron Microscope

Chapter Three

Results and Discussion

3.1 Characterization Techniques

3.1.1 Fourier Transform Infrared Spectroscopy (FTIR)

Figure (3.1) shows the FTIR spectrum of pomegranate peel powder. The major identification absorption bands are listed in table (3.1). The spectrum confirmed the complex nature of the peels and proved the presence of wide variety of compounds. It has been reported by many studies that pomegranate peels contains different natural compounds with biological nature ⁽⁶⁰⁾. A wide broad peak at 3383.14 cm^{-1} of O-H band confirms the presence of alcohols compounds and carboxylic acids. The sharp mid-intense peak at 1728.22 cm^{-1} attributed to carbonyl group C=O which lead to presence of aldehydes, ketones and carboxylic acids. The moderate sharp peak at 1620.21 cm^{-1} indicates the presence of unsaturated compounds (alkenes). The presence of alkanes confirmed by presence of stretching band at 2935.66 cm^{-1} . The absorption peak at 1219 cm^{-1} confirms the presence of esters and ethers.

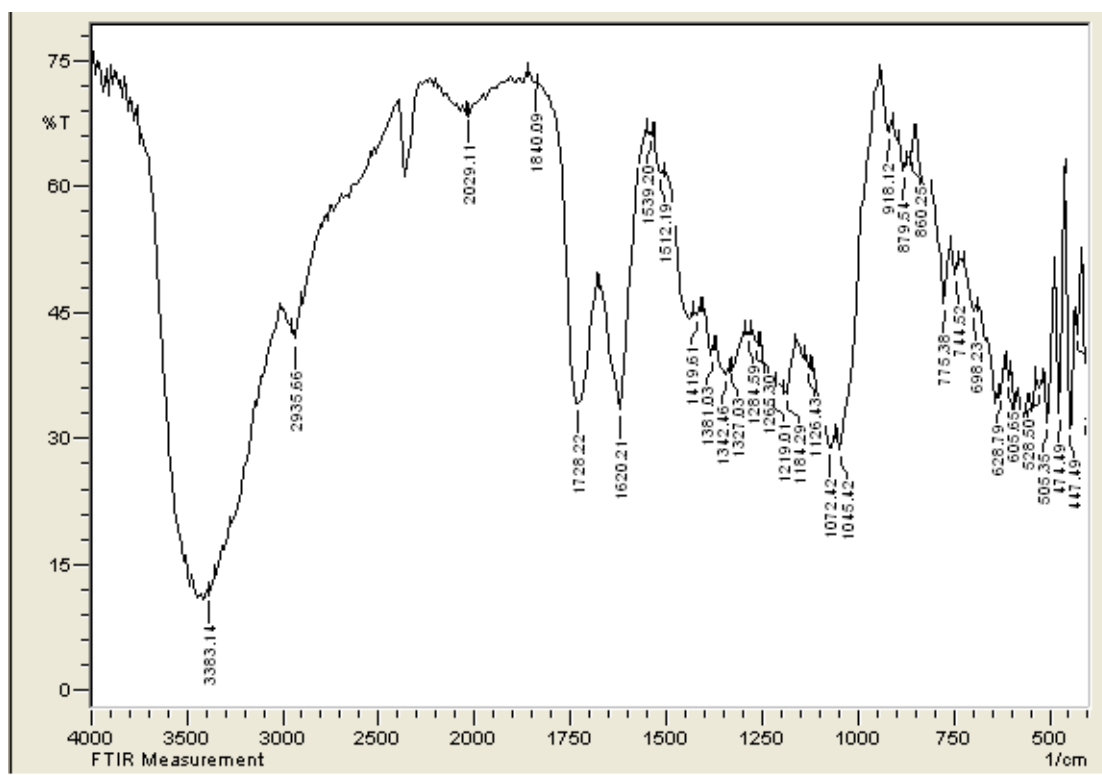


Figure (3.1): FTIR spectrum of pomegranate peels powder.

Due to the complex chemical nature of the peels there are many peaks have been interfered with each other however, the other important peaks have been listed in the table below.

Table (3.1): The main FTIR bands in pomegranate peel powder.

NO.	Peak number (cm ⁻¹)	Bond	Group assignment
1	3383.14	O-H	Alcohols and carboxylic acids
2	2935.66	C-H	Alkanes
3	1728.22	C=O	Carbonyl compounds
4	1620	C=C	Alkenes
5	1512.19	N=O	Nitro Compounds
6	1219	C-O	Ethers
7	1072	C-N	Amides
8	918.12	C-H	Alkenes

* The standard wavenumbers of absorption bands that used to interpret and compare the spectra are based on Y.R.SHARMA "Elementary Organic Spectroscopy" ⁽⁶¹⁾

The FTIR spectrum for red apple peels powder's spectrum, the spectrum has some similarities in compare with pomegranate peel powder's spectrum. Figure (3.2) shows the FTIR spectrum for red apple peels powder. The spectrum shows major identification peaks, an O-H absorption peak at 3398.57 cm⁻¹ which corresponds to alcohols and carboxylic acids and interfered absorption peak at 3309.85 cm⁻¹ for stretching N-H peak that attributed to presence of nitrogen-containing compounds such as amines and amides. The presence of alkynes has been confirmed by appearing an absorption peak at 3224.98 cm⁻¹ for C≡C-H. The mid-intense peak at 1735.93 cm⁻¹ attributed to C=O of carbonyl compounds. Unsaturated alkenes presence corresponds to stretching band at 1635.64 cm⁻¹ other identification peaks are listed in table (3.2).

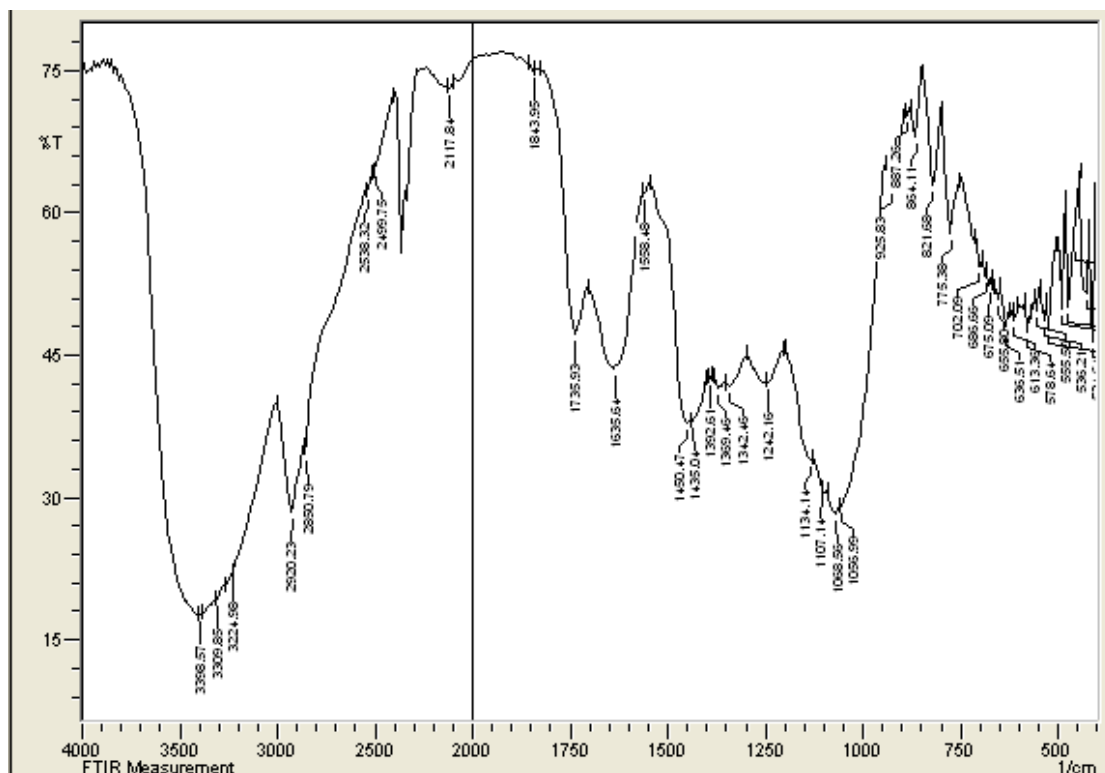


Figure (3.2): FTIR spectrum of red apple peel powder.

Table (3.2): The main FTIR bands red apple peel powder.

NO.	Peak number (cm^{-1})	Bond	Group assignment
1	3398.57	O-H	Alcohols and carboxylic acids
2	3309.85	N-H	Amines and amides
3	3224.98	$\text{C}\equiv\text{C-H}$	Alkynes
4	2920.23	C-H	Alkanes
5	2850.79	C-H_{ald}	Aldehydes
6	2117.84	$\text{C}\equiv\text{C}$	Alkynes
7	1735.93	C=O	Carbonyl compounds
8	1635.64	C=C	Alkenes
9	1134.14	C-O	Ethers and esters
10	1072	C-N	Amides
11	1056	C-F	Fluoro- containing compounds

The spectra of both of pomegranate and red apple peels have confirmed the presence of wide assorted compounds (nitrogen-containing compounds, oxygen-containing compounds, sulphur-containing compounds and unsaturated compounds) such of those compounds play a crucial role in the corrosion

inhibition process as they have numerous hetero atoms which responsible for inhibitive action. Further study involves the existence of the compounds; their chemical structure and nomenclature have been accomplished by GC-MS technique.

3.1.2 Gas Chromatography Mass Spectroscopy (GC-MS)

The GC-MS spectrum of methanolic extract of pomegranate peels is shown in figure (3.3). The spectrum confirmed the presence of sixteen phytochemicals constituents their chemical structure, nomenclature, molecular weight and retention times are listed in table (3.3).

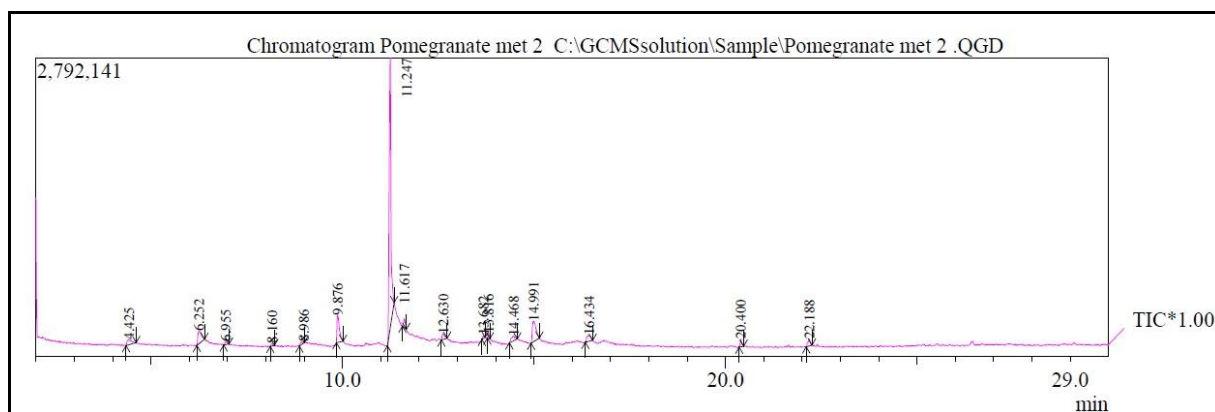


Figure (3.3): Chromatogram of methanolic extract of pomegranate peel.

GC-MS detects the compounds by their abundance (Y-axis) with respect to retention time (X-axis). The sixteen identified active compounds have the most abundance percentages in the methanolic extract of pomegranate peels more than other existed compounds that didn't appeared in the spectrum. According to the data that obtained from GC-MS analysis of methanolic extract of pomegranate peel that presented in table (3.2), it's found out that the 5-Hydroxymethylfurfural is the most existed compound as have highest abundance percentage 68.96% this natural compound is existed in many nutritional substances such as sugar and honey ⁽⁶²⁾ its chemical structure is shown in figure (3.4).

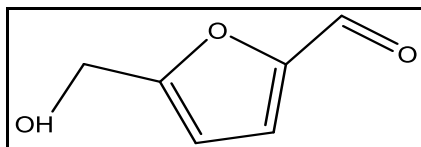
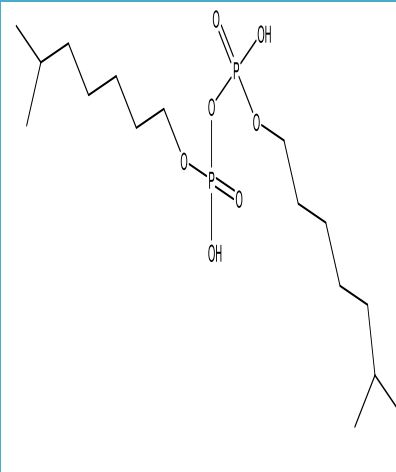
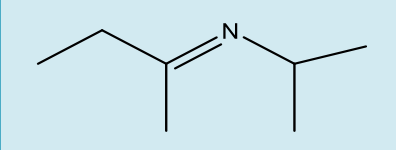
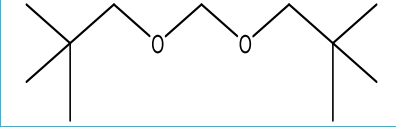
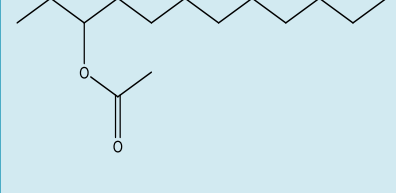
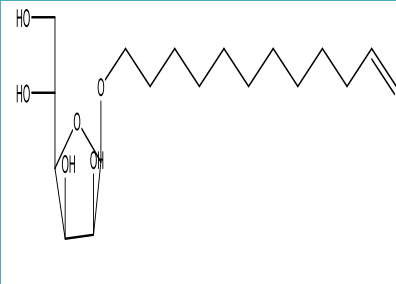
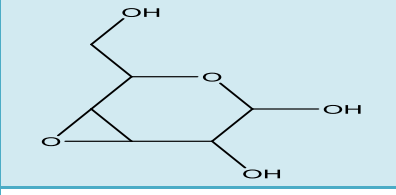
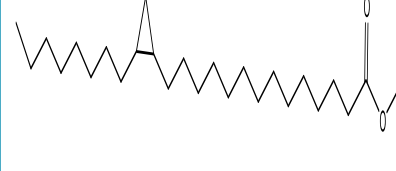


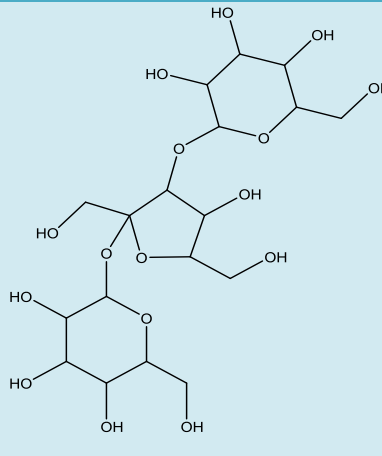
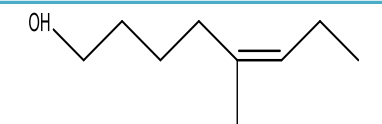
Figure (3.4): Chemical structure of 5-Hydroxymethylfurfural

The spectrum confirms the presence of ketones, esters, amines, carboxylic acids and alcohols compounds which fit the data obtained from FTIR spectrum.

Table (3.3): Major identification compounds in methanolic extract of pomegranate peels.

NO.	Name of Compound	RT (min)	Chemical formula	M.Wt (g/mole)	Structure
1	2-Furancarboxaldehyde	4.425	C ₅ H ₄ O ₂	96	
2	(Z)-Aconitic anhydride	6.252	C ₆ H ₄ O ₅	156	
3	3-Acetamido-6-methyl-7H-s-triazolo[5,1-c]-s-triazole	6.955	C ₆ H ₉ N ₇ O	195	
4	1-Methyl-1-nitrosoethyl acetate	8.160	C ₅ H ₉ NO ₃	131	
5	(3E)-3,4-Dimethyl-3-hexen-2-one	8.986	C ₈ H ₁₄ O	126	
6	3,5-Dihydroxy-6-methyl-2,3-dihydro-4H-pyran-4-one	9.876	C ₆ H ₈ O ₄	144	
7	5-Hydroxymethylfurfural	11.247	C ₆ H ₆ O ₃	126	

8	Bis(6-methyl heptyl dihydrogen diphosphate)	11.617	$C_{16}H_{36}O_7P_2$	402	
9	2-Propanamine, N-(1-methyl propylidene)	12.630	$C_7H_{15}N$	113	
10	2,2-Dimethyl-1-[(neopentyloxy) methoxy propane]	13.682	$C_{11}H_{24}O_2$	188	
11	3-Acetoxydodecane	13.816	$C_{14}H_{28}O_2$	228	
12	beta-D-Mannofuranoside	14.468	$C_{17}H_{32}O_6$	332	
13	3,4-Altrosan	14.991	$C_6H_{10}O_5$	162	
14	Methyl-14-(2-octylcyclopropyl) tetradecanoate	16.434	$C_{26}H_{50}O_2$	394	

15	6,6-((4-hydroxy-2,5-bis(hydroxymethyl) tetrahydrofuran-2,3-diyl) bis(oxy) bis(2-hydroxymethyl) tetrahydro-2H-pyran-3,4,5-tiol)	20.400	$C_{18}H_{32}O_{16}$	504	
16	5-methyl-5-octen-1-ol	22.188	$C_9H_{18}O$	142	

For the red apple peels, the chromatogram of methanolic extract of the peels is shown in figure (3.5). The spectrum confirmed the presence of twenty six phytochemicals compounds which have been listed in table (3.4) along with chemical structures, molecular weight and retention times. Only twenty four compounds have been identified the last two remaining compounds weren't identified by database library of the spectrometer this may be because two reasons, first their abundance is very nominal that makes it unrecognizable to the database and the second one is because the library that used in the mass spectrometer doesn't have standards mass spectra to match the sample with.

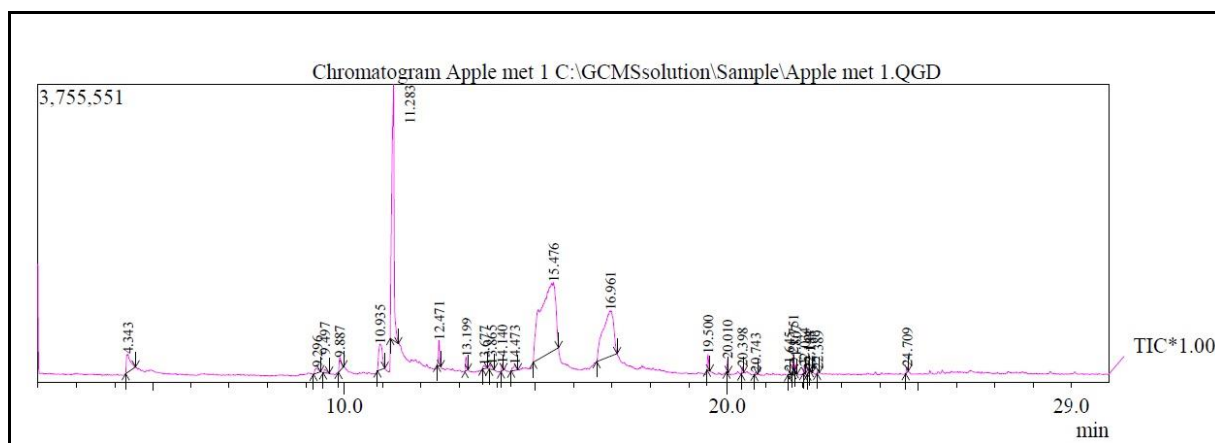


Figure (3.5): Chromatogram of methanolic extract of red apple peel.

According to the obtained data of the chromatogram presented in table (3.4), it found that cyclobutyl decyl oxalate is the most dominant compound with abundance percentage 44.02 % the chemical structure is shown below in figure (3.6).

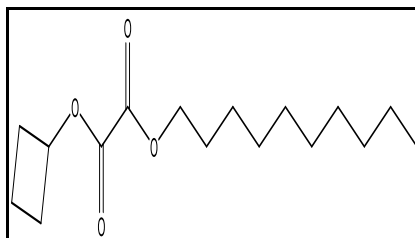
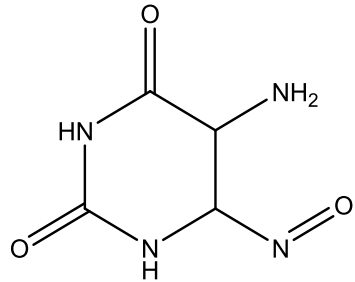
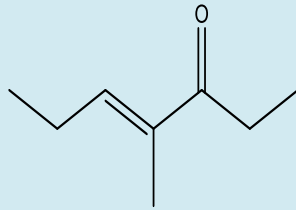
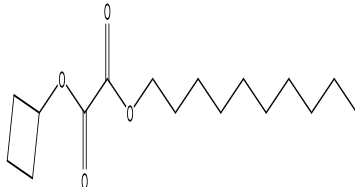
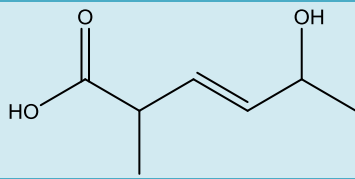
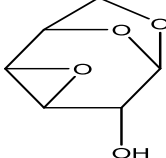
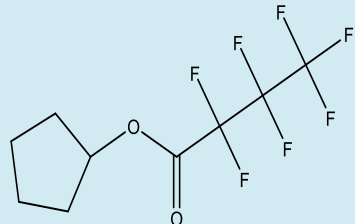
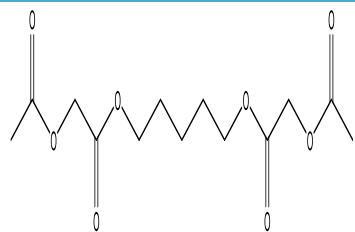
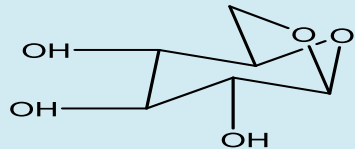


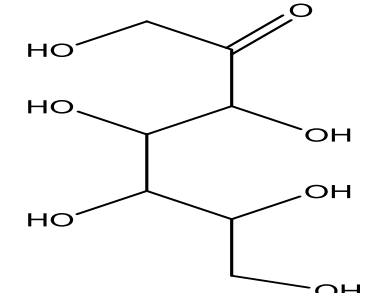
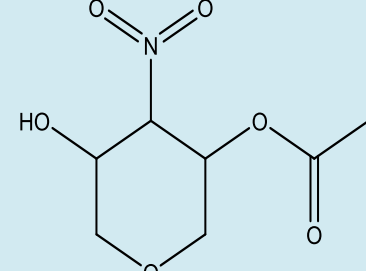
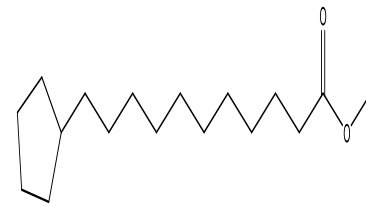

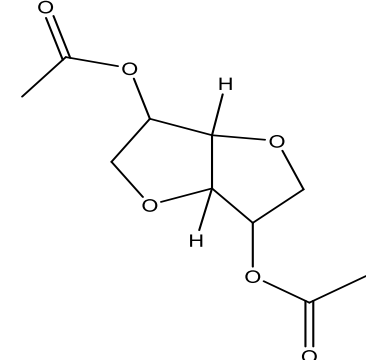
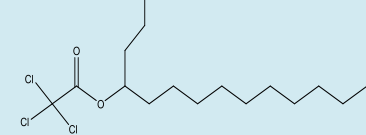
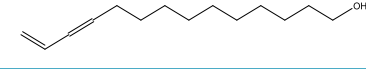

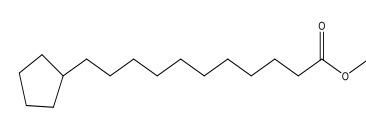
Figure (3.6): Chemical structure of cyclobutyl decyl oxalate

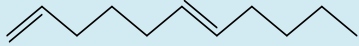
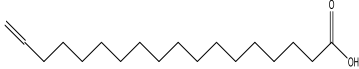
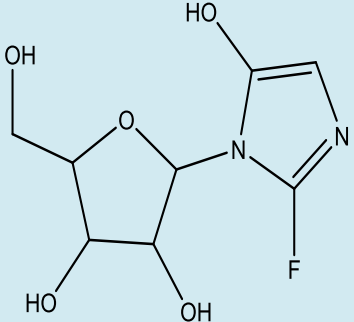
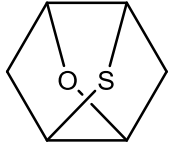
The chromatogram confirmed the presence of alcohols, carboxylic acids, amides, amines, esters, ethers and unsaturated compounds which consistent the obtained data from FTIR spectrum.

Table (3.4): Major identification compounds in methanolic extract of red apple peels.

NO.	Name of Compound	RT (min)	Chemical formula	M.Wt (g/mole)	Structure
1	1-Methyl-L-histidin	4.343	$C_7H_{11}N_3O_2$	169	
2	5-(3,7-Dimethylocta-2,6-dienyl)-4-methyl-2,3-dihydrothiophene-1,1-dioxide	9.296	$C_{15}H_{24}O_2S$	268	
3	4-(1,1-dimethylethoxy)-3-hydroxy methyl ester	9.497	$C_9H_{18}O_4$	190	

4	5-amino-6-nitrosodihydropyrimidine-2,4(1H,3H)-dione	9.887	$C_4H_4N_4O_3$	156	
5	(E)-4-Methylhept-4-en-3-one	10.935	$C_8H_{14}O$	126	
6	cyclobutyl decyl oxalate	11.283	$C_{16}H_{28}O_4$	284	
7	(3E)-5-Hydroxy-2-methyl-3-hexenoic acid	12.471	$C_7H_{12}O_3$	144	
8	3,4-Anhydro-d-galactosan	13.199	$C_6H_8O_4$	144	
9	Cyclopentyl-2,2,3,3,4,4,4-heptafluorobutanoate	13.677	$C_9H_9F_7O_2$	282	
10	Pentane-1,5-diyl bis(2-acetoxyacetate)	13.865	$C_{13}H_{20}O_8$	304	
11	Anhydro-d-mannosan	14.140	$C_6H_{10}O_5$	162	

12	Galacto-heptulose	14.473	$C_7H_{14}O_7$	210	
13	Acetic acid, 5-hydroxy-4-nitrotetrahydropyran-3-yl ester		$C_7H_{11}NO_6$	205	
14	Methyl-11-cyclopentylundecanoate	16.961	$C_{17}H_{32}O_2$	268	
15	Palmitic acid	19.500	$C_{16}H_{32}O_2$	256	
16	D-Glucitol-1,4,3,6-dianhydrodiacetate	20.010	$C_{10}H_{14}O_6$	230	
17	Tetradecan-4-yl-2,2,2-trichloroacetate	20.398	$C_{16}H_{29}Cl_3O_2$	358	
18	13-tetradecene-11-yn-1-ol	20.743	$C_{14}H_{24}O$	208	
19	Octadecadienoic acid methyl ester	21.645	$C_{19}H_{36}O_2$	296	
20	Methyl-11-cyclopentylundecanoate	21.751	$C_{17}H_{32}O_2$	286	

21	E-1,6-Undecadiene	21.807	$C_{11}H_{20}$	152	
22	Octadec-17-enoic acid	22.034	$C_{18}H_{32}O_2$	280	
23	2-(2-fluoro-5-hydroxy-1H-imidazol-1-yl)-5-(hydroxymethyl)tetrahydrofuran-3,4-diol	22.144	$C_8H_{11}FN_2O_5$	234	
24	2-Oxa-7-thiatricyclo [4.4.0.0(3,8)] decane	22.188	$C_8H_{12}OS$	156	

The mass spectra of methanolic extract of both pomegranate and red apple peels provide other evidence on the natural organic compounds that exist in the peels. The qualitative measurements (GC-MS and FTIR) of the peels confirmed the red apple peels have more natural active organic compounds than pomegranate peels which mean that the red apple peels may be more active corrosion inhibitor than the pomegranate peels due to have large number of hetero atoms (N, S, O, P) these atoms responsible for corrosion inhibition as they have free lone pair (electronic density) which makes capable of forming a coordinate bond with vacant d-orbitals of a metal.

3.2 Potentiostatic Polarization Measurements

Figures (3.7 – 3.12) show the polarization curves for α -brass alloy in the acidic media (H_2SO_4 and HCl) in absence and presence different concentrations of pomegranate and red apple peels extracts (200, 300, 400 and 500) ppm over temperature range between (293-313) K.

The obtained corrosion parameters from polarization curves are corrosion current density (i_{corr}), corrosion potential (E_{corr}), anodic Tafel slope (b_a), cathodic Tafel slope (b_c), corrosion rate (CR) and penetration rate (PR) are listed in tables (3.5 – 3.10).

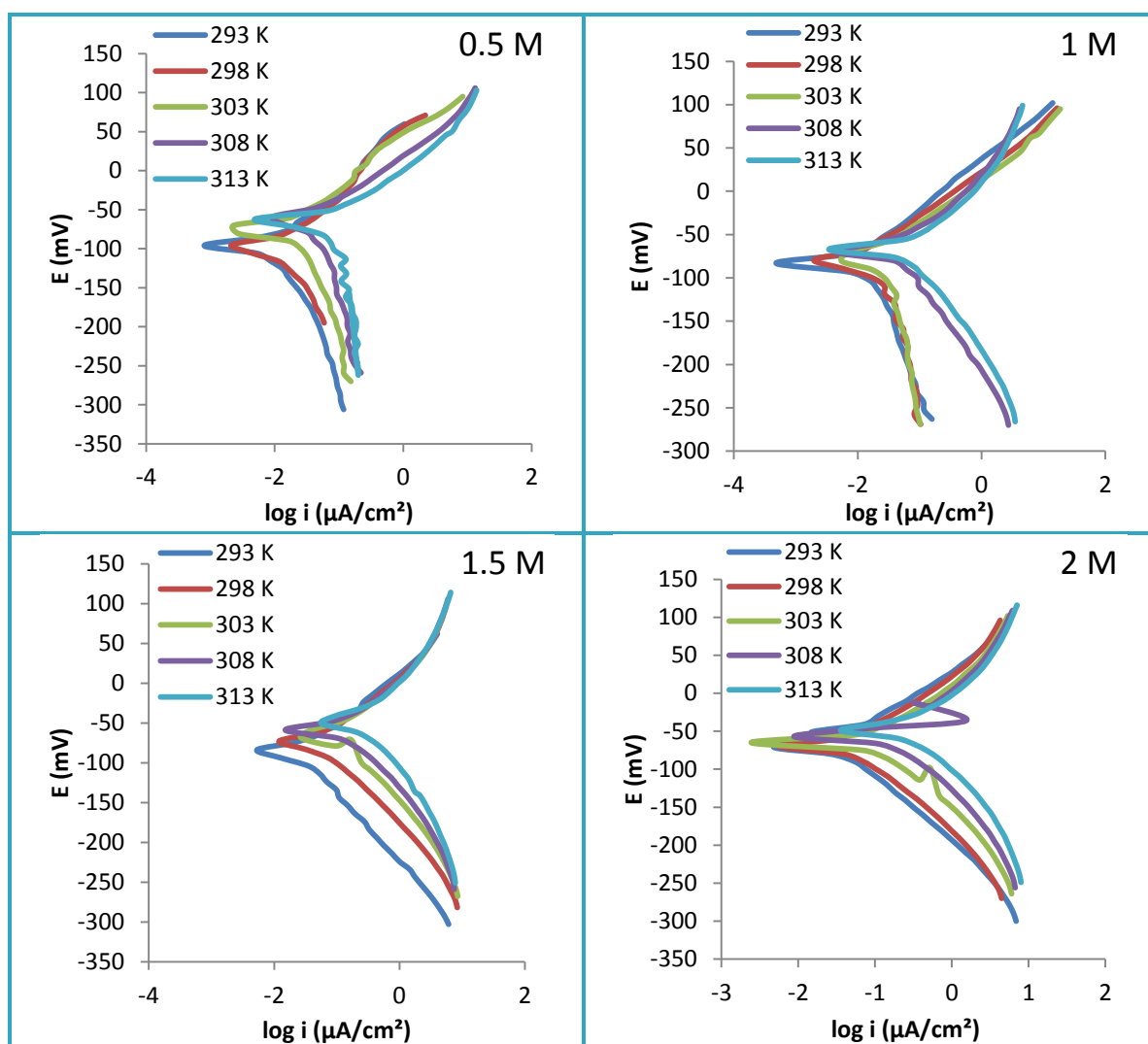


Figure (3.7): Polarization curves for α -brass corrosion in blank acidic medium (H_2SO_4 solution) at different concentrations at temperature range (293-313) K.

Table (3.5): Corrosion parameters of α -brass in blank acidic medium (H_2SO_4 solution) at different concentrations at temperature range (293-313) K.

Blank. (M)	T (K)	$-E_{corr}$ (mV)	i_{corr} ($\mu A/cm^2$)	Tafel slope (mV/dec)		CR (g/m ² d)	PR (mm/Y)
				$-b_c$	$+b_a$		
0.5	293	94.9	8.2	127.1	60.5	2.33	0.0955
	298	96	11.08	127.9	61.4	3.15	0.129
	303	73.1	20.2	183.6	64.4	5.51	0.226
	308	60	45.3	281.3	56.5	12.6	0.516
	313	63.1	82	233.1	61.5	23	0.943
1	293	74	11	111.1	61.6	2.98	0.122
	298	77.5	12.5	120.6	50.3	3.29	0.134
	303	76	20.6	87.2	58.5	5.57	0.237
	308	70	46.2	108	67.4	13.1	0.531
	313	69	89.3	93	69	24.6	0.976
1.5	293	84.1	26.12	92.2	59.2	7.43	0.304
	298	74.8	48.78	75.8	53.7	13.6	0.556
	303	67	89.34	73.2	67.7	25.4	1.04
	308	73.3	122.73	78.2	69.4	34.9	1.43
	313	68.8	231.56	90.7	82.8	46.4	2.76
2	293	68.1	29.34	77.9	63.1	8.35	0.342
	298	69.3	57.03	75.8	66.2	15.02	0.664
	303	67.3	141.61	89.2	82.1	33.2	1.65
	308	56.7	148.99	83.9	75.9	41.08	1.93
	313	47.1	239.77	85	74.2	47.9	2.79

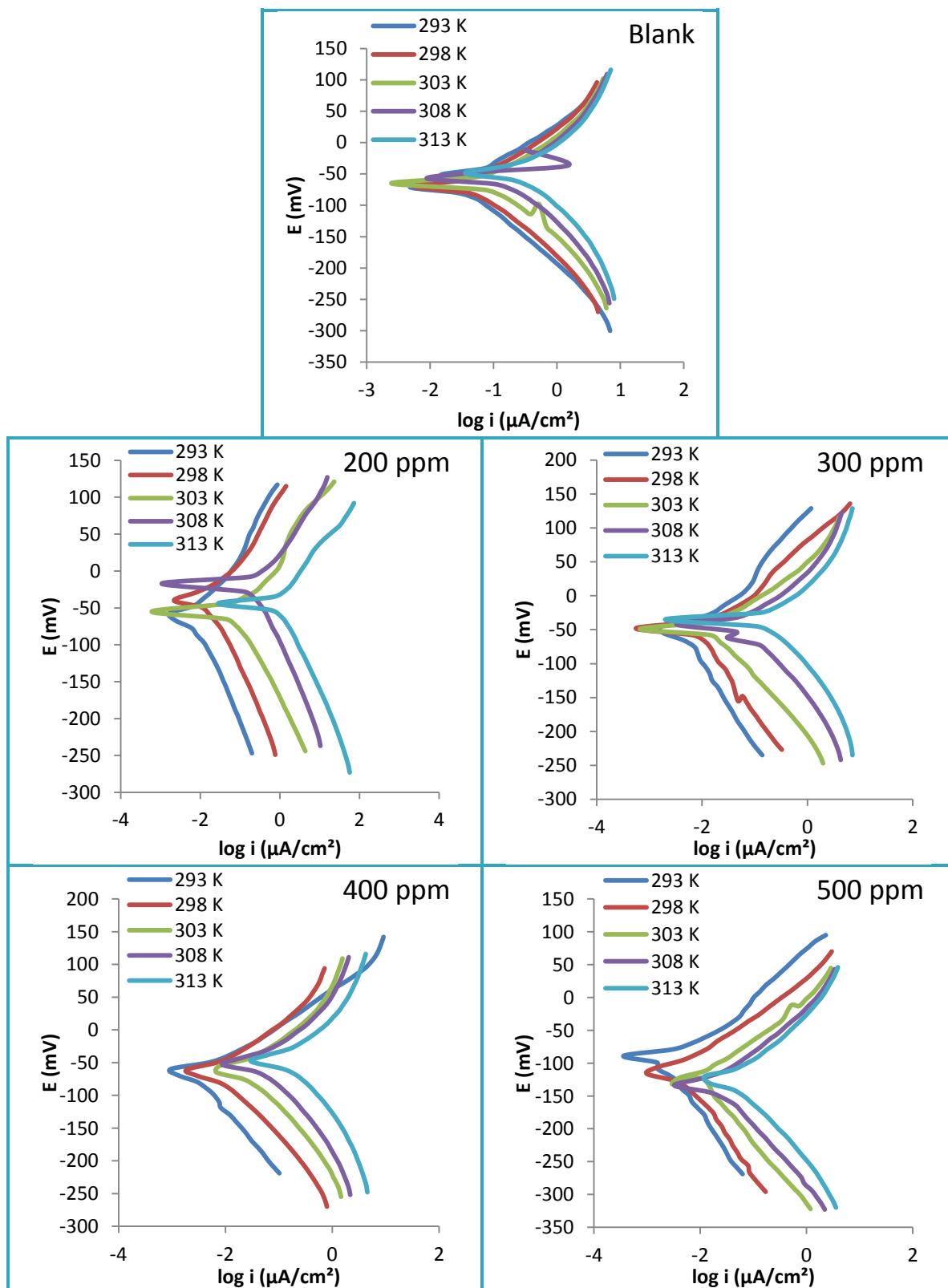


Figure (3.8): Polarization curves for α -brass corrosion in the blank (H_2SO_4 solution) and in presence of different pomegranate peel concentrations at temperature range (293-313) K.

Table (3.6): Corrosion parameters of α -brass in the blank (H_2SO_4 solution) and in presence of different pomegranate peel concentrations at temperature range (293-313) K.

Inh. (ppm)	T (K)	$-E_{corr}$ (mV)	i_{corr} ($\mu A/cm^2$)	Tafel slope (mV/dec)		CR (g/m^2d)	PR (mm/Y)
				$-b_c$	$+b_a$		
0	293	68.1	29.34	77.9	63.1	8.35	0.342
	298	69.3	57.03	75.8	66.2	15.02	0.664
	303	67.3	141.61	89.2	82.1	33.2	1.65
	308	56.7	148.99	83.9	75.9	41.08	1.93
	313	47.1	239.77	85	74.2	47.9	2.79
200	293	51	11.34	140.1	84.7	2.96	0.13
	298	39.9	22.4	128.6	93.4	6.27	0.257
	303	67	57.3	122.6	96.7	15.9	0.649
	308	17.3	62.28	89.1	74.3	17.1	0.702
	313	44	108.18	103	87.1	30.8	1.26
300	293	47.3	5.8	151.3	70.2	1.66	0.0643
	298	48.6	12.3	142.7	86	3.42	0.14
	303	49.2	31.4	93.4	78.5	9.21	0.375
	308	43	47.82	107.5	90.6	13.6	0.557
	313	34.8	79.92	97.1	84.4	22.1	0.903
400	293	60.2	3.1	94	48.7	0.866	0.0354
	298	61.7	9.1	126	79.9	2.55	0.107
	303	64.8	23.15	121	96.3	6.6	0.27
	308	53.2	27.25	82	68.3	7.91	0.324
	313	48.8	51.14	102	84.7	14.5	0.592
500	293	89.8	2.4	151.9	81.7	0.682	0.0279
	298	115.5	4.81	118	62.8	1.37	0.0559
	303	120.4	13.25	101.4	78.3	1.68	0.0639
	308	133	20.97	106.5	81.3	3.27	0.201
	313	123	39.24	124.8	98.5	10.2	0.418

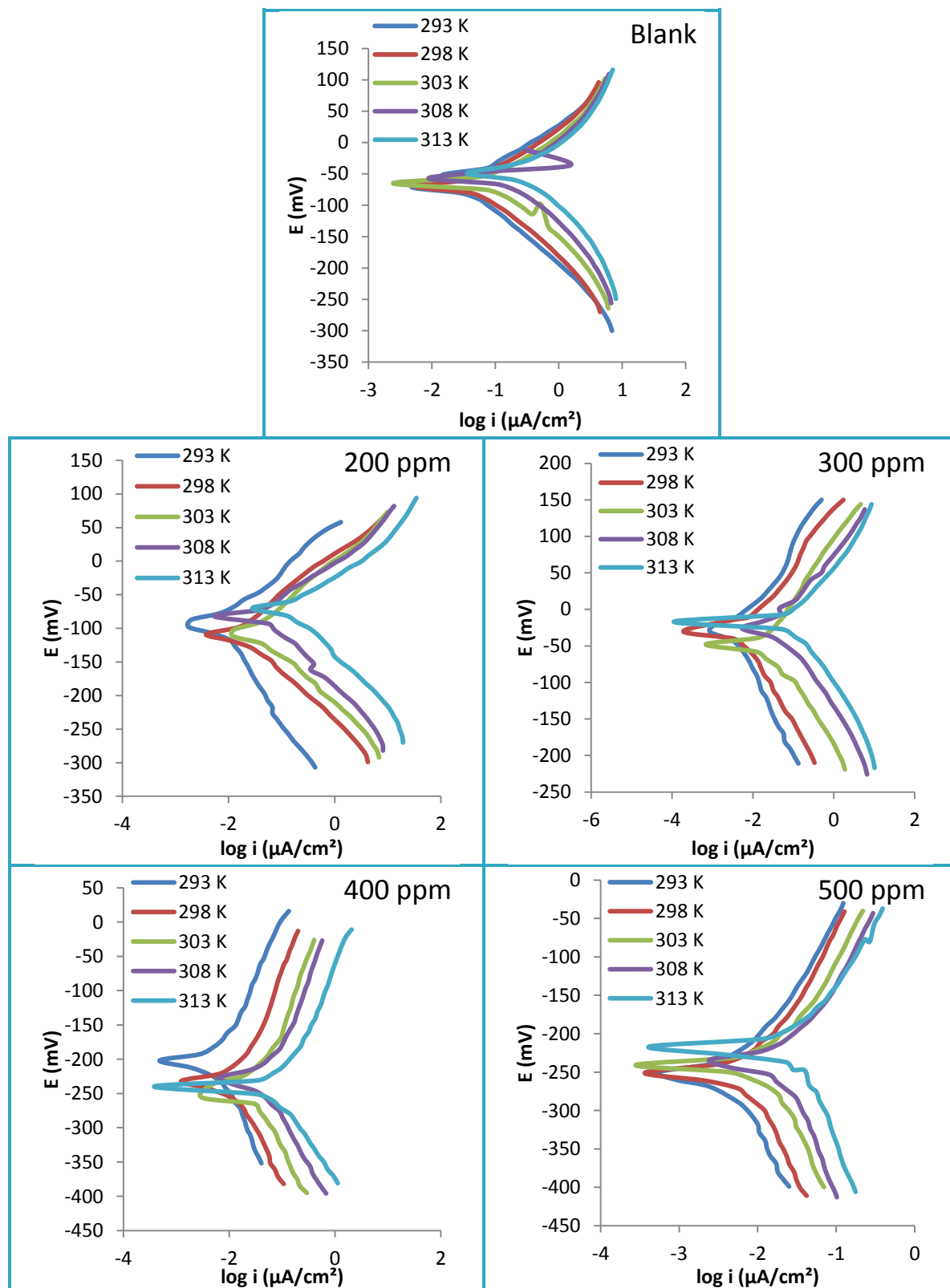


Figure (3.9): Polarization curves for α -brass corrosion in the blank (H_2SO_4 solution) and in presence of different red apple peel concentrations at temperature range (293-313) K.

Table (3.7): Corrosion parameters of α -brass in the blank (H_2SO_4 solution) and in presence of different red apple peel concentrations at temperature range (293-313) K.

Inh. (ppm)	T (K)	$-E_{corr}$ (mV)	i_{corr} ($\mu A/cm^2$)	Tafel slope (mV/dec)		CR (g/m^2d)	PR (mm/Y)
				$-b_c$	$+b_a$		
0	293	68.1	29.34	77.9	63.1	8.35	0.342
	298	69.3	57.03	75.8	66.2	15.02	0.664
	303	67.3	141.61	89.2	82.1	33.2	1.65
	308	56.7	148.99	83.9	75.9	41.08	1.93
	313	47.1	239.77	85	74.2	47.9	2.79
200	293	97.4	6.02	132.2	87.1	2.61	0.107
	298	108.9	13.1	113.4	82.6	5.84	0.238
	303	112.7	36.31	121.6	96.7	14.6	0.597
	308	82	44.12	92.1	78	17.6	0.721
	313	70.6	73.59	118	92.2	32.9	1.35
300	293	31.1	3.99	106.6	67.9	1.14	0.0464
	298	30.6	8.6	96.9	71	2.72	0.098
	303	47.2	27.55	122.5	98.6	7.82	0.321
	308	25.1	34.19	91.5	76.3	12.1	0.495
	313	17.2	64.73	79	68.2	22.3	0.913
400	293	202.8	2.91	72.9	50.9	1.07	0.033
	298	232.4	7.8	149.1	104.1	2.29	0.0936
	303	225.9	21.14	128	97.1	5.16	0.211
	308	227.9	29.5	94.9	78.1	7.83	0.328
	313	241.1	48.4	119	95.3	11.6	0.677
500	293	250.7	1.85	86.8	61.4	0.528	0.0216
	298	253.1	4.6	93	69.1	0.87	0.0356
	303	261.2	12.8	173.7	96.2	3.96	0.162
	308	241.6	18.5	179.5	110	4.79	0.196
	313	237.4	30.2	132	94	6.53	0.267

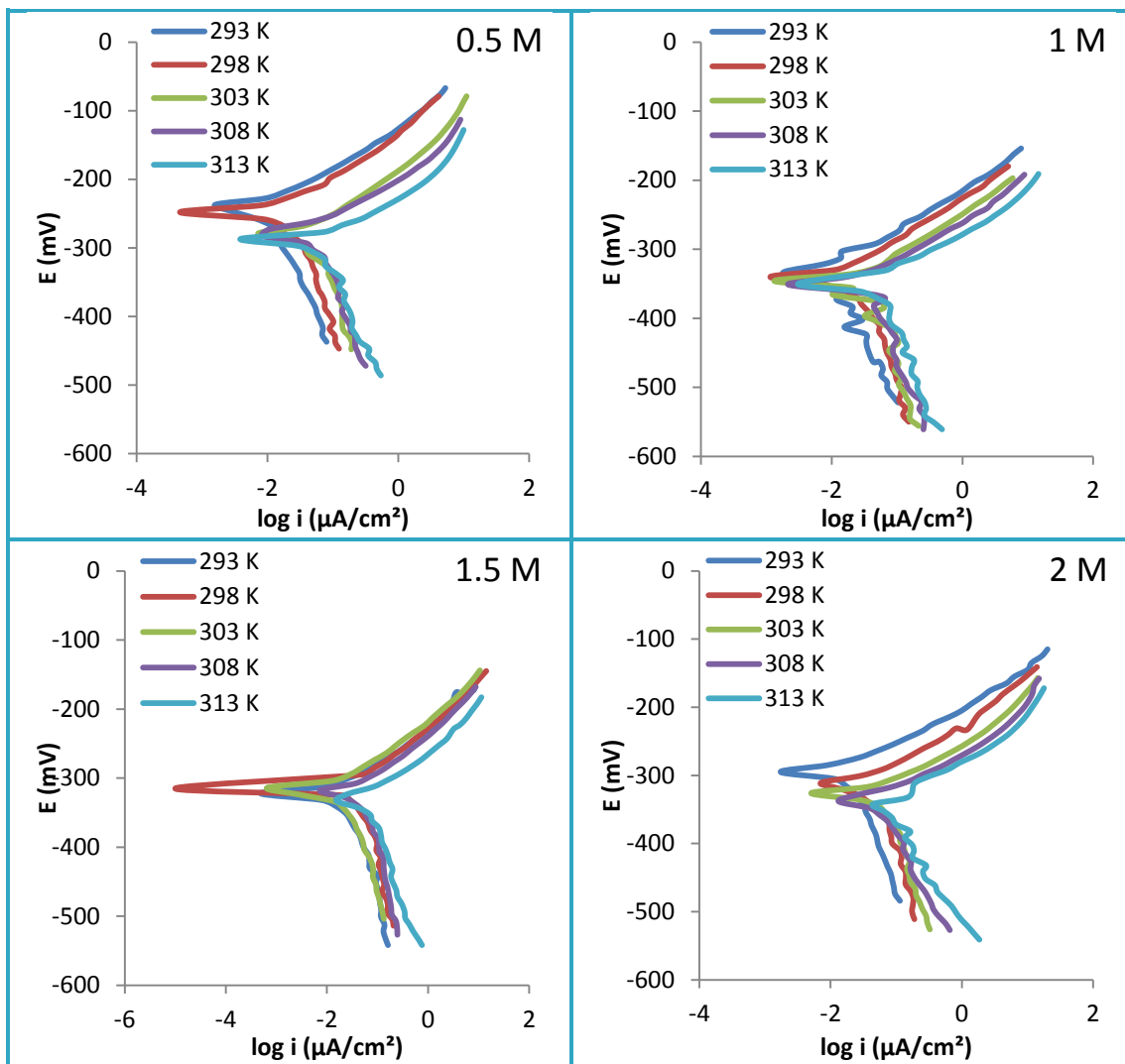


Figure (3.10): Polarization curves for α -brass corrosion in blank acidic medium (HCl solution) at different concentrations at temperature range (293-313) K.

Table (3.8): Corrosion parameters of α -brass in blank acidic medium (HCl solution) at different concentrations at temperature range (293-313) K.

Blank. (M)	T (K)	$-E_{\text{corr}}$ (mV)	i_{corr} ($\mu\text{A}/\text{cm}^2$)	Tafel slope (mV/dec)		CR ($\text{g}/\text{m}^2\text{d}$)	PR (mm/Y)
				$-b_c$	$+b_a$		
0.5	293	240.5	8.34	180.0	51.9	2.37	0.0971
	298	270.7	15.53	119.4	53.5	4.42	0.1800
	303	279.5	32.00	162.0	53.3	9.10	0.3720
	308	278.8	46.53	197.7	50.9	13.2	0.5420
	313	295.2	54.70	154.7	52.9	15.6	0.6380
1	293	316.9	9.490	260.4	43.5	9.70	0.110
	298	334.7	14.35	141.1	58.5	4.08	0.160
	303	354.2	21.10	132.4	56.7	6.00	0.246
	308	348.7	25.14	140.7	55.0	7.15	0.29
	313	341.4	49.00	249.3	48.2	13.9	0.57
1.5	293	317.3	14.8	148.6	49.2	4.26	0.174
	298	313	26.39	140.5	51.9	7.51	0.307
	303	302.3	53.44	280.6	57.3	15.2	0.622
	308	318.5	74.37	228.4	49.6	21.2	0.866
	313	336	56.53	198.3	53.1	29	1.02
2	293	292.5	24.62	89.6	75.7	4.17	0.117
	298	305.5	36.21	77.3	68.4	10.3	0.422
	303	327.7	62.2	91.6	82.9	17.7	0.724
	308	338.2	71.31	76.0	69.6	20.3	0.830
	313	343.0	83.28	90.9	81.6	23.7	0.970

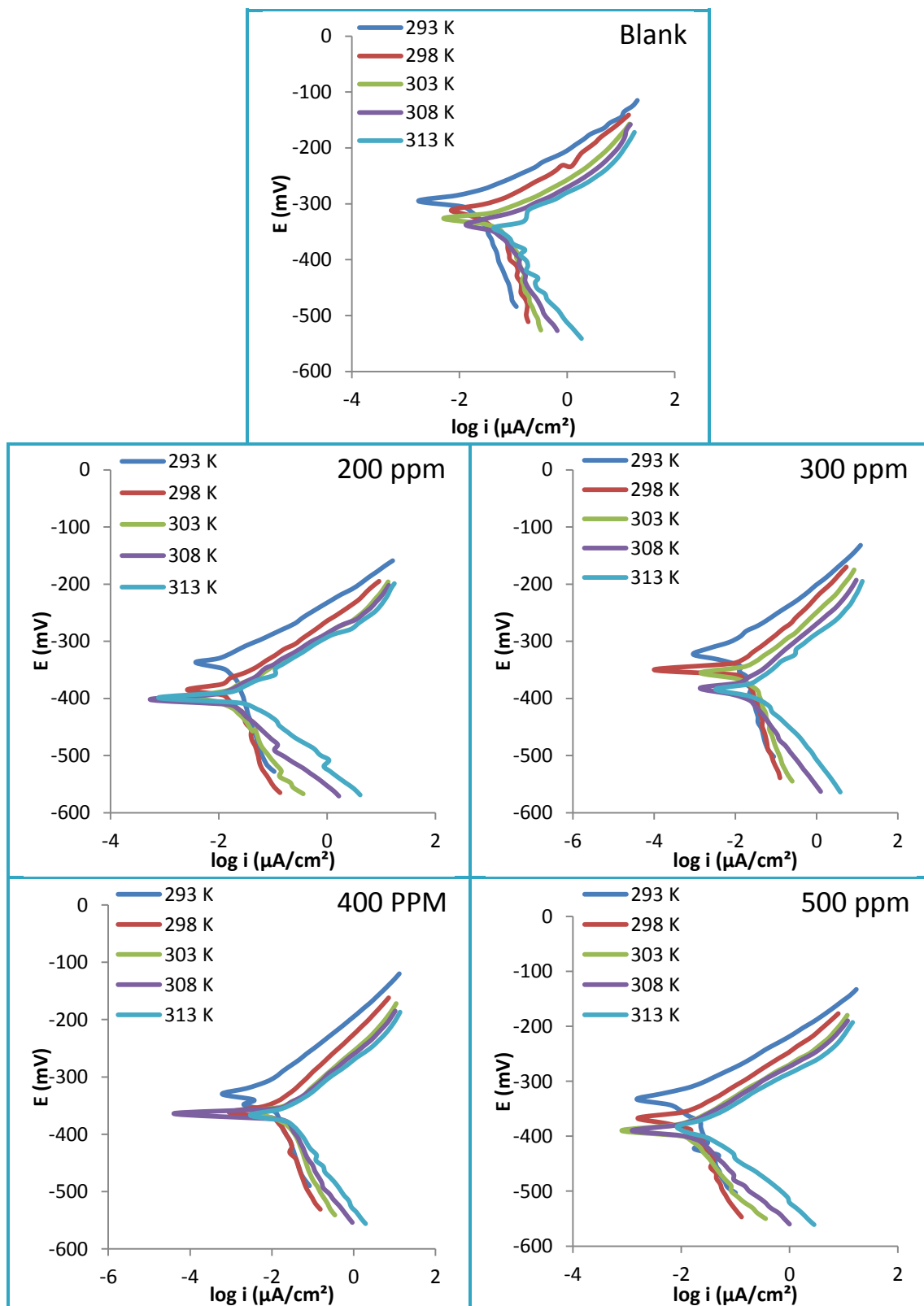


Figure (3.11): Polarization curves for α -brass corrosion in the blank (HCl solution) and in presence of different pomegranate peel concentrations at temperature range (293-313) K.

Table (3.9): Corrosion parameters of α -brass in the blank (HCl solution) and in presence of different pomegranate peel concentrations at temperature range (293-313) K.

Inh. (ppm)	T (K)	$-E_{\text{corr}}$ (mV)	i_{corr} ($\mu\text{A}/\text{cm}^2$)	Tafel slope (mV/dec)		CR ($\text{g}/\text{m}^2\text{d}$)	PR (mm/Y)
				$-b_c$	$+b_a$		
0	293	292.5	24.62	89.6	75.7	4.17	0.117
	298	305.5	36.21	77.3	68.4	10.3	0.422
	303	327.7	62.20	91.6	82.9	17.7	0.724
	308	338.2	71.31	76.0	69.6	20.3	0.830
	313	343.0	83.28	90.9	81.6	23.7	0.970
200	293	341.8	13.32	87.8	69.1	2.49	0.102
	298	385.1	20.41	91.2	73.8	5.71	0.234
	303	397.0	38.10	81.7	72.9	10.9	0.448
	308	398.9	44.50	75.8	67.5	13.0	0.520
	313	400.5	53.80	90.4	78.6	16.3	0.655
300	293	318.4	10.83	103.4	77.5	2.02	0.0825
	298	344.6	18.75	83	69.4	4.70	0.209
	303	352.6	33.09	105.6	90.5	9.62	0.039
	308	380.5	39.50	78.5	69.6	10.8	0.444
	313	384.6	48.10	82.9	72.2	13.6	0.556
400	293	326.8	9.94	122.8	91.3	1.95	0.0796
	298	351.3	17.10	101.1	80.9	4.21	0.130
	303	361.2	31.40	107.3	92.4	7.11	0.220
	308	362.1	37.20	90.2	78.6	7.90	0.291
	313	363.3	44.60	102.9	88.2	8.40	0.410
500	293	331.4	8.02	110.2	84.2	1.46	0.0599
	298	371.0	13.46	98.1	77.3	3.83	0.157
	303	389.3	25.43	116.4	98.1	4.30	0.310
	308	389.8	29.50	79.8	69.8	5.70	0.507
	313	383.0	37.22	82.1	71.7	6.30	0.710

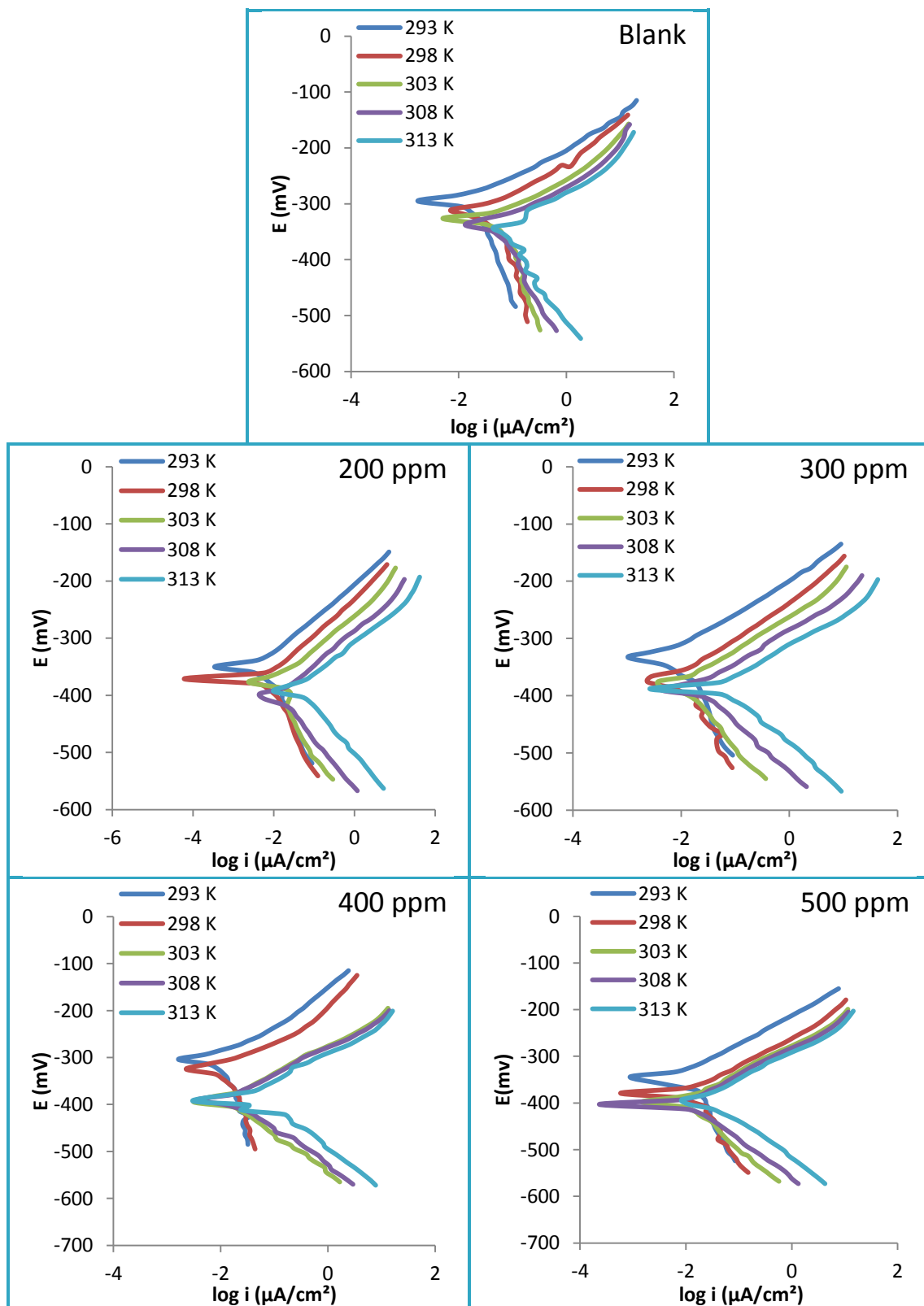


Figure (3.12): Polarization curves for α -brass corrosion in the blank (HCl solution) and in presence of different red apple peel concentrations at temperature range (293-313) K.

Table (3.10): Corrosion parameters of α -brass in the blank (HCl solution) and in presence of different red apple peel concentrations at temperature range (293-313) K.

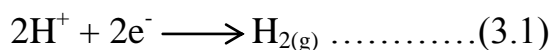
Inh. (ppm)	T (K)	$-E_{\text{corr}}$ (mV)	i_{corr} ($\mu\text{A}/\text{cm}^2$)	Tafel slope (mV/dec)		CR ($\text{g}/\text{m}^2\text{d}$)	PR (mm/Y)
				$-b_c$	$+b_a$		
0	293	292.5	24.62	89.6	75.7	4.17	0.117
	298	305.5	36.21	77.3	68.4	10.3	0.422
	303	327.7	62.20	91.6	82.9	17.7	0.724
	308	338.2	71.31	76.0	69.6	20.3	0.830
	313	343.0	83.28	90.9	81.6	23.7	0.970
200	293	349.7	7.53	171.4	94.4	2.06	0.0842
	298	372.4	11.69	141.4	89.8	3.33	0.136
	303	377.6	21.19	125.8	92.6	6.03	0.247
	308	397.4	25.3	98.5	78.5	7.2	0.295
	313	403.6	30.09	91.9	74.6	8.53	0.349
300	293	332.9	6.12	86.6	61.9	1.74	0.071
	298	366.3	9.06	115.9	75.8	2.58	0.105
	303	386.4	17.04	109.5	82.3	4.85	0.168
	308	390.4	19.9	120.5	89.7	5.46	0.232
	313	388.5	24.5	127.22	94.2	6.3	0.449
400	293	305	5.1	83.5	61.1	1.4	0.073
	298	325.7	7.61	97.3	68.2	2.3	0.098
	303	389.1	13.36	84.1	64.7	3.94	0.161
	308	386.5	16.23	73.6	59.7	4.62	0.891
	313	393.6	21.05	81.3	66.8	5.99	0.245
500	293	346.1	3.88	123.2	84.9	1.1	0.045
	298	379.1	5.83	55.7	48.5	1.66	0.067
	303	398.5	11.59	104.1	76.3	3.3	0.135
	308	405	14.3	72.1	58.6	3.9	0.186
	313	407	19.15	68.6	57.7	5.45	0.223

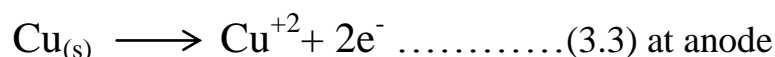
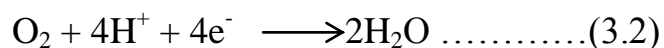
3.2.1 Corrosion Parameters

The corrosion behavior of α -brass in the blank solutions was tested over range of concentrations from 0.5 M up to 2 M of each of H_2SO_4 and HCl individually in order to provide information on the concentration effect of the hydrochloric and sulfuric acids on the corrosion of the alloy and giving a clear

idea about which acid under study leads to more corrosion of it. The data presented in tables (3.5) and (3.8). The obtained data show that with increasing the concentration of the corrosive media (H_2SO_4 and HCl) the corrosion current density increase this is because increasing the concentration of aggressive ions (chloride ions or sulfate ions) these ions can attack the alloy surface and begin to degrade it leading to form many types of corrosion.

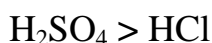
In H_2SO_4 solution the corrosion current density values were found to be increased with increasing temperature at constant concentration. At 0.5 M the values of corrosion current were increased gradually from $8.2 \mu\text{A}/\text{cm}^2$ at 293 K reaching up to $82 \mu\text{A}/\text{cm}^2$ at 313 K. The rising in temperature increasing the rate of corrosion reactions by accelerating the attack of the corrosive ions. The same trend is observed when the concentration of corrosive solution is increased at 1 M and 1.5 M. At 2 M concentration the corrosion current density values were remarkably increase reaching up to $239.77 \mu\text{A}/\text{cm}^2$ at 313 K this noticeable increase in corrosion current densities is attributed to the fact that H_2SO_4 is an oxidizing acid which means that the cathodic reactions represents by reduction of oxygen in addition to hydrogen evolution as shown in equations (3.1 – 3.3) for anodic and cathodic reactions. Since the polarization measurement take place in aerated environment the oxidizing power of the acid is increased because increase the concentration of dissolved oxygen that occurred at Air/solution interface. The corrosion potential values were found to be varied at all the concentrations and temperatures this behavior could be attributed that the sulfate ions SO_4^{2-} act as inorganic inhibitor by forming a temporary protective film at low concentration which result to shift the corrosion potential towards noble direction (anodic polarization) then the protective film breaks down by the successive sulfate ions then the potential shifts towards active direction (cathodic polarization).





In HCl solution the corrosion current density follows the same trend in case of H₂SO₄ which increase gradually with increasing temperature at constant concentration. The maximum obtained value of corrosion current density was 83.28 μA/cm² at 313 K which attributed to the presence of chloride ions which being aggressive ions these ions can attack the alloy surface successivly and form a visible pits. The crrosion potencial values weren't varied as the same case as observed in H₂SO₄ the corrosion potencial were found to be cathodically polarized with increase temperature that could be attributed to the aggressive nature of chloride ions.

The corrosion behavior of α- Brass alloy in 2 M acidic media H₂SO₄ or HCl show that the *i*_{corr} values are smaller in HCl solution 83.28 μA/cm² as compared with H₂SO₄ solution 239.77 μA/cm² at the same temperature. This behavior is in according with the variation in such acid properties as the oxidizing ability for the two acids (H₂SO₄ is an oxidizing acid while HCl is non-oxidizing acid)⁽⁶³⁾. The corrosion trend of α-brass in acidic media is shown:



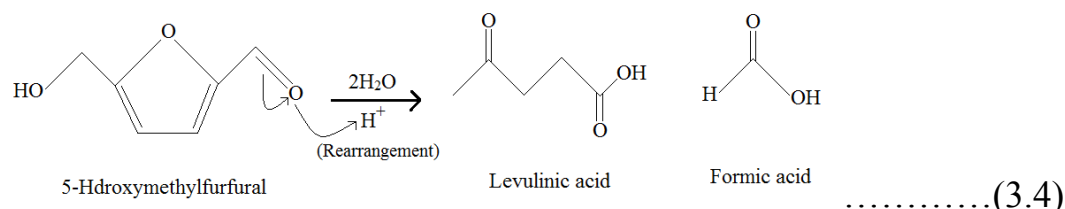
The behavior of each inhibitor that used in the research is summarized as follows:

❖ *Pomegranate Peels Extract*

The polarization curves for α-brass in the acidic media and in presence of different concentrations of pomegranate peels extract were shown in figures (3.8 and 3.11) and the obtained corrosion parameters were listed in tables (3.6 and 3.9).

❖ *The Proposed Inhibition Mechanism of Pomegranate Peels Extract*

In H_2SO_4 solution it's found that the corrosion current densities reduced significantly with increase the concentration of pomegranate peels extract from $239.77 \mu\text{A}/\text{cm}^2$ in blank solution to its minimal value $2.4 \mu\text{A}/\text{cm}^2$ at 293 K and at maximum extract concentration 500 ppm. The inhibitive activity of pomegranate peels comes from the fact that it's contain a numerous of oxygen-containing compounds, nitrogen-containing compounds and unsaturated compounds. Those compounds contain unsaturated π electrons and hetero atoms that possess lone pair (electronic density) that interact with the vacant d-orbitals of the metal and promote a protective layer [Cu-Pome] complex on the surface that can isolate the alloy from the corrosive solution. As mention previously in GC-MS analysis of pomegranate peels that 5-Hdroxymethylfurfural is the major constituent that present in the peels this compound is unstable and reactive in aqueous acidic solutions and can undergo hydrolysis and acidic decomposition to form levulinic acid and formic acid ⁽⁶⁴⁾ as shown in equation:

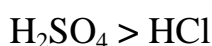


These resulted compounds can adsorb on the metal surface via the lone pair that located on oxygen atoms and promote a protective layer to isolate the metal from the corrosive species. The corrosion potential values were found to be varied at all the extract concentrations and shifted the potential values of the blank solution towards cathodic and anodic directions which indicates that the pomegranate peels act as mixed-type inhibitor ⁽⁶⁵⁾.

For HCl the addition of various concentrations of pomegranate peels leads to decrease the values of corrosion current densities from $83.28 \mu\text{A}/\text{cm}^2$ at the blank solution to $37.22 \mu\text{A}/\text{cm}^2$ at 500 ppm of pomegranate peel extract which

suggests that formation of a protective layer via adsorption. The inhibiting effect of pomegranate peel extract (decrease of the corrosion current density values) in HCl medium was relatively less than observed behavior in H₂SO₄ medium which is likely to be due to the presence of aggressive chloride ions. These corrosive species could be attack locally and form a blug type corrosion (pitting corrosion) besides to weaken the adhesive of inhibitive layer that formed on the alloy surface. The corrosion potentials of the blank solution were shifted towards cathodic direction (active direction) in addition of pomegranate peels which suggest that the pomegranate peels in HCl solution act as cathodic type inhibitor.

Generally, the inhibition performance of pomegranate peels in acidic media can be arranged as follows:



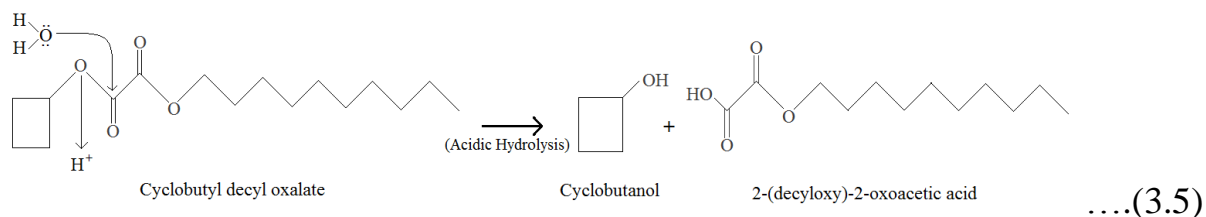
❖ *Red Apple Peels Extract*

The polarization curves for α -brass in the acidic media and in presence of different concentrations of red apple peels extract were shown in figures (3.9 and 3.12) and the obtained corrosion parameters were listed in tables (3.7 and 3.10).

❖ *The Proposed Inhibition Mechanism of Red Apple Peels Extract*

The red apple peels show a remarkable inhibitive performance in H₂SO₄ solution by decreasing the corrosion current density values from 239.77 $\mu\text{A}/\text{cm}^2$ in blank solution up to 1.85 $\mu\text{A}/\text{cm}^2$ at 500 ppm of red apple extract which attributed that red apple peels contain a greater number of compounds that contain many hetero atoms (N, O, S and P) and unsaturated π electrons these atoms adsorb onto the metal surface and improve a protective layer. The GC-MS analysis of red apple peels reported that the cyclobutyl decyl oxalate is the major constituent in the peels. This diester derivative undergoes acidic hydrolysis

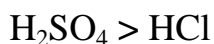
process in acidic media to yield cyclic alcohol and carboxylic acid because cyclic alkyl is more reactive than n-chain of alkyl groups as shown in equation:



These resulted compounds can adsorb on metal surface via lone pair located on oxygen atoms and form protective film other another advantage of these compounds is that the long chain of hydrocarbon can also adsorb physically by Vander Waals forces which giving rise of adherent and insoluble protective film then resulted strong inhibitive performance. The corrosion potential values were shifted cathodically at 200, 400 and 500 ppm and anodically at 300 ppm of red apple peels extract which is suggested that red apple peels act as mixed-type inhibitor in H_2SO_4 solution.

Red apple peels show good inhibitive performance in HCl solution by decreasing the corrosion current density of blank from $83.28 \mu\text{A}/\text{cm}^2$ to $3.88 \mu\text{A}/\text{cm}^2$. The results show that the protective layer formed by red apple peels is stable, insoluble and protect the alloy from aggressive chloride ions. The corrosion potential values were slightly shifted towards cathodic direction which indicates that the red apple peels act as cathodic type inhibitor.

The inhibitive performance of red apple peels in acidic media as follows:



To summarize the overall performance of each inhibitor in acidic media one can concludes the follows:

1. 2 M concentration of H_2SO_4 and HCl was selected as the main concentration of blank solutions.

2. The results show that α -brass corroded more in H_2SO_4 than HCl.
3. Both of pomegranate and red apple peels show better inhibitive performance in H_2SO_4 than HCl.
4. Red apple peels was better inhibitor than pomegranate peels in both of H_2SO_4 and HCl.
5. In H_2SO_4 solution both of the inhibitors act as mixed-type inhibitor while in HCl solution they act as cathodic type inhibitor.

The obtained results of corrosion and penetration rates for α -brass in the acidic media are summarized as follow:

1. Both of corrosion rate and penetration rates corresponding to corrosion current density which they increase with increasing temperature.
2. CR and PR values were found to be decreased with increasing the concentration of pomegranate and red apple peels.

3.2.2 Tafel Slopes and Transfer Coefficients

The values of anodic and cathodic transfer coefficients (α_a , α_c) were calculated from equations (1.13) and (1.14) are listed in tables (3.11 – 3.14).

The values of anodic and cathodic slopes that obtained from the polarization curves are listed in tables (3.5 – 3.10).

Table (3.11): Values of transfer coefficient (α_c , α_a), the polarization resistance (R_p) and equilibrium exchange current density (i_o) for corrosion of α -brass in 2 M H_2SO_4 solution in the absence and presence of pomegranate peels at temperature range (293-313) K.

Conc. (M)	T (K)	α_c	α_a	$R_p \times 10^3$ ($\Omega \cdot \text{cm}^2$)	$i_o \times 10^{-5}$ (A/cm ²)
Blank	293	0.373	0.460	4.915	0.514
	298	0.390	0.446	3.979	0.645
	303	0.337	0.366	3.162	0.826
	308	0.364	0.402	2.319	1.144
	313	0.365	0.418	1.057	2.550
200	293	0.207	0.343	8.201	0.308
	298	0.229	0.316	6.614	0.388
	303	0.267	0.310	5.189	0.503
	308	0.342	0.411	3.098	0.856
	313	0.301	0.356	2.264	1.191
300	293	0.192	0.414	9.804	0.258
	298	0.207	0.344	7.640	0.336
	303	0.321	0.383	6.804	0.384
	308	0.284	0.337	5.232	0.507
	313	0.319	0.368	3.505	0.769
400	293	0.309	0.597	14.154	0.178
	298	0.234	0.370	10.420	0.246
	303	0.248	0.312	8.848	0.295
	308	0.372	0.447	6.514	0.407
	313	0.304	0.366	4.240	0.636
500	293	0.179	0.399	31.984	0.079
	298	0.250	0.470	12.118	0.212
	303	0.296	0.383	11.263	0.232
	308	0.286	0.375	7.114	0.373
	313	0.248	0.315	5.172	0.521

Table (3.12): Values of transfer coefficient (α_c , α_a), the polarization resistance (R_p) and equilibrium exchange current density (i_o) for corrosion of α -brass in 2 M H_2SO_4 solution in the absence and presence of red apple peels at temperature range (293-313) K.

Conc. (M)	T (K)	α_c	α_a	$R_p \times 10^3$ ($\Omega \cdot \text{cm}^2$)	$i_o \times 10^{-5}$ (A/cm ²)
Blank	293	0.373	0.460	4.915	0.514
	298	0.390	0.446	3.979	0.645
	303	0.337	0.366	3.162	0.826
	308	0.364	0.402	2.319	1.144
	313	0.365	0.418	1.057	2.550
200	293	0.206	0.343	18.415	0.137
	298	0.230	0.317	10.080	0.255
	303	0.267	0.311	5.647	0.462
	308	0.343	0.411	5.014	0.529
	313	0.302	0.357	2.488	1.084
300	293	0.192	0.414	20.353	0.124
	298	0.207	0.344	13.413	0.191
	303	0.322	0.383	7.965	0.328
	308	0.284	0.337	5.833	0.455
	313	0.320	0.3680	3.346	0.806
400	293	0.309	0.597	25.167	0.100
	298	0.235	0.370	19.201	0.134
	303	0.248	0.312	8.262	0.316
	308	0.373	0.447	6.447	0.412
	313	0.304	0.367	4.293	0.628
500	293	0.180	0.400	49.248	0.051
	298	0.251	0.471	25.381	0.101
	303	0.297	0.384	7.314	0.355
	308	0.287	0.376	6.668	0.398
	313	0.249	0.315	4.695	0.574

Table (3.13): Values of transfer coefficient (α_c , α_a), the polarization resistance (R_p) and equilibrium exchange current density (i_o) for corrosion of α -brass in 2 M HCl solution in the absence and presence of pomegranate peels at temperature range (293-313) K.

Conc. (M)	T (K)	α_c	α_a	$R_p \times 10^3$ ($\Omega \cdot \text{cm}^2$)	$i_o \times 10^{-5}$ (A/cm ²)
Blank	293	0.324	0.384	8.606	0.293
	298	0.383	0.432	7.124	0.360
	303	0.328	0.363	6.093	0.428
	308	0.402	0.439	5.033	0.527
	313	0.342	0.381	4.158	0.649
200	293	0.331	0.421	10.576	0.239
	298	0.324	0.401	8.229	0.312
	303	0.368	0.412	7.713	0.338
	308	0.403	0.453	6.015	0.441
	313	0.344	0.395	4.869	0.555
300	293	0.281	0.375	12.405	0.204
	298	0.356	0.426	9.809	0.262
	303	0.285	0.332	8.305	0.314
	308	0.389	0.439	6.748	0.393
	313	0.375	0.430	5.050	0.534
400	293	0.237	0.318	15.548	0.162
	298	0.292	0.365	10.282	0.250
	303	0.280	0.325	9.202	0.284
	308	0.339	0.389	7.096	0.374
	313	0.302	0.352	6.011	0.449
500	293	0.264	0.345	19.322	0.131
	298	0.301	0.383	11.761	0.218
	303	0.258	0.306	10.654	0.245
	308	0.383	0.438	8.199	0.324
	313	0.378	0.433	6.603	0.408

Table (3.14): Values of transfer coefficient (α_c , α_a), the polarization resistance (R_p) and equilibrium exchange current density (i_o) for corrosion of α -brass in 2 M HCl solution in the absence and presence of red apple peels at temperature range (293-313) K.

Conc. (M)	T (K)	α_c	α_a	$R_p \times 10^3$ ($\Omega \cdot \text{cm}^2$)	$i_o \times 10^{-5}$ (A/cm^2)
Blank	293	0.324	0.384	8.606	0.293
	298	0.383	0.432	7.124	0.360
	303	0.328	0.363	6.093	0.428
	308	0.402	0.439	5.033	0.527
	313	0.342	0.381	4.158	0.649
200	293	0.170	0.308	12.117	0.208
	298	0.209	0.329	9.140	0.281
	303	0.239	0.325	7.190	0.363
	308	0.310	0.389	6.635	0.391
	313	0.338	0.416	5.719	0.472
300	293	0.336	0.470	15.398	0.163
	298	0.255	0.390	10.491	0.245
	303	0.275	0.365	8.443	0.309
	308	0.254	0.341	7.657	0.347
	313	0.244	0.330	6.432	0.419
400	293	0.348	0.474	19.392	0.130
	298	0.304	0.434	13.011	0.197
	303	0.357	0.465	9.116	0.286
	308	0.415	0.512	8.457	0.314
	313	0.382	0.465	7.726	0.349
500	293	0.236	0.342	30.563	0.083
	298	0.531	0.610	27.945	0.092
	303	0.289	0.394	10.704	0.244
	308	0.424	0.522	9.503	0.279
	313	0.453	0.538	8.234	0.328

The obtained values of transfer coefficient as well as Tafel slopes were found to be varied at all the concentrations and temperatures which indicates of the variation of rate-determining step since the anodic reaction involves transfer of metal ions into the solution and cathodic reaction involves reduction of discharge hydrogen ions into hydrogen gas or/both reduction of oxygen ions the

variation of Tafel slopes (cathodic and anodic) values indicates that the pomegranate and red apple peels inhibitors effected these reactions ⁽⁶⁶⁾.

3.2.3 Polarization Resistances and Exchange Current Densities

The results of R_p and i_o were calculated from equations (1.15) and (1.17) are listed in tables (3.11 – 3.14). The outcome results can be summarized as follow:

1. R_p values decrease with increasing temperature.
2. R_p values in absence of the inhibitors (blank solutions) were found to be higher in HCl than H_2SO_4 .
3. R_p values increase with increasing in concentration of both of pomegranate and red apple peels.
4. The highest values of R_p were obtained in presence of red apple peels.

Since the exchange current density represents corrosion rate at equilibrium, its values were increased with increasing temperature. When the inhibitors are added the values of exchange current densities decreased dramatically as the concentration of the inhibitor increased. The highest reduction in values of exchange current was observed in presence of red apple peels in both of acidic media (H_2SO_4 and HCl).

3.3 Surface Coverage and Inhibition Efficiency

The inhibition efficiency (IE%) and surface coverage (θ) are evaluated by using the eqautions (3.6) and (3.7) respectively ^(67, 68):

$$IE\% = \frac{i_{corr}^{\circ} - I_{corr}}{i_{corr}^{\circ}} \dots\dots\dots(3.6)$$

Where I_{corr}° and I_{corr} represent corrosion current densities in absence and presence of the inhibitors respectively.

$$\theta = \frac{IE\%}{100} \dots\dots\dots(3.7)$$

The obtained values of the IE% and θ were listed in tables (3.15) and (3.16).

Table (3.15): Inhibition efficiencies and surface coverages of pomegranate and red apple peels at various concentration with temperature range (293-313)K in 2 M H₂SO₄.

Inh.	T (K)	200 ppm		300 ppm		400 ppm		500 ppm	
		IE%	θ	IE%	θ	IE%	θ	IE%	θ
Pomegranate Peels	293	61.35	0.6135	80.23	0.8023	89.34	0.8934	91.86	0.9186
	298	60.65	0.6065	78.43	0.7843	85.79	0.8579	91.58	0.9158
	303	59.53	0.5953	77.82	0.7782	83.65	0.8365	90.64	0.9064
	308	57.93	0.5793	67.90	0.679	81.70	0.8170	85.92	0.8592
	313	54.82	0.5482	66.66	0.6666	79.50	0.7950	83.63	0.8363
Red apple Peels	293	79.48	0.7948	86.40	0.864	90.08	0.9008	93.69	0.9369
	298	77.03	0.7703	84.92	0.8492	86.32	0.8632	91.93	0.9193
	303	74.36	0.7436	81.95	0.8195	85.07	0.8507	90.96	0.9096
	308	70.39	0.7039	77.05	0.7705	80.02	0.8002	88.25	0.8825
	313	69.31	0.6931	73.00	0.7300	79.81	0.7981	87.40	0.8740

Table (3.16): Inhibition efficiencies and surface coverages of pomegranate and red apple peels at various concentration with temperature range (293-313)K in 2 M HCl.

Inh.	T (K)	200 ppm		300 ppm		400 ppm		500 ppm	
		IE%	θ	IE%	θ	IE%	θ	IE%	θ
Pomegranate Peels	293	45.90	0.4590	56.01	0.5601	59.63	0.5963	67.42	0.6742
	298	43.64	0.4364	48.21	0.4821	52.77	0.5277	62.82	0.6282
	303	38.74	0.3874	46.80	0.4680	49.51	0.4951	59.11	0.5911
	308	37.59	0.3759	44.60	0.4460	47.83	0.4783	58.63	0.5863
	313	35.39	0.3539	42.24	0.4224	46.83	0.4683	55.30	0.5530
Red apple Peels	293	69.41	0.6941	75.14	0.7514	79.28	0.7928	84.24	0.8424
	298	67.71	0.6771	74.97	0.7497	78.97	0.7897	83.89	0.8389
	303	65.93	0.6593	72.60	0.726	78.52	0.7852	81.36	0.8136
	308	64.52	0.6452	72.09	0.7209	77.55	0.7755	79.90	0.799
	313	63.86	0.6386	70.58	0.7058	74.72	0.7472	77.05	0.7705

The results show that the highest inhibition efficiencies were obtained in H_2SO_4 solution for both of pomegranate and red apple peels which were 91.86% and 93.69% respectively while in HCl solution the inhibition efficiencies were 67.42% and 84.24% for pomegranate and red apple peels respectively which suggest that red apple was best inhibitor in both of acidic media which attributed to the mechanism that discussed earlier. While pomegranate peels show good inhibition performance only in H_2SO_4 . The surface coverage and inhibition efficiency depend on many factors such as concentration of the inhibitor, chemical structure of inhibitor, temperature and the environment. The IE% and θ values are greatly affected by these factors. The IE% values were found to increase with increasing the concentration of the inhibitors and decrease with increase temperature ⁽⁶⁹⁾.

The adsorption inhibitors (also known as organic inhibitors) are widely believed that its remarkable inhibitive characteristic comes from its tendency to adsorb on the metal surface via hetero atoms or unsaturated π electrons. The adsorption either chemisorption a strong adsorption type that involves a

formation of a covalent-coordinated bond and/or physisorption that occurred due to an electrostatic interaction between polarized inhibitor groups and metal surface.

3.4 Activation Parameters of α -Brass Corrosion

The activation parameters of α -brass in acidic media and in absence and presence of pomegranate and red apple peels over temperature range (293-313) K were calculated using Arrhenius equation (1.18). Can be converted it to logarithmic form as:

$$\log i_{corr} = \frac{-E_a}{2.303 RT} + \log A \dots\dots\dots(3.8)$$

Figures (3.13) and (3.15) represent Arrhenius plots of $\log i_{corr}$ vs $1/T$ of both of blank solutions and the inhibitors. The E_a and A values were obtained from slopes and intercepts of these plots respectively. Their values were listed in tables (3.17) and (3.18).

An alternative form of Arrhenius equation has been used to evaluate other activation parameters as follow:

$$i_{corr} = \left(\frac{RT}{Nh}\right) \exp\left(\frac{\Delta S_a}{R}\right) \exp\left(\frac{-\Delta H_a}{RT}\right) \dots\dots\dots(3.9)$$

Where h is planks constant's, N is Avogadro's number, ΔS_a is the entropy of activation energy and ΔH_a is the enthalpy of activation. The equation (3.9) would take the form:

$$\ln \frac{i_{corr}}{T} = \ln \left(\frac{R}{Nh}\right) + \left(\frac{\Delta S_a}{R}\right) - \left(\frac{\Delta H_a}{RT}\right) \dots\dots\dots(3.10)$$

Figures (3.14) and (3.16) show the variation of $\ln (i_{corr}/T)$ values for the both acids in the presence of both inhibitors with the variation of reciprocal temperatures ($1/T$). Values of ΔH_a and ΔS_a have been then determined

respectively from the slopes and intercepts of figures (3.14) and (3.16) and presented in tables (3.17) and (3.18).

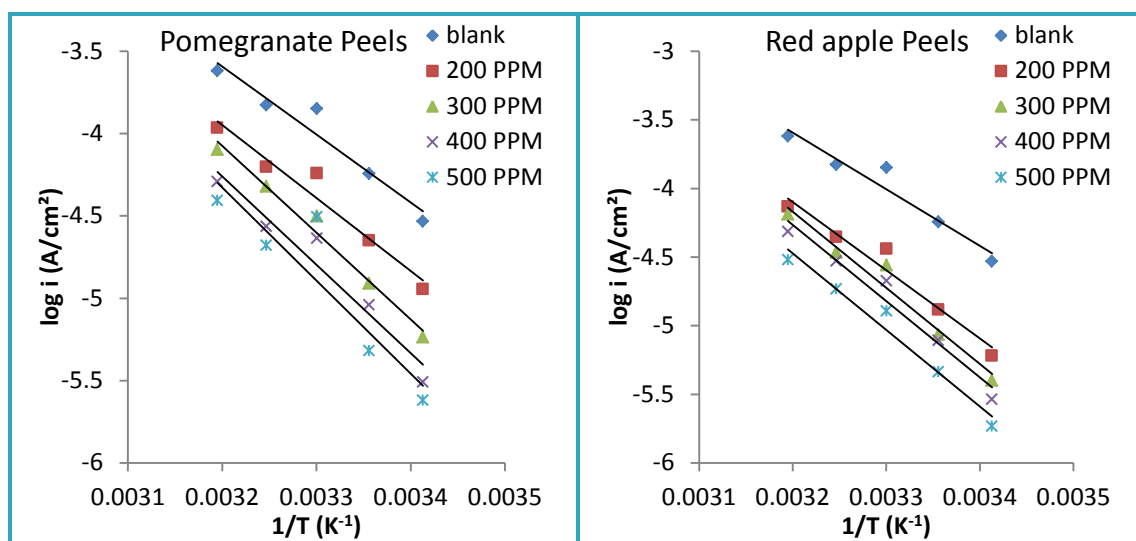


Figure (3.13): Arrhenius plots of $\log i_{\text{corr}}$ versus $1/T$ for the corrosion of α -brass in 2 M H_2SO_4 and in the presence of inhibitors (Pomegranate and Red apple Peels) at various concentrations.

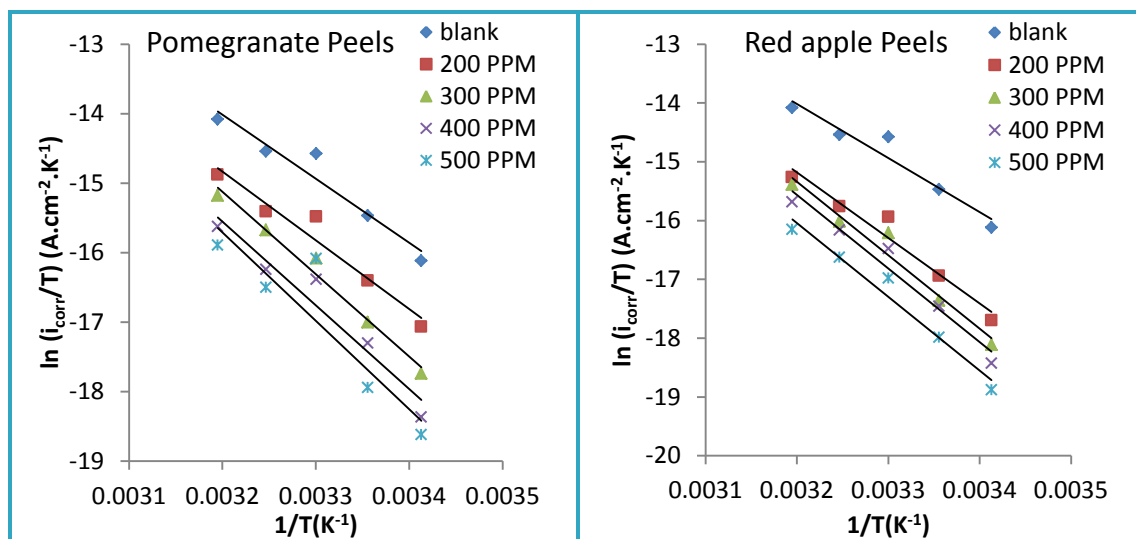


Figure (3.14): Arrhenius plots of $\ln (i_{\text{corr}}/T)$ versus $1/T$ for the corrosion of α -brass in 2 M H_2SO_4 and in the presence of inhibitors (Pomegranate and Red apple Peels) at various concentrations.

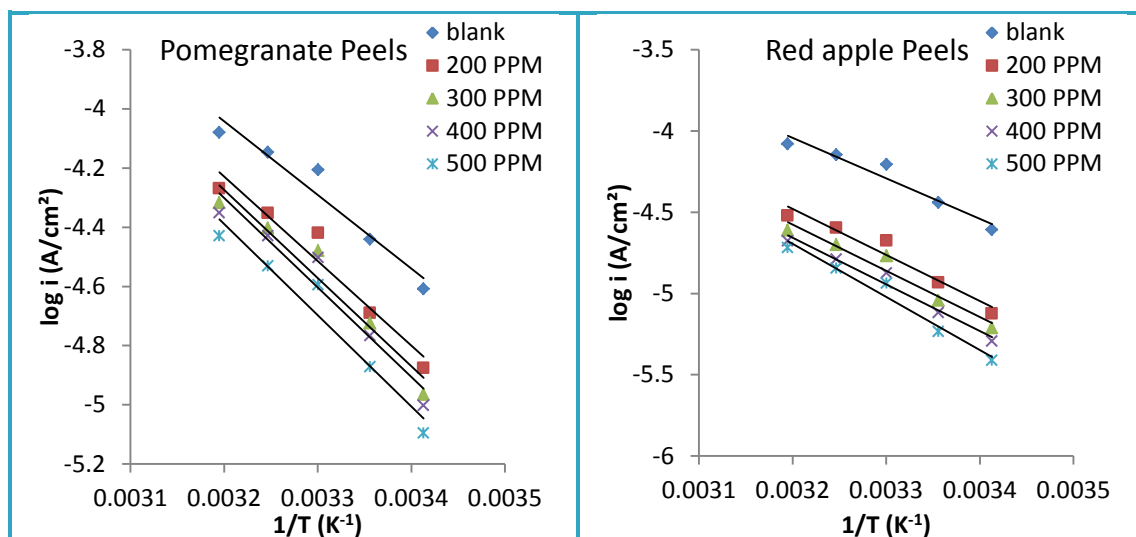


Figure (3.15): Arrhenius plots of $\log i_{\text{corr}}$ versus $1/T$ for the corrosion of α -brass in 2 M HCl and in the presence of inhibitors (Pomegranate and Red apple Peels) at various concentrations.

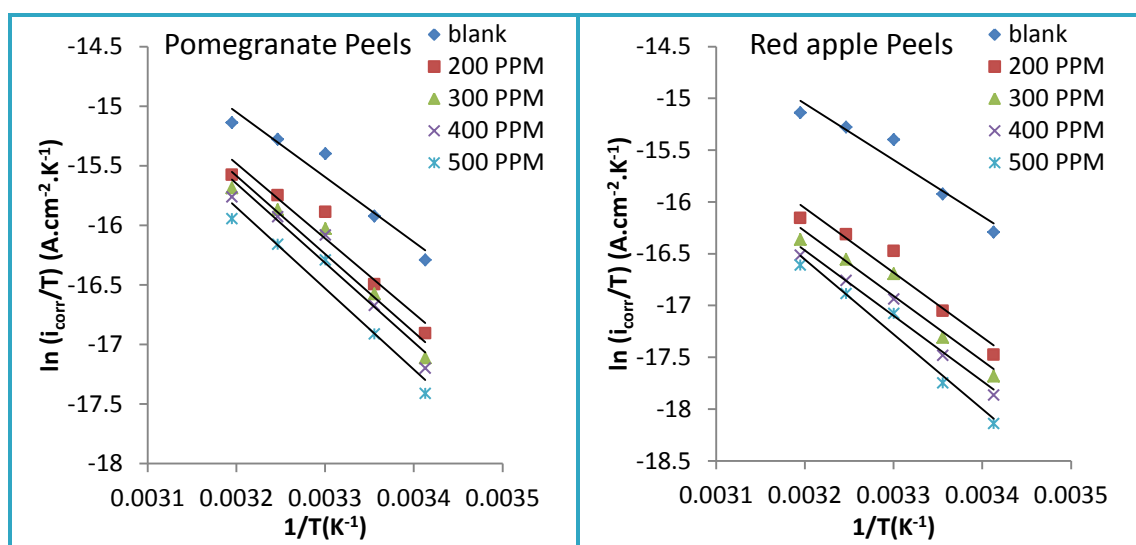


Figure (3.16): Arrhenius plots of $\ln (i_{\text{corr}}/T)$ versus $1/T$ for the corrosion of α -brass in 2 M HCl and in the presence of inhibitors (Pomegranate and Red apple Peels) at various concentrations.

Table (3.17): Activation energy (E_a), activation enthalpy (ΔH_a), and the entropy of activation (ΔS_a) for the corrosion of α -brass in 2 M H_2SO_4 and in the presence of inhibitors (Pomegranate and Red apple Peels) at various concentrations.

Inh.	Conc. (ppm)	E_a ($kJ.mol^{-1}$)	A ($molecules.cm^{-2}.s^{-1}$)	ΔH_a ($kJ.mol^{-1}$)	ΔS_a ($J.K^{-1}.mol^{-1}$)
Blank	-	79.02	2.47×10^{33}	76.49	-69.31
Pomegranate Peels	200	84.73	9.81×10^{33}	82.20	-57.85
	300	100.96	3.77×10^{36}	98.42	-8.36
	400	102.64	4.71×10^{36}	100.10	-6.54
	500	108.28	3.53×10^{37}	105.74	10.21
Red apple Peels	200	95.21	3.92×10^{35}	92.90	-27.21
	300	106.33	2.41×10^{37}	103.79	7.04
	400	106.44	2.01×10^{37}	103.90	5.54
	500	106.77	1.41×10^{37}	104.23	2.61

Table (3.18): Activation energy (E_a), activation enthalpy (ΔH_a), and the entropy of activation (ΔS_a) for the corrosion of α -brass in 2 M HCl and in the presence of inhibitors (Pomegranate and Red apple Peels) at various concentrations.

Inh.	Conc. (ppm)	E_a ($kJ.mol^{-1}$)	A ($molecules.cm^{-2}.s^{-1}$)	ΔH_a ($kJ.mol^{-1}$)	ΔS_a ($J.K^{-1}.mol^{-1}$)
Blank	-	47.72	5.16×10^{27}	45.20	-178.06
Pomegranate Peels	200	54.70	4.92×10^{28}	52.17	-159.32
	300	57.03	1.09×10^{29}	54.50	-152.71
	400	57.93	1.44×10^{29}	55.40	-150.37
	500	59.04	1.81×10^{29}	56.51	-148.47
Red apple Peels	200	54.26	2.33×10^{28}	51.73	-165.52
	300	54.51	2.06×10^{28}	51.99	-166.55
	400	54.95	2.02×10^{28}	52.42	-166.71
	500	62.55	3.45×10^{29}	60.02	-143.12

The resulted data revealed that E_a values were found to be higher in presence of the inhibitors than in blank solution which indicated that the addition of the inhibitors increase the energy barrier of the corrosion process. The values of E_a were increased with increasing the concentration of the inhibitors which suggested that the presence of inhibitor molecules increase the energy barrier

when the reactants transform to the hypothetical transition state or activated complex as the concentration of the inhibitor increases, the energy required by reactants to move into products increases in other words the corrosion process occurrence became difficult ^(70,71).

The positive sign of enthalpy of activation (ΔH_a) values in absence and presence of the inhibitors reflects the endothermic nature of α -brass dissolution process and their positivity increase with increasing the inhibitor concentration which suggest the difficulty of α -brass corrosion in presence of pomegranate and red apple peels ⁽⁷²⁾. The values of entropy of activation (ΔS_a) in the blank acids solutions were found to be negative and their negativity decreased gradually with increasing inhibitors concentration. For H_2SO_4 solution the increase of ΔS_a values was remarkably observed and its values were positive at higher concentrations for both of the inhibitors. On the other hand, ΔS_a values for HCl solution were negative in absence and presence of both inhibitors and negativity decrease with increasing inhibitors concentrations. The increase of ΔS_a values can be interpreted to the increase in randomness (degree of freedom) that take place when the corrosion reaction going from reactants to the transition state (activated complex) and also suggest that the rate determining step is association rather than dissociation ⁽⁷³⁾.

3.5 Thermodynamic Parameters of Adsorption Isotherm Modeling

The adsorption behavior of pomegranate and red apple peels on α -brass in both acids was investigated using Langmuir adsorption isotherm model.

The adsorption of pomegranate and red apple peels on α -brass depends on surface coverage (θ) that had been calculated from equation (3.7) for both acids and can be employed in Langmuir equation (1.19).

The equilibrium (K_{ads}) adsorption constant which have been evaluated from the intercept in plots of c/θ vs c as shown in figures (3.17) and (3.18). The correlation coefficient (R^2) values are between (0.92-0.99). The resulting data of K_{ads} for both acids in the absence and presence of both inhibitors are presented in tables (3.19) and (3.20).

From calculated values of K_{ads} . The Gibbs free energy of adsorption has been calculated using the equation ⁽⁷⁴⁾:

$$\Delta G^{\circ}_{ads} = -RT \ln(1000K_{ads}) \dots\dots\dots(3.11)$$

Where R is gas constant, T is absolute temperature and the value 1000 represents the molar concentration of water in g/L. The values of ΔG°_{ads} are also listed in tables (3.19) and (3.20).

Other thermodynamic parameters the enthalpy of adsorption (ΔH°_{ads}) and entropy of adsorption (ΔS°_{ads}) have been calculated by plotting the ΔG°_{ads} against temperature for both acids in the presence of both inhibitors as shown in figures (3.19) and (3.20) using well known equation ⁽⁷⁵⁾:

$$\Delta G^{\circ}_{ads} = \Delta H^{\circ}_{ads} - T\Delta S^{\circ}_{ads} \dots\dots\dots(3.12)$$

The intercept and slope represent ΔH°_{ads} and ΔS°_{ads} respectively.

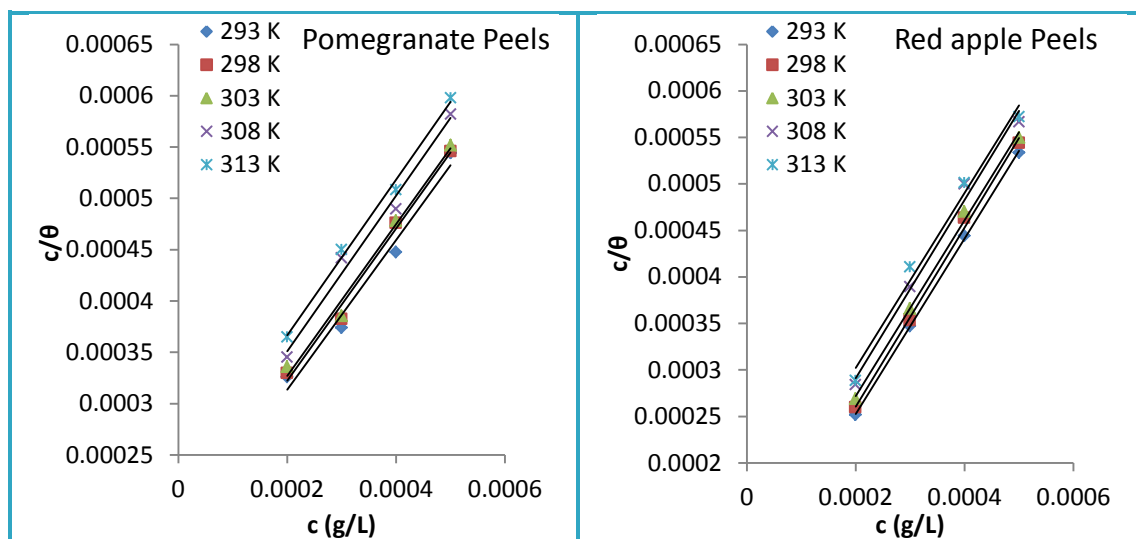


Figure (3.17): Langmuir isotherm plots for the adsorption of (Pomegranate and Red apple Peels) on α -brass in 2 M H_2SO_4 .

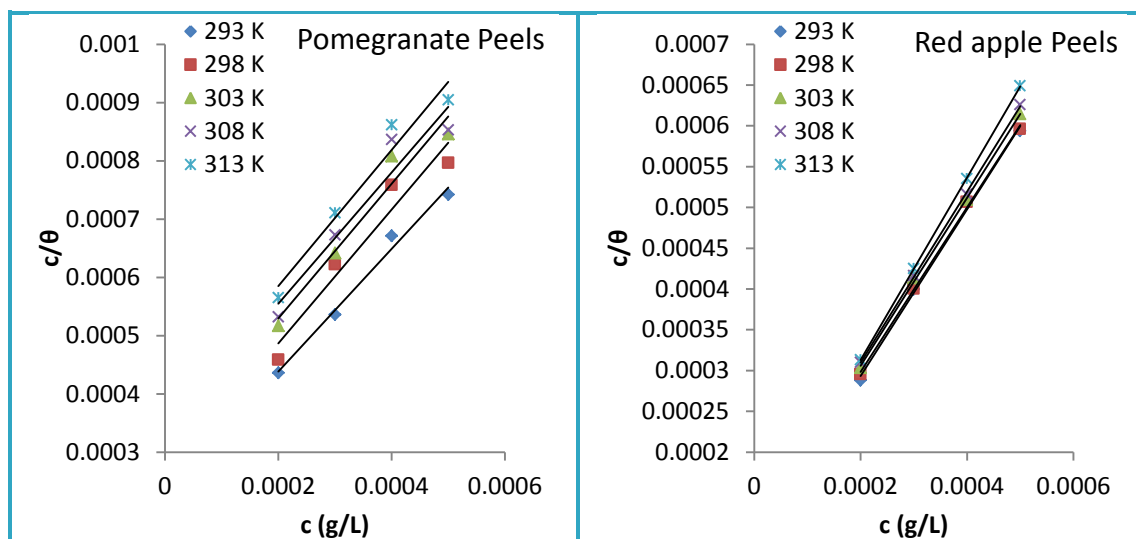


Figure (3.18): Langmuir isotherm plots for the adsorption of (Pomegranate and Red apple Peels) on α -brass in 2 M HCl .

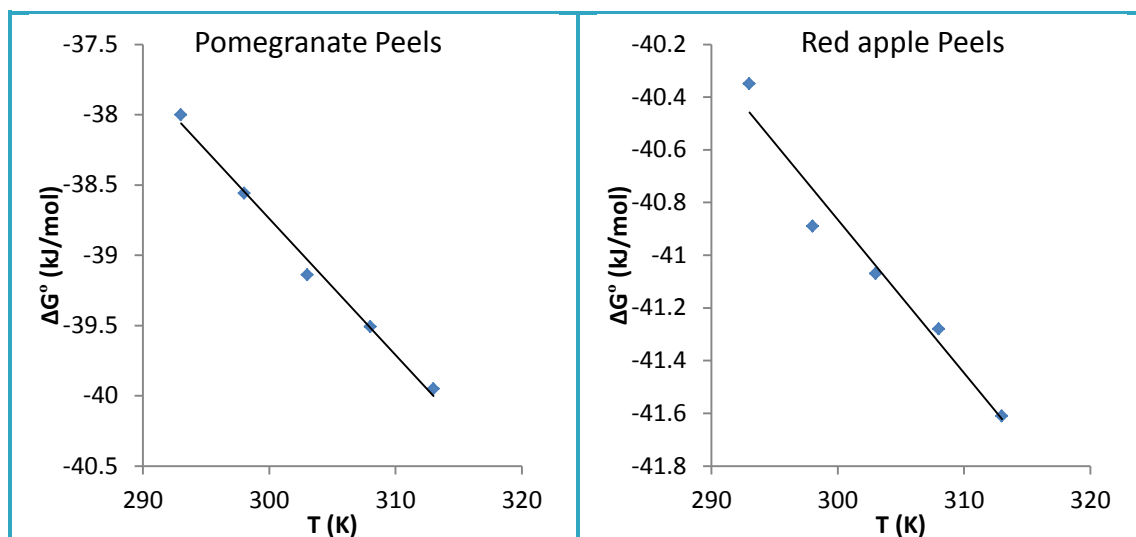


Figure (3.19): The variation of Gibbs free energies ($\Delta G^\circ_{\text{ads}}$) with temperature for the adsorption of (Pomegranate and Red apple Peels) on α -brass in 2 M H_2SO_4 .

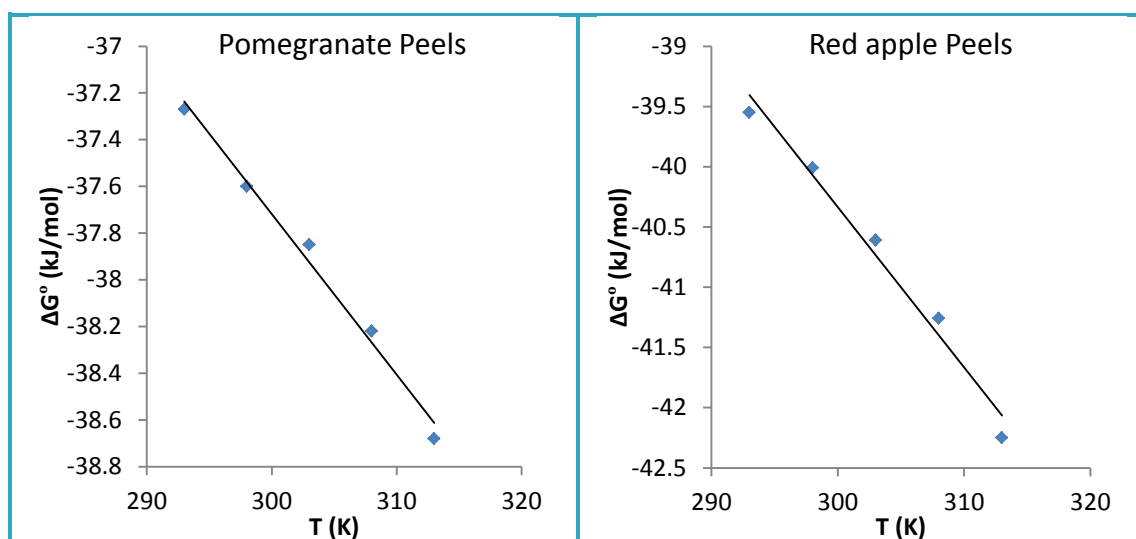


Figure (3.20): The variation of Gibbs free energies ($\Delta G^\circ_{\text{ads}}$) with temperature for the adsorption of (Pomegranate and Red apple Peels) on α -brass in 2 M HCl.

Table (3.19): Thermodynamic parameters for adsorption of (Pomegranate and Red apple Peels) on α -brass in 2 M H_2SO_4 .

Inh.	T (K)	K_{ads} ($g^{-1}.L$)	$-\Delta G_{ads}^{\circ}$ ($kJ.mol^{-1}$)	$-\Delta H_{ads}^{\circ}$ ($kJ.mol^{-1}$)	ΔS_{ads}° ($J.K^{-1}.mol^{-1}$)
Pomegranate Peels	293	5952.38	38.00	9.64	97
	298	5747.13	38.56		
	303	5586.60	39.14		
	308	5025.13	39.51		
	313	4651.16	39.96		
Red apple Peels	293	15600.62	40.35	23.41	58.2
	298	14705.88	40.89		
	303	12048.19	41.07		
	308	10030.09	41.28		
	313	8779.631	41.61		

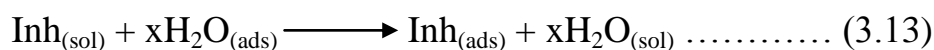
Table (3.20): Thermodynamic parameters for adsorption of (Pomegranate and Red apple Peels) on α -brass in 2 M HCl.

Inh.	T (K)	K_{ads} ($g^{-1}.L$)	$-\Delta G_{ads}^{\circ}$ ($kJ.mol^{-1}$)	$-\Delta H_{ads}^{\circ}$ ($kJ.mol^{-1}$)	ΔS_{ads}° ($J.K^{-1}.mol^{-1}$)
Pomegranate Peels	293	4405.286	37.27	17.08	68.8
	298	3891.051	37.60		
	303	3355.705	37.85		
	308	3039.514	38.22		
	313	2849.003	38.68		
Red apple Peels	293	11235.96	39.55	0.45	133
	298	10309.28	40.01		
	303	10030.09	40.61		
	308	9950.25	41.26		
	313	11235.96	42.25		

The large and negative values of ΔG_{ads}° indicates the spontaneity and stable adsorbed film that formed by inhibitor molecules which supported by obtained large values of adsorption constant ⁽⁷⁶⁾. The values of ΔG_{ads}° were ranged between (37.27 – 42.25) $kJ.mole^{-1}$ the maximum value was obtained for red apple inhibitor in H_2SO_4 solution. The obtained results give an indication that the adsorption process of those inhibitors are likely via chemisorption and

physisorption mechanisms but mainly via chemisorption mechanism due to highly values of free Gibbs energy of adsorption for both of inhibitors especially in H₂SO₄ medium. Chemisorption mechanism is a strong adsorption that involves formation of semi-bond between lone pairs that located on hetero atoms and d-vacant orbitals of the metal. Unlike physisorption, chemisorption increase with increasing temperature ^(77, 78).

The negative values of $\Delta H_{\text{ads}}^{\circ}$ reflects the exothermic nature of the adsorption of pomegranate and red apple peels extract on α -brass surface. The positive sign of $\Delta S_{\text{ads}}^{\circ}$ values indicates the increase in randomness or degree of freedom that accompany of adsorption process of both inhibitors. This behavior can be attributed is that the water molecules that located on the metal surface will be displaced by aqueous inhibitor molecules which results decrease in disorder of inhibitor molecules and increase the disorder of the solution. The increase in entropy of adsorption occurred as the reactant goes from solution to metal/solution interface ⁽⁷⁹⁾ as shown in equation (3.13).



3.6 Surface Characterization Techniques

3.6.1 X-Ray Diffraction (XRD) Powder

The interpreted XRD patterns for α -brass alloy in absence and presence of the inhibitors are shown in figures (3.21 – 3.24).

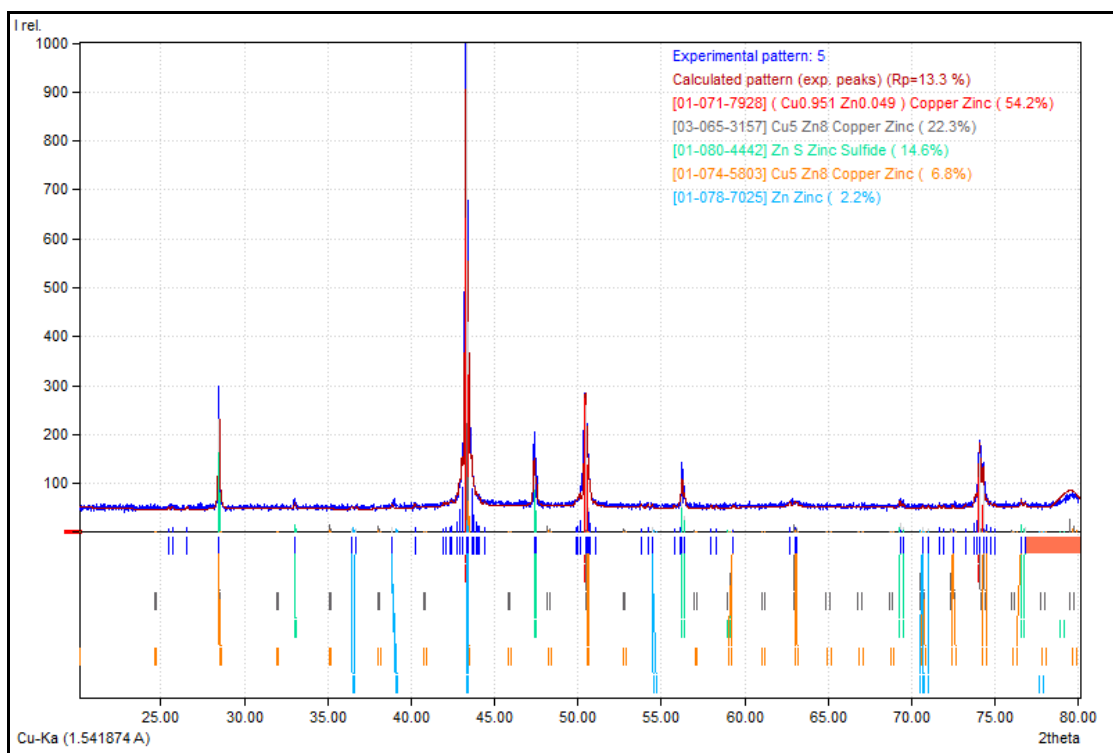


Figure (3.21): XRD interpreted patterns for α -brass in 2 M of blank solution (H_2SO_4).

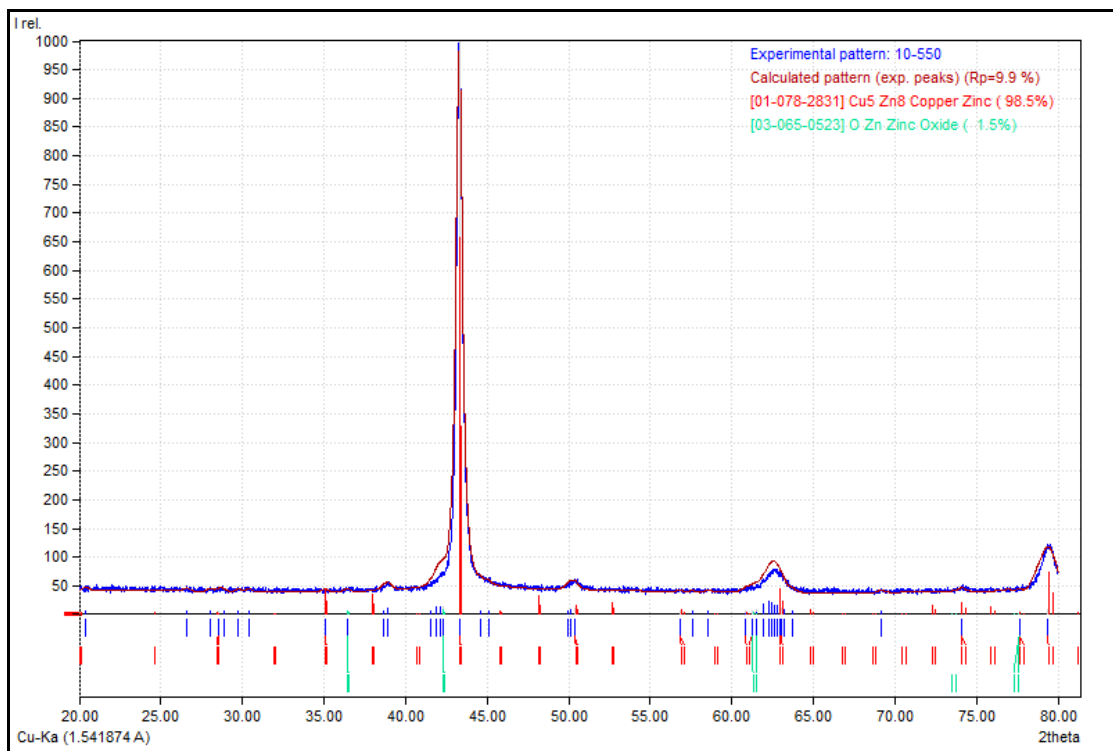


Figure (3.22): XRD interpreted patterns for α -brass in 2 M of blank solution (H_2SO_4) and in presence of 500 ppm of pomegranate peels.

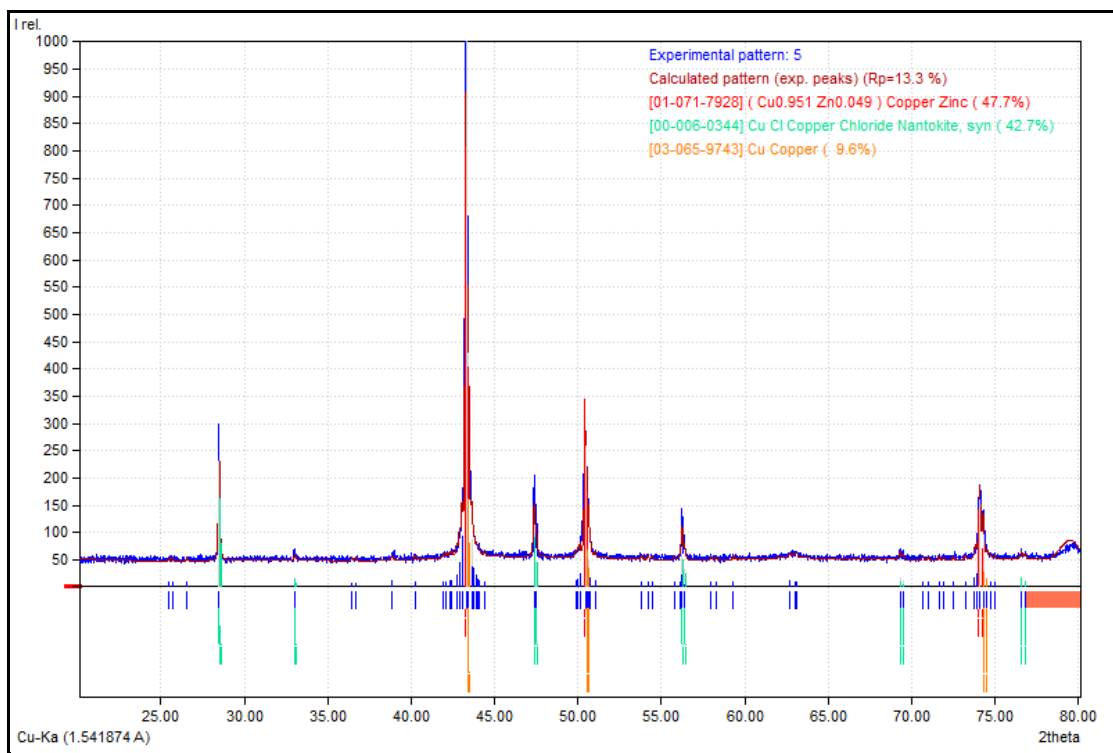


Figure (3.23): XRD interpreted patterns for α -brass in 2 M of blank solution (HCl).

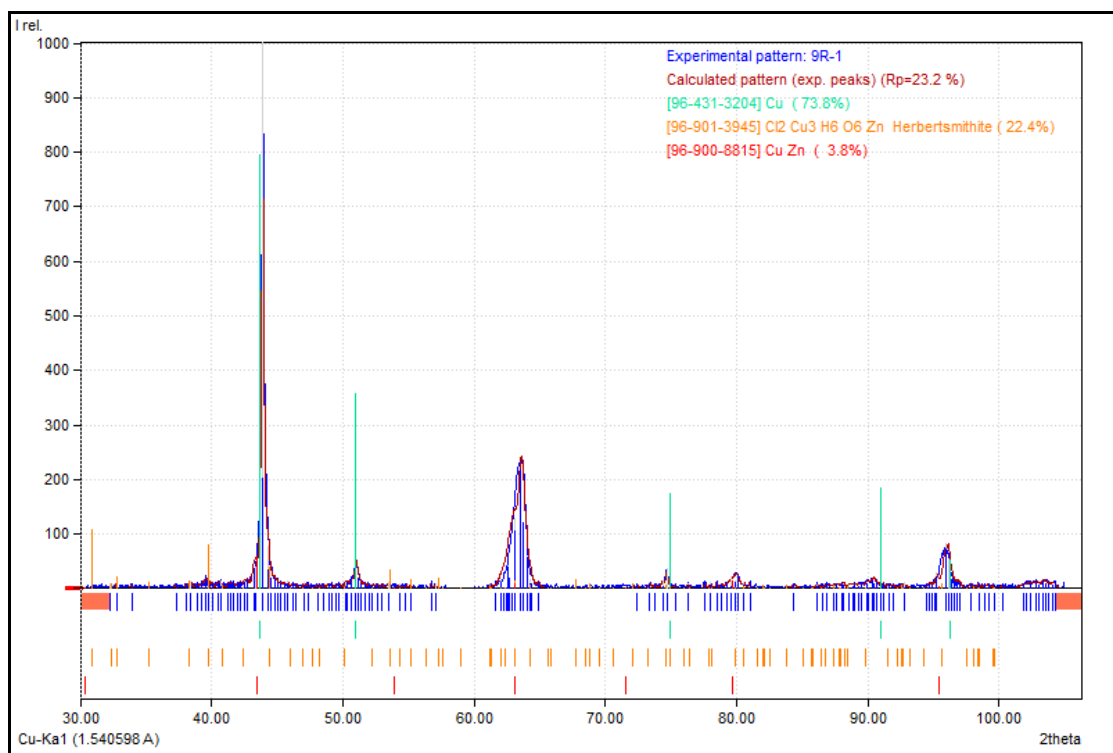
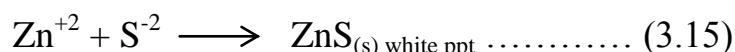
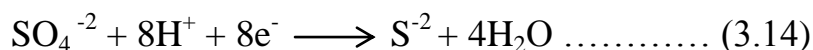


Figure (3.24): XRD interpreted patterns for α -brass in 2 M of blank solution (HCl) and in presence of 500 ppm of red apple peels.

The diffractograms of the alloy in both acids (H_2SO_4 , HCl) approved that the alloy is experienced corrosion on large scale due to the presence of aggressive ions. The mainly reason of using XRD is to investigate the corrosion products that will be formed after the polarization measurements. The corrosion products were identified by comparing the diffractograms to standard XRD database (provided by International Centre for Diffraction Data) the comparison is based on 2θ values and the intensities of the peaks.

The interpreted diffractogram for alloy in H_2SO_4 solution show peaks at (28, 48, and 56) 2θ are attributed to formation of zinc sulfide. The proposed mechanism about formation of ZnS may be explained as follow: Firstly zinc atoms suffer oxidation to form zinc ions Zn^{+2} and then leaching out from alloy surface due to dezincification phenomenon and then dissolved in the solution.

The aggressive sulfate ions SO_4^{-2} undergo a reduction reaction to form sulfide ions S^{-2} . Then the sulfide and zinc ions reacted to form zinc sulfide which is observed as a white precipitate formed on the alloy surface ⁽⁸⁰⁾ as indicated by the following reactions:



The diffractogram (figure 3.21) show very intense peak at (43) 2θ which assign to intermetallic copper crystal phase Cu 0.951 Zn 0.049 another intermetallic copper phase observed at (52, 74) 2θ for Cu5Zn8 XRD patterns also revealed that very traces amount of zinc are deposited on the surface which clearly indicated in the diffractogram. When the inhibitor (pomegranate peels) is added (as shown in figure (3.22)) the peaks of ZnS and Zn are disappeared and only very traces of zinc oxide is formed at (63) 2θ with very intense peak of intermetallic phase Cu5Zn8 (43) 2θ which bring another evidence about the inhibitive performance of the natural peels that formed a protective layer which prevents the dezincification and formation of other compounds.

The XRD patterns for α -brass alloy in HCl solution shown important observations such the completely leaching out of zinc atoms and also the diffractogram shows the formation of cupreous chloride (CuCl) that formed due to primarily oxidation of copper as described in the reactions:

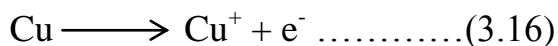


Figure (3.23) observed that forms Cu^+ ions that react with chloride that can be observed in peaks at (28, 48) 2θ with deposited red spongy of copper which approved with appearance peak at (51) 2θ . On the other hand, presence of inhibitor (red apple peels) (as shown in figure (3.24)) leads to disappearance of cupreous chloride peaks and a new intense peak (43) 2θ appear refer to

deposited copper metal on the alloy surface. The diffractogram also show the presence of copper intermetallic halide layer which known as Herbertsmithite with a chemical formula $\text{Cl}_2\text{Cu}_3\text{H}_6\text{O}_6\text{Zn}$.

3.6.2 Scanning Electron Microscope (SEM)

The examination of adsorption of inhibitor molecules on the alloy surface was done by using scanning electron microscope. Figures (3.25) and (3.26) show the obtained micrographs for α -brass alloy for both acids in the absence and presence of pomegranate and red apple peels extract. The micrographs (a) show a smooth polished surface before immersed in the acidic media. When the specimens immersed in the blank solutions for 24 hrs at room temperature a clearly observed corrosion is noticeable in the micrograph (b) which shows that the surface of the alloy gets cracked and rough due to the presence of aggressive ions. Micrographs (c and d) show a remarkable accumulation on the alloy surface by adsorbed inhibitors which bring more evidence that a protective film is formed via adsorption process that's lead to isolate the alloy surface form the corrosive medium.

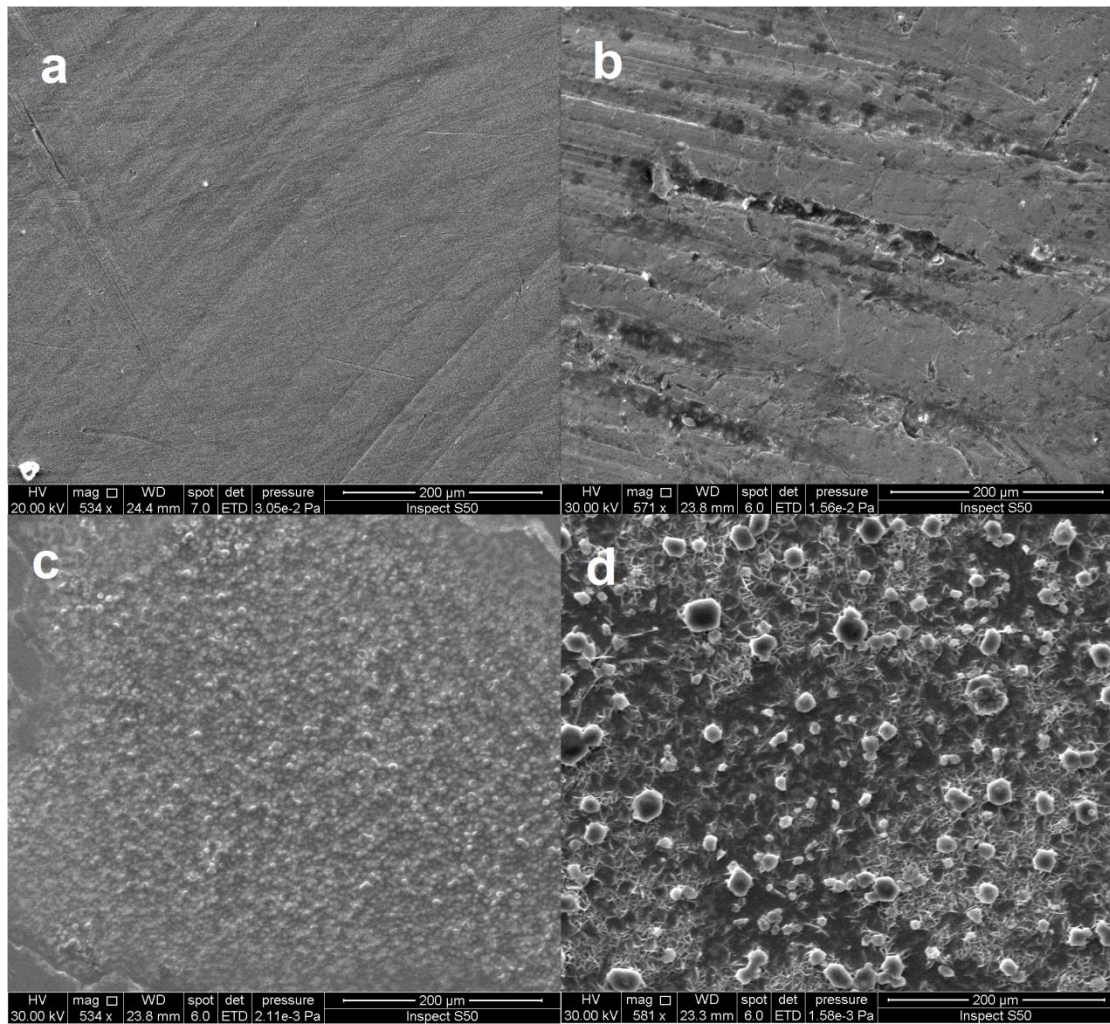


Figure (3.25): Scanning electron micrographs of (a) Polished α -brass alloy (b) α -brass alloy immersed 24 hrs in 2 M H_2SO_4 solution (c) α -brass alloy immersed 24 hrs in 2 M H_2SO_4 solution and in presence of 500 ppm red apple peels extract and (d) α -brass alloy immersed 24 hrs in 2 M H_2SO_4 solution and in presence of 500 ppm pomegranate peels extract.

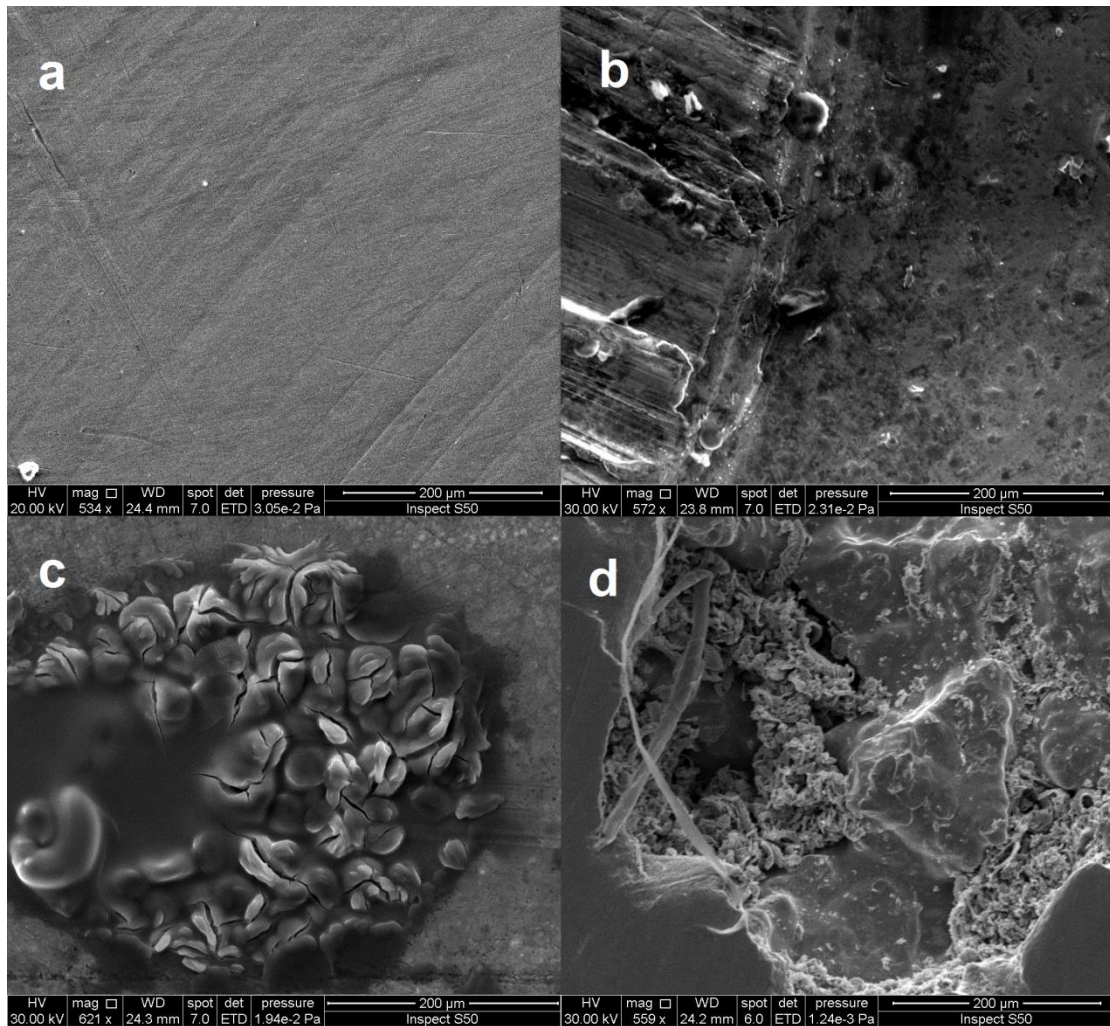


Figure (3.26): Scanning electron micrographs of (a) Polished α -brass alloy (b) α -brass alloy immersed 24 hrs in 2 M HCl solution (c) α -brass alloy immersed 24 hrs in 2 M HCl solution and in presence of 500 ppm red apple peels extract and (d) α -brass alloy immersed 24 hrs in 2 M HCl solution and in presence of 500 ppm pomegranate peels extract.

Chapter Four

Conclusions and

Recommendations

4.1 Conclusions

The outcome highlights that can be concluded from the results and discussion are listed as follow:

1. The characterization techniques (GC-MS) and (FT-IR) for pomegranate and red apple peels are proved the presence of many natural organic compounds and these compounds having large number of hetero atoms that responsible for the inhibition performance of those inhibitors. According to obtained GC-MS spectra the number of phytochemicals were found as:

Red apple peels > Pomegranate peels

2. The potentiostatic results proved that α -brass alloy suffer corrosion the most in H_2SO_4 than in HCl:

$H_2SO_4 > HCl$

3. The corrosion parameters such as corrosion current density, corrosion rate and penetration rate are increasing with increase temperature and decreasing with increase inhibitors concentration.
4. The inhibition efficiency was increased with increasing the concentration of inhibitors. The outcome results show that red apple peels was better inhibitor than pomegranate peels in both of acidic media.

Red apple peels > Pomegranate peels in H_2SO_4 and HCl

5. Both of the inhibitors act as mixed-type inhibitor in H_2SO_4 solution while as cathodic inhibitor in HCl solution.
6. The activation parameters indicated that the energy of activation (E_a) values increasing with increase inhibitor concentration which indicates the decreasing in the rate of corrosion process. The enthalpy of activation (ΔH_a) values was positive and increasing with inhibitor concentration due

- to endothermic nature of corrosion process. And the large values of ΔS_a indicate the increase in randomness as reactants going into the transition state of activated complex.
7. The thermodynamic parameters of adsorption for those inhibitors can be highlighted as $\Delta G_{\text{ads}}^\circ$ values were large and negative which indicates that the adsorption of the inhibitors is spontaneous and operates mostly via chemisorption mechanism. The large values of adsorption constant (K_{ads}) approved the stability and strength of the adsorbed layer that formed by adsorption of those inhibitors. The negative sign of $\Delta H_{\text{ads}}^\circ$ indicate the exothermic nature of the adsorption process. The positive sign of $\Delta S_{\text{ads}}^\circ$ indicates the increase in degree of freedom accompanied the adsorption process.
 8. The surface examination techniques (XRD and SEM) give important observations about the α -brass alloy behavior as well as the inhibitors behavior in the acidic medium.
 9. The investigation on the corrosion products was carried out using XRD analysis that proved the formation of ZnS and CuCl compounds in blank solutions H_2SO_4 and HCl respectively. While in presence of the inhibitors hinders the formation of those compounds which gives another evidence of the inhibitive activity of the used inhibitors.
 10. SEM images of the blank solutions and the inhibitors are proved the aggressive nature of the blank solutions and also confirmed the formation of protective film that formed by the inhibitor molecules via adsorption process.

4.2 Recommendations

Here some suggestions for further studies that concerning about α -brass alloy and its corrosion behavior:

1. Further studies needed about the corrosion behavior of α -brass alloy in acidic media especially the acidic oxidizing agents.
2. Despite the importance of α -brass alloy in industrial fields, there are significant lack studies about using natural derivatives such as plants and peels on α -brass. So further studies required using natural derivatives as green corrosion inhibitors for α -brass alloy.
3. Study the inhibitive performance of new approach that use recycled polymers that derived from plastic waste which they seem to be promised as active corrosion inhibitor for copper alloys.

References

References:

1. Richardson H. W., (1997), "Handbook of Copper Compounds and Applications", Marcel Dekker, Inc., (18).
2. Barak P., Helmke P. A., (1993), The Chemistry of Zinc, Springer, 55(1-13).
3. Cicek V, (2013), "Cathodic Protection", Scrivener Publishing Wiley, (1).
4. Roberge P. R, (2000), "Handbook of Corrosion Engineering", 1st ed., McGraw-Hill Book Company, (833).
5. Roberge P. R., (2008), "Corrosion Engineering Principles and Practice", McGraw-Hill Companies, (82, 86, 112).
6. Bardal E., (2004), "Corrosion and Protection", Springer, (6,7).
7. Antonijevic M. M. and Petrovic M. B, (2008), Copper Corrosion Inhibitors. A review, Int. J. Electrochem. Sci., 3(1-28).
8. Mihajlović M. B. and Antonijević M. M., (2015), Copper Corrosion Inhibitors. Period 2008-2014. A Review, Int. J. Electrochem. Sci., 10(1027-1053).
9. Refaey S. A., Abd El Malak A. M, Abdel-Fatah H. T. and Taha F, (2007), Corrosion and Inhibition of Cu-Zn Alloys in NaCl Solution by Using Permanganate and Phosphate Anions, Int. J. Electrochem. Sci, 2(563-571).
10. The Copper Advantage a Guide to Working with Copper and Copper Alloys, Copper Development Association, 260 Madison Avenue, New York, NY 10016-2401.
11. D. D. Davies, Dip. App. Chem., MIM., (1993), A Note on the Dezincification of Brass and the Inhibiting Effect of Elemental Additions, Copper Development Association Inc., 260 Madison Avenue, New York, NY 10016.

12. Loto C. A. and Loto R. T., (2016), Inhibition Effect of Garlic Extracts on the Corrosion of Alpha Brass in Nitric Acid, *Der Pharma Chemica*, 8(162-171).
13. Dadgarinezhad A. and Baghaei F., (2010), Effect of a New Schiff Base on the Corrosion and Dezincification of Brass in 1 M HCl, *G.U. Journal of Science*, 23(287-293).
14. Kumar S., Narayanan T. S., Kumar M. S. and Manimaran A., (2006), Dezincification of Brass in Sulfide Polluted Sodium Chloride Medium: Evaluation of the Effectiveness of 2-Mercaptobenzothiazole, *Int. J. Electrochem. Sci.*, 1(456-469).
15. Abbas M. I., (1991), Effects of Temperature on Dezincification and Electrochemical Behaviour of 70-30 Brass in Sulphuric Acid, *Dr. Corros. J.*, 26(273-278).
16. Hegazy H. S., Ashour E. A. and Ateya B. G., (2001), Effect of Benzotriazole on the Corrosion of Alpha Brass in Sulfide Polluted Salt Water, *Journal of Applied Electrochemistry*, 31(1261-1265).
17. Refaey S. A., Abd El Malak A. M, Taha F and Abdel-Fatah H. T., (2008), Corrosion and Inhibition of Cu-Zn Alloys in Acidic Medium by Using Isatin, *Int. J. Electrochem. Sci*, 3(167-176).
18. Abdallah M., Al- Agez M. and Fouda A. S., (2009), Phenylhydrazone Derivatives as Corrosion Inhibitors for α -Brass in Hydrochloric Acid Solutions, *Int. J. Electrochem. Sci.*, 4(336-352).
19. Raj X. J. and Rajendran N., (2011), Corrosion Inhibition Effect of Substituted Thiadiazoles on Brass, *Int. J. Electrochem. Sci.*, 6(348-366).
20. Abd-El-Nabey B. A., Abdel-Gaber A. M., Khamis E., Morgaan A. I. and Ali N. M., (2013), Inhibition of Corrosion of Brass in 0.1 M H₂SO₄ by Thioxopyrimidinone Derivatives, *Int. J. Electrochem. Sci.*, 8(11301-11326).

21. Rangana, Banerjee R. and Nandi M. M., (2013), Corrosion Inhibition of Brass in Presence of 1, 4, 5, 6-tetrahydropyrimidine Derivatives in Chloride Solution, Indian Journal of Chemical Technology, 20(237-244).
22. Gowrani T., (2014), Effect of 5-Methylbenzotriazole on the Corrosion Inhibition of Brass in NaCl Solution, Chem Sci Trans., 3(1007-1012).
23. Ramdé T., Rossi S. and Bonou L., (2016), Corrosion Inhibition Action of Sulfamethoxazole for Brass in Acidic Media, Int. J. Electrochem. Sci., 11(6819-6829).
24. Damej M., Benassaoui H., Chebabe D., Benmessaoud M., Erramli H., Dermaj A., Hajjaji N. and Srhiri A., (2016), Inhibition Effect of 1,2,4-triazole-5-thione Derivative on the Corrosion of Brass in 3% NaCl Solution", J. Mater. Environ. Sci. 7(738-745).
25. "High-Performance Alloys for Resistance to Aqueous Corrosion", (2000), Special Metals Corporation, Publication number SMC-026, (1-2).
26. Dr. Uster D. H., "Corrosion for Engineers", (10-1)-(10-5).
27. Maaß P. and Peißker P., (2011), "Handbook of Hot-dip Galvanization", WILEY-VCH Verlag GmbH & Co. KGaA, Weinheim, (3).
28. Biresaw G. and Mittal K. L., (2014), "Surfactants in Tribology", Volume 4, CRC Press, (390).
29. Li Z., BRANZ Corrosion Scientist, (2009), "Galvanic corrosion"
30. Aliofkhazraei M., (2014), "Developments in Corrosion Protection", InTech, (438).
31. Yadla S. V., Sridevi V., Lakshmi C. M. and Kumari S. P., (2012), A Review on Corrosion of Metals and Protection, IJESAT, 2(637-644).
32. Mansfeld F., (2006), Classic Paper in Corrosion Science and Engineering with a Perspective", NACE International, 62(843-855).
33. Sequeira C. A., (2010), Some Considerations on the Background of Passivity, Corros. Prot. Mater., 4(126-137).

34. Basics of Corrosion Measurements, Application Note CORR-1, Princeton Applied Research, 801 S. Illinois Ave., Oak Ridge, TN 37830.
35. Obuka, Sylvester N., Celestine O. N., Ikwu, Reuben G., Chukwumuanya and Okechukwu E., (2012), Review of Corrosion Kinetics and Thermodynamics of CO₂ and H₂S Corrosion Effects and Associated Prediction/Evaluation on Oil and Gas Pipeline System, IJSTR, 1(156-162).
36. Fontana M. G., (1987), "Corrosion Engineering", 3rd ed., McGraw-Hill Book Company, (19).
37. Davis J. R., (2000), "Corrosion: Understanding the Basics", ASM International, (84).
38. Hughes A. E. et al. (eds.), (2016), "Active Protective Coatings", Springer Science + Business Media Dordrecht, (21,22).
39. Zhang J., (2008), "PEM Fuel Cell Electrocatalysts and Catalyst Layers, Fundamentals and application", Springer, (56).
40. Etor A., (2009), Electrochemical Measurement of Crevice Corrosion of Type AISI 304 Stainless Steel.
41. Stansbury E. E. and Buchanan R. A., (2000), "Fundamentals of Electrochemical Corrosion", ASM International, (147-149).
42. Woods R. and Doyle F. M., (2000), "Electrochemistry in Mineral and Metal Processing", 5th ed., The Electrochemical Society, Inc., (40-44).
43. Kear G., Flatley I. and Jones S., (2006), Application of Polarization Resistance Measurements for the Estimation of Corrosion Rates of Galvanised Steel Structures in Soils, BRANZ, 127(1-15).
44. Tang D., Lu J., Zhuang L. and Liu P., (2010), Calculations of the Exchange Current Density for Hydrogen Electrode Reactions: A Short Review and a New Equation, Journal of Electroanalytical Chemistry 644(144-149).

45. Yaro A. S., Wael R. K. and Khadom A. A., (2010), Reaction Kinetics of Corrosion of Mild Steel in Phosphoric Acid, *Journal of the University of Chemical Technology and Metallurgy*, 45(443-448).
46. Ansari K. R., Quraishi M. A. and Singh A., (2015), Pyridine Derivatives as Corrosion Inhibitors for N80 Steel in 15% HCl: Electrochemical, Surface and Quantum Chemical Studies, *Measurement*, 76(136-147).
47. Ibrahim T. H., Chehade Y. and Abou Zour M., (2011), Corrosion Inhibition of Mild Steel using Potato Peel Extract in 2 M HCl Solution, *Int. J. Electrochem. Sci.*, 6(6542-6556).
48. Rani B. E. and Basu B. B., (2012), Green Inhibitors for Corrosion Protection of Metals and Alloys: An Overview, *International Journal of Corrosion*, (1-15).
49. Revie R. W., (2011), "Uhlig's Corrosion Handbook", 3rd ed., John Wiley & Sons, Inc., (1022-1025).
50. Sharma S. K., Peter A. and Obot I. B., (2015), Potential of Azadirachta Indica as a Green Corrosion Inhibitor Against Mild Steel, Aluminum, and Tin: A Review, *Journal of Analytical Science and Technology*, 6(1-16).
51. Ibrahim T. H. and Abou Zour M., (2011), Corrosion Inhibition of Mild Steel using Fig Leaves Extract in Hydrochloric Acid Solution, *Int. J. Electrochem. Sci.*, 6(6442-6455).
52. Mahmoud, S. S., (2006), Corrosion Inhibition of Muntz (63% Cu, \approx 37% Zn) Alloy in HCl Solution by Some Naturally Occurring Extracts, *Portugaliae Electrochimica Acta*, 24(441-445).
53. Rocha J. C., Gomes J. A., D'Elia E., Cruz A. P., Cabral L. M., Torres A. G. and Monteiro M. V., (2012), Grape Pomace Extracts as Green Corrosion Inhibitors for Carbon Steel in Hydrochloric Acid Solutions, *Int. J. Electrochem. Sci.*, 7(11941-11956).

54. Agarwal K., (2014), Fenugreek Leaves and Lemon Peel as Green Corrosion Inhibitor for Mild Steel in 1 M HCl Medium, *Journal of Materials Science & Surface Engineering*, 1(44-48).
55. Ismail A. and Tajuddin M. A., (2014), Banana Peel as Green Corrosion Inhibitor for Stainless Steel 304, *International Conference on X-Rays & Related Techniques in Research & Industry*, (109-110).
56. Al-Fakih A. M., Aziz M. and Sirat H. M., (2015), Turmeric and Ginger as Green Inhibitors of Mild Steel Corrosion in Acidic Medium, *J. Mater. Environ. Sci.* 6(1480-1487).
57. Bashraheil B. O., al-ahmary J. A., al-zahrani N. A. and Arab S. T., (2011), Inhibition of Aluminum Corrosion in 1.25 M HCl by Pomegranate Aqueous Extract, *Journal of King Abdulaziz University*, (1-42).
58. Umoren S., Obot I. B., Gasem Z. and Odewunmi N. A., (2015), Experimental and Theoretical Studies of Red Apple Fruit Extract as Green Corrosion Inhibitor for Mild Steel in HCl Solution, *Journal of Dispersion Science and Technology*, 36(789-802).
59. Avci G. and Keles Y., (2011), Aqueous Extract of Acacia Cyanophylla Leaves as Environmentally Friendly Inhibitor for Mild Steel Corrosion in 1 M H₂SO₄ Solution, *Surf. Interface Anal.*, 43(1311-1317).
60. Mohammed G. J., Al-Jassani M. J. and Hameed I. H., (2016), Antibacterial, Antifungal Activity and Chemical Analysis of Punica Granatum (Pomegranate Peel) Using GC-MS and FTIR Spectroscopy, *IJPPR*, 8(480-494).
61. Sharma Y. R., (2010), "Elementary Organic Spectroscopy", S Chand, (93-130).
62. Kumar K. A. and Vijayalakshmi K., (2011), GC-MS Analysis of Phytochemical Constituents in Ethanolic Extract of Punica Granatum Peel

- and Vitis Vinifera Seeds, International Journal of Pharma and Bio Sciences, 2(461-468).
63. Shukla J. and Pitre K. S., (2002), Electrochemical Behavior of Brass in Acid Solutions and the Inhibitive Effect of Imidazole, Purdue University Libraries Authenticated, 20(217-229).
64. Girisuta B., Janssen L. P. and Heeres H. J., (2006), A kinetic Study on the Decomposition of 5-hydroxymethylfurfural into Levulinic Acid, The Royal Society of Chemistry, 8(701-709).
65. Gunavathy N. and Murugavel S. C., (2012), Corrosion Inhibition Studies of Mild Steel in Acid Medium Using Musa Acuminata Fruit Peel Extract, E-Journal of Chemistry, 9(487-495).
66. Al-Amiery A. A., Kadhum A. H., Alobaidy A. M., Mohamad A. and Hoon P. S., (2014), Novel Corrosion Inhibitor for Mild Steel in HCl, 7(662-672).
67. Kumara S. A., Sankar A. and Kumarb S. R., (2013), Vitamin B-12 Solution as Corrosion Inhibitor for Mild Steel in Acid Medium, IJCES, 3(57-61).
68. Al Juhaiman L. A., Abu Mustafa A. and Mekhamer W. K., (2012), Polyvinyl Pyrrolidone as a Green Corrosion Inhibitor of Carbon Steel in Neutral Solutions Containing NaCl: Electrochemical and Thermodynamic Study, Int. J. Electrochem. Sci., 7(8578-8596).
69. Abdallah M., AL Jahdaly B. A. and Al-Malyo O. A., (2015), Corrosion Inhibition of Carbon Steel in Hydrochloric Acid Solution using Non-Ionic Surfactants Derived from Phenol Compounds, Int. J. Electrochem Sci., 10(2740-2754).
70. Wang H., Liu Y., Xie J., Tang J., Duan M., Wang Y. and Chamas M., (2016), 3-(diethylamino)-1-phenylpropan-1-one as a Corrosion Inhibitor for N80 Steel in Acidization of Petroleum Exploitation, Int. J. Electrochem. Sci., 11(4943-4956).

71. Zarrouk A., Hammouti B., Zarrok H., Al-Deyab S. S. and Messali M., (2011), Temperature Effect, Activation Energies and Thermodynamic Adsorption Studies of L-Cysteine Methyl Ester Hydrochloride as Copper Corrosion Inhibitor in Nitric Acid 2 M, *Int. J. Electrochem. Sci.*, 6(6261-6274).
72. Hassan R. M. and Zaafarany I. A., (2013), Kinetics of Corrosion Inhibition of Aluminum in Acidic Media by Water-Soluble Natural Polymeric Pectates as Anionic Polyelectrolyte Inhibitors, *Materials*, 6(2436-2451).
73. Ouali I. E., Hammouti B., Aouniti A., Ramli Y. and Azougagh M., (2010), Thermodynamic Characterisation of Steel Corrosion in HCl in the Presence of 2-phenylthieno (3, 2-b) quinoxaline, *J. Mater. Envir. Sci.*, 1(1-8).
74. Chaubey S. N., Mourya P., Singh V. K. and Singh M. M., (2015), Fruit Extract as a Green Inhibitor for Copper Corrosion in Nitric Acid Solution, *IJIRSET*, 4(4545-4553).
75. Rubaye A. Y., Abdulsahib H. T. and Abdulwahid A. A., (2015), Corrosion Inhibition Properties of Norepinephrine Molecules on Mild Steel in Acidic Media, *Journal of Encapsulation and Adsorption Sciences*, 5(155-164).
76. Yadav M., Gope L., Kumari N. and Yadav P., (2016), Corrosion Inhibition Performance of Pyranopyrazole Derivatives for Mild Steel in HCl Solution: Gravimetric, Electrochemical and DFT Studies, *Journal of Molecular Liquids*, 216(78-86).
77. Singh P. and Quraishi M. A., (2016), Corrosion Inhibition of Mild Steel Using Novel Bis Schiff's Bases as Corrosion Inhibitor: Electrochemical and Surface Measurement, *Measurement*, 86(114-124).
78. Laabaissi T., Bouassiria M., Oudda H., Zarrok H., Zarrouk A., Elmidaoui A., Lakhri L., Lakhri B., Essassi E. M. and Tourir R., (2016),

- Adsorption and Corrosion Inhibition Effect of Benzodiazepine Derivative on Carbon Steel in 2.0 M H_3PO_4 Medium, J. Mater. Environ. Sci., 7(1538-1548).
- 79.Khaled K. F., Elhabibc O. A., El-mghrabya A., Ibrahima O. B. and Ibrahimd M. A., (2010), Inhibitive effect of thiosemicarbazone derivative on corrosion of mild steel in hydrochloric acid solution, J. Mater. Environ. Sci., 1(139-150).
- 80.Bouroushian M., (2010), "Electrochemistry of Metal Chalcogenides", Springer, (59).

- على ان نوع التفاعل هو باعث للحرارة. ووجدت ان قيم الانتروبي هي موجبة مما يدل على زيادة في عشوائية النظام اثناء حدوث عملية الامتزاز.
٨. بينت نتائج حيود الاشعة السينية على تكون مركبات (ZnS) و (CuCl) في حامض الكبريتيك وحامض الهيدروكلوريك على التوالي في حين عند اضافة المثبطات حالت دون تكون هذه المركبات مما يدل على فعاليتها كمثبط.
٩. اظهرت الصور الناتجة من المجهر الالكتروني الماسح على مدى الضرر الناتج للسبيكة عند غمرها في الاوساط الحامضية واكدت الصور ايضا على حدوث عملية الامتزاز للمثبطات على سطح السبيكة وتكوين طبقة حماية للسبيكة.

الملخص:

تتضمن الرسالة الحالية من اربعة فصول رئيسية تسلط الضوء على دراسة سلوك تاكل سبيكة الفايبراص الحامضية باستخدام الطريقة الاستقطابية يتناول كل فصل عدة مواضيع مهمة كالموضحة كالتالي:

١. الفصل الاول يناقش مواضيع تعريفية فيما يخص التاكل، انواعه، مفاهيم كهروكيميائية و سبائك النحاس.
٢. الفصل الثاني يناقش الجزء العملي من حيث طرق التحضير والتقنيات المستخدمة حول تشخيص قشور الرمان والتفاح الاحمر وكذلك الدراسة الاستقطابية.
٣. الفصل الثالث يناقش اهم النتائج الي تم التوصل اليها من الجزء العملي ومن حسابات دوال ارينوس وحسابات الامتزاز
٤. الفصل الرابع يوضح اهم الاستنتاجات المستحصلة من النتائج وكذلك بعض التوصيات .
اهم النتائج التي تم الحصول عليها من استخدام التقنيات اعلاه يمكن تلخيصها كالتالي :
١. ان تقنيات التشخيص الطيفية اثبتت على وجود انواع عديدة من المركبات العضوية الطبيعية في القشور وان هذه المركبات هي المسؤولة عن الفعالية التثييطية لقشور الرمان والتفاح الاحمر.
٢. نتائج القياس الاستقطابية اثبتت ان كثافات تيار التاكل ومعدلات التاكل تزداد مع زيادة درجة الحرارة.
٣. قيم كفاءة التثييط وتغطية السطح تزداد مع زيادة تركيز قشور الرمان والتفاح الاحمر وتقل مع زيادة درجة الحرارة.
٤. كذلك بينت النتائج بان قشور التفاح الاحمر كانت افضل مثبت لسبيكة في الوسطين.
٥. اظهرت النتائج بان كلا من قشور الرمان والتفاح الاحمر يسلكان كمثبطات (كاثودية وانودية معاً) في حامض الكبريتيك في حين سلكا كمثبطات كاثودية في حامض الهيدروكلوريك.
٦. اظهرت نتائج حساب المعامل الحركية للسبيكة بان قيم طاقة التنشيط تزداد مع زيادة تركيز المثبط مما يدل على صعوبة حدوث عملية التاكل في وجود المثبط. ووجدت ان قيم الانثالبي موجبة في وجود وعدم وجود المثبط مما يدل على ان نوع التفاعل ماص للحرارة. وان قيم الانتروبي سالبة وتتجه نحو الموجب مع زيادة تركيز المثبط مما يؤكد على زيادة في عشوائية التفاعل.
٧. الحسابات الثيرموديناميكية لعملية امتزاز المثبطات على سطح السبيكة اظهرت ان قيم الطاقة الحرة سالبة مما يدل على تلقائية حدوث عملية الامتزاز وان قيمها تراوحت ما بين (٣٧,٢٧-٤٢,٢٥) كيلو جول/مول مما يؤكد على ان نوع ميكانيكية الامتزاز هي كيميائية وفيزيائية ولكنها كيميائية بدرجة اكبر. وكذلك اظهرت الحسابات ان قيم الانثالبي للامتزاز هي سالبة مما يؤكد



جمهورية العراق
وزارة التعليم العالي
والبحوث العلمي
جامعة النهرين
كلية العلوم
قسم الكيمياء

تشخيص مستخلصات قشور التفاح والرمان الاحمر كمثبطات لتآكل سبيكة الفا (نحاس- خارصين) في الوسط الحامضي

رسالة
مقدمه إلى كلية العلوم / جامعة النهرين
كجزء من متطلبات نيل درجة الماجستير في علوم الكيمياء

من قبل
مصطفى صبري جواد
بكالوريوس ٢٠١٥

إشراف
الأستاذ المساعد الدكتورة
تغريد علي سلمان

شباط ٢٠١٨م

جمادى الأولى ١٤٣٩هـ